Cranfield University

MHMOD A A HAMEL

Condition Monitoring of Helical Gears Using Acoustic Emission (AE) Technology

School of Engineering

Doctor of Philosophy

July, 2013

Cranfield University

School of Engineering

PhD Thesis

July, 2013

MHMOD A A HAMEL

Condition Monitoring of Helical Gears Using Acoustic Emission (AE) Technology

Under Supervision: Prof. David Mba
Dr. A Addali

Academic Year 2012 - 2013

ABSTRACT

Techniques such as vibration monitoring, thermal analysis and oil analysis are well established as means to have been used to improve reliability of gearboxes and extend time-to-failure. In this area Acoustic Emission (AE) technology is still in its infancy but the attention shown by researchers towards this method has increased dramatically because several studies have shown the AE offers the important advantage of improved sensitivity over more conventional monitoring tools for the early detection and prediction of gear failure.

Helical gear lubrication is critically important for maintaining the integrity of operating gears and the oil also prevents asperity contact at the gear mesh thereby protecting the gears from a deterioration process and surface failures. In gear systems, there are three types of lubrication regimes: Dry Running, Boundary Lubrication (BL), Hydrodynamic Lubrication (HL) and Elastohydro-dynamic Lubrication (EHL). The last regime is associated with the normal operating running condition of gears.

Acoustic emissions were acquired from gears and analysed for different lubrication regimes (dry, BL, HL and EHL regimes at different temperatures), and corresponding specific film thicknesses (λ) levels. The results showed an inverse relationship between AE signal levels and specific film thickness (λ) of the oil. This relation was used to determine the lubrication regime from the measured AE signals. For instance, dry running had the highest AE levels which were attributed to the metal-to-metal contact of the gear mesh. The BL regime had relatively high AE levels which also attributed to the level of asperity contact is greater than the oil film thickness. The HL regime was characterized by the lowest AE levels due to the lubricant oil completely separating the teeth during gear meshing. Finally, the EHL regime showed intermediate AE levels compared to the BL and HL regimes because the oil film was less than for the HL regime but greater than for the BL regime.

It is shown that the application of advanced signal processing methods is necessary for monitoring helical gears; Kurtosis and Spectral Kurtosis were used to investigate the

AE signatures and found to be effective in de-noising (spectral kurtosis) acquired signals. Acoustic Emission proved to be a powerful tool to detect the oil regime for both defective and non-defective conditions.

It is concluded that the experimental findings of this research programme will provide the foundations for significant advancement in the application of AE for the determining the lubrication regime present within a helical gearbox and for the detection of developing gear faults. This should give a new impetus in the field of maintenance and prevention of human and material catastrophes.

Several papers presenting the findings of this research have been published in international journals and given at conferences.

Papers for Journals:

1. Journal of lubricants (mdpi): Using of Acoustic Emission for Monitoring Oil Film Regimes**.** Manuscript ID (Research Paper): lubricants-34202 (published)

2. Journal of Engineering Tribology**:** Employing of Acoustic Emission for Monitoring Oil Film Regimes**.** The number assigned to work (Research Paper) is TRIB-12-1205 (accepted)

3. Journal of Applied Acoustics: Investigation of the influence of oil film thickness on helical gear defect detection using Acoustic Emission. the reference number: APAC-D-13-00027 (accepted)

Papers for Conferences:

1. Oil Regime Monitoring in Helical Gears Using Acoustic Emission. *M Hamel, A Addali and D Mba.* AMME-15 conference 29-31 May 2012 , Cairo, Egypt

2. Employing acoustic emission for monitoring oil film regime. *M Hamel, A Addali and D Mba.* The 51st Annual Conference of The British Institute of Non-Destructive Testing, 11-13 September 2012, Northamptonshire, UK.ISBN: 978 0 903132 55 9

3. Investigation of the influence of oil film thickness on helical gear defect detection using Acoustic Emission. *M Hamel, A Addali and D Mba.* CM 2013 and MFPT 2013, 18-20 June 2013, Kraków, Poland

4. Babak Eftekharnejad, Mhmod Hamel, Abdulmajid Addali and David Mba. Condition Monitoring of Machinery in Non-Stationary Operations ,"Proceedings of the Second International Conference "Condition Monitoring of Machinery in Non-Stationnary Operations" CMMNO'2012", March 26 - 28, 2012 - Hammamet – Tunisia, Part 4, 425-437, DOI: 10.1007/978-3-642-28768-8_45.

Acknowledgment

*First of all, I thank **Allah**, the almighty, for giving me the strength to carry on this project. Next, I would like to express my gratitude to Department Power and Propulsion of School of Engineering, Cranfield University, and specially to my supervisor Prof David for the useful comments, remarks and engagement through the learning process of this PhD thesis. Furthermore I would like to express my gratitude to staff of Advanced Centre of Technology, ACT-Tripoli, and specially for Dr Mohmmed Ateeg for introducing me to the topic as well for the support on the way. Also, I like to thank everyone who helped me in my research, who have willingly shared their precious time during the process of my research. I would like to thank my loved ones, who have supported me throughout entire process. I will be grateful forever for you.*

*'' Deep gratitude and love for **my parents**, my wife, my children Aws and Farah and all of my brothers and sisters''*

TABLE OF CONTENTS

ABSTRACT ..... **i**

List of Tables **1**

List of Figure s **2**

1 Introduction **8**

1.1 Project Aim and Objectives 11

1.2 Project Contribution 11

2 Gears **14**

2.1 Background 14

2.1.1 A historical Note 14

2.1.2 Gear Types and Terminology 15

2.1.3 Helical Gears 17

2.1.4 Advantages of Helical Gear 19

2.1.5 Gear Life Predictions 20

2.2 Gear Lubrication 21

2.2.1 Gear Tooth Temperature 22

2.2.2 Purposes of Lubrication 22

2.2.3 Lubricant Selection 23

2.2.4 Lubrication Properties 23

2.3 Lubrication Methods 24

2.3.1 Spray Lubrication (Forced oil circulation lubrication). 25

2.3.2 Splash Lubrication Systems 26

2.3.3 Grease Lubrication 26

2.4 Lubrication Regimes in Gears 26

2.4.1 Boundary Lubrication (BL) 27

2.4.2 Elastohydrodynamic Lubrication (EHL) 28

2.4.3 Hydrodynamic Lubrication (HL) 30

2.4.4 The Stribeck Curve 31

2.5 Specific Oil Film Thickness (λ) 33

2.6 Gear Failures 37

2.6.1 Lubrication Related Failures 39
2.6.2 Non Lubrication Related Failure 42
3 Gearbox Condition Monitoring Review: 45
3.1 Signal Processing Techniques 46
3.2 Temperature Monitoring: 52
3.3 Oil Debris Monitoring: 53
3.4 Vibration analysis: 57
Chapter 4 60
Acoustic Emission 60
4 Acoustic Emission 61
4.1 Brief history of Acoustic Emission 61
4.2 Acoustic Emission Sources 62
4.3 Acoustic Emission Applications 64
4.4 Acoustic Emission's, Advantages and Disadvantages 65
4.5 Acoustic Emission Sensors 66
4.6 Sensor Couplant 67
4.7 AE Measuring 69
4.8 Wear Conditions and Acoustic Emission 71
4.9 Gear faults monitoring using acoustic emission. 74
4.10 Acoustic Emission Activities Constraints 75
4.11 Acoustic Emission and lubricant 75
Chapter 5 78
Experimental Setup and procedure 78
5 Experimental Setup and procedure 79
5.1 Experimental Gearbox 79
5.1.1 Gears 81
5.1.2 Electrical Motor 81
5.1.3 Lubrication 82
5.1.4 Loading Plates 82
5.1.5 AE Sensors 83

5.1.6 Thermocouples 83
5.1.7 Slip Ring 84
5.1.8 Pre-Amplifier 84
5.1.9 Accelerometers 85
5.2 Data Acquisition (DAQ) Cards 85
5.2.1 Data Acquisition (DAQ) Software 85
5.3 Experimental Procedure 86
5.3.1 Capability of AE Technology for Gearbox Diagnosis 87
5.3.2 Influence of Lubrication Film Conditions on AE Signal 89
Chapter 6 94
Results and Discussion 94
6 Results and Discussion 95
6.1 Capability of AE Technology for Gearbox Diagnosis 95
6.1.1 Test Instrumentation and Procedure 95
6.1.2 Results Based on Acoustic Emission AE Monitoring 97
6.2 Influence of Lubrication Film Conditions on AE 103
6.2.1 Test Instrumentation and Procedure 103
6.2.2 Observations of AE Under Lubricated Conditions 104
6.3 Diagnosis During Dry and Lubricated Contact 108
6.3.1 Test Instrumentation and Procedure 108
6.3.2 Observations of AE Under Dry and Lubricated Conditions 108
6.4 Applicability of AE in Monitoring Defects During Dry and Lubricated Contact 112
6.4.1 Test Instrumentation and Procedure 112
6.4.2 Observation of The Signals in Time and Frequency Domains 113
6.5 Spectral Kurtosis of AE Signal from Defective and Non-Defective Gear ... 117
6.6 Correlation of AE r.m.s With Specific Film Thickness (λ) 126
6.7 General Observations 127
Chapter 7 128
Conclusions and Future Work 128
7 Conclusions and Future Work 129

7.1 Conclusions 129
7.2 Future Work 131
8 References 134
9 Appendixes 148

List of Tables

Table 1: Ranges of tangential speed for gears (Handbook of metric gears,). 25
Table 2: Film thickness regimes, mechanisms and applications (Dowson, 1995; Dowson and Ehret, 1999) 27
Table 3: Specifications of helical gears used in the experimental work (Appendix A) ... 81
Table 4: Specification of the lubricant (Appendix C) 82
Table 5: K&J-type Thermocouple Specification (Appendix D for data sheet) 83
Table 6: Experimental stages 93
Table 7: Estimated optimum frequencies and bandwidths from Kurtogram 120

List of Figure s

Figure 1: Illustration of (a) spur and (b) helical gears (Gitin M, 1994)..... 14
Figure 2: Gear Types (Ham et al., 1958)..... 16
Figure 3: Gear Terminology (Ham et al., 1958)..... 16
Figure 4: Helical gear geometry (Becker and Shipley, 2002)..... 18
Figure 5: Tooth contact lines on a spur gear (a), a bevel gear (b), and helical gear(c). (Stokes, 1992)..... 19
Figure 6: Relative gear surface fatigue life as a function of (λ) (Townsend and Shimski, 1994)..... 21
Figure 7: Lubricant spray arrangement (ASM., 1992)..... 25
Figure 8: Splash (Bath) Lubrication System (Pirro and Wessol, 2001)..... 26
Figure 9: Boundary lubrication. (Richard Booser, P. D. (1983)..... 28
Figure 10: Distribution of pressure, temperature, pressure path in Hertz and film thickness in an EHL contact (Dowson, 1977)..... 29
Figure 11: Elastohydrodynamic Lubrication (EHL) (. Richard Booser, P. D. (1983).... 30
Figure 12: Hydrodynamic lubrication (HL) (. Richard Booser, P. D. (1983)..... 31
Figure 13: Stribeck Curve (Stribeck, 1902)..... 31
Figure 14 : Diagram of gear pair..... 35
Figure 15: Gear failure modes..... 38
Figure 16: Combination of sliding and rolling in gear teeth (Walton and Goodwin, 1998)..... 39
Figure 17: Stress distribution at and near contacting surfaces under rolling contact..... 41
Figure 18: Modes of gear failures (Boyer, 1975)..... 43
Figure 19: condition based monitoring techniques..... 46
Figure 20: Classical Bath-tub curve for wear (Roylance and Hunt, 1999)..... 54
Figure 21: Schematic of the Acoustic Emission principle (NDT, 2013)..... 62
Figure 22: Example of Kaiser Effect (NDT, 2013)..... 64
Figure 23: Schematic diagram of typical AE sensor(Miller and McIntire, 1987b)..... 67
Figure 24: Hsu-Nielsen calibration head (Brüel and Kjaer., 1981)..... 68
Figure 25: Pencil lead break test raw signal, (Brüel and Kjaer., 1981)..... 69
Figure 26: Different AE signal types (Holroyd, 2000)..... 70
Figure 27: The typical AE signal features (Physical Acoustic Co., 2007)..... 71

Figure 28: Back-to-back gearbox 79
Figure 29: Schematic diagram of the test arrangement..... 80
Figure 30: Loading plates..... 83
Figure 31: Slip ring 84
Figure 32: Schematic diagram of the Data Acquisition Systems 86
Figure 33: Schematic diagram showing the different test positions at which the Nielsen source was located 88
Figure 34: Seeded defect on single tooth..... 89
Figure 35: Cooling arrangement showing nitrogen gun nozzle 90
Figure 36: Liquid nitrogen gun location and gear wheel 90
Figure 37: Defective gear..... 92
Figure 38: Schematic diagram of the experimental procedure 93
Figure 39: AE and vibration sensors locations 96
Figure 40: AE waveform associated with a defect free condition..... 98
Figure 41: AE waveform associated with a tooth defect 98
Figure 42: Oil temperature with time; defect free and with seeded defect 99
Figure 43: AE r.m.s values at each sensor with oil temperature 100
Figure 44: AE Energy values at each sensor with oil temperature 101
Figure 46: Statistical parameters of the AE first channel signals, a) kurtosis and b) Crest Factor. 102
Figure 47: Locations of the AE sensor and thermocouples..... 103
Figure 48: Gear temperature, specific film thickness and AE r.m.s with lubrication regime (system started dry, then oil was added and then system cooled). 105
Figure 49: Influence of gear temperature and specific film thickness on AE waveforms (the waveforms corresponded the regions in Figure 48)..... 107
Figure 50: Influence of gear temperature and specific film thickness on AE r.m.s (system started dry, then oil was added and then system cooled). 109
Figure 51: Gear temperature, specific film thickness and AE r.m.s as Figure 50 but enlarged..... 110
Figure 52: Influence of gear temperature and specific film thickness on AE waveforms (the waveforms correspond to the regions in Figure 50) 110
Figure 53: Defective Teeth – spalls of 2 mm diameter and 2 mm depth..... 112
Figure 54: Influence of gear temperature and specific film thickness on AE r.m.s 113

Figure 55: AE waveforms associated with regions ‘A’, ‘B’, ‘C’ in Figure 54 114
Figure 56: Statistical parameters associated with AE waveform for different lubrication regimes. 116
Figure 57: Kurtogram for defect free test; waveforms ‘A’ to ‘D’ correspond to regions ‘A’ to ‘D’ in Figure 50 118
Figure 58: Kurtogram for defective gear test; waveforms ‘A’ to ‘D’ correspond to regions ‘A’ to ‘D’ in Figure 54 119
Figure 59: AE waveforms associated with filtered signals (defect free test) 121
Figure 60: AE waveforms associated with filtered signals (test with defective gear) .. 122
Figure 61: Effect of band pass filtering of raw AE signal on KURT and CF (Defect free gear test) 124
Figure 62: Effect of band pass filtering of raw AE signal on KURT and CF (defective gear test) 125

LIST OF EQUATIONS

$\lambda = \frac{h}{\sigma_{rms}}$ ……1 33

$\sigma_{rms} = \sqrt{(\sigma 1^2 + \sigma 2^2)}$.....2 33

$\ln(\text{In}(\nu + 0.7)) = A + B\ln(T)$.....3 34

$\nu = e^{e^{(A-B\ln T)}} - 0.7$…….....…… 4 34

$h = 1.6(\eta ouR)^{0.5}$……..……5 34

$R = \frac{(R_1 sin\,\Phi + S)\,(R_2 sin\Phi - S)}{(R_1 + R_2) sin\Phi}$.....6 35

$u = \frac{\pi N_1}{30}(R_1 sin\,\Phi - \frac{S}{2} + (r-1))$..... 7 35

$r = \frac{R_2}{R_1}$.....8 36

$R = R1(\frac{r}{r+1})\sin\emptyset$ 9 36

$h = \frac{k(\eta 0u)^{0.7} R^{0.43}}{w^{0.13}}$ μm ……..……..10 37

$\lambda = hmin = \frac{h}{\sigma_{rms}}$…….....11 37

$\overline{x} = \frac{1}{T}\int_0^T x(t)dt$……...12 47

$r.m.s = \sqrt{(\frac{1}{T}\int_{-\infty}^{\infty} x^2(t)dt)}$……13 47

$Fc = = \frac{P}{rms}$……..……..…14 48

$K = \frac{\sum_{i=1}^{N}(x_i - \bar{x})^4/N}{(\sigma^2)^2} - 3$……...15 48

$Y(t) = \int_{-\infty}^{\infty} e^{2\pi ft} H(t,f)dH(f)$……..16 51

$(C_{4Y}) = S_{4Y}(f) - 2{S_{2Y}}^2(f)$……..…17 51

$$\frac{S_{2nY(t,f)=E\{|H(t,f)dx\,(f)|^{2n\omega}\}}}{df} = |H(t,f)|^{2n}\, S_{2nX} \quad \text{.....18} \qquad 52$$

$$K_Y(f) = \frac{C_{4Y(f)}}{S_{2y(f)}{}^2} = \frac{S_{4Y(f)}}{S_{2y(f)}{}^2} - 2 \quad \text{.....19} \qquad 52$$

Chapter 1

Introduction

1 Introduction

Gearboxes are an essential component in all rotating machinery. A gearbox is a transmission mechanism that provides both torque and speed conversions from a power source that is rotating (such as an electric motor) to other devices in proportion to its gear ratios. The often heavy financial losses associated with machine breakdown and commercial pressure for greater efficiency, performance, and safety have made effective machine fault detection and diagnosis increasingly important (Choy et al., 1994)

To ensure survival in the modern competitive market place it is vital for industries to improve product reliability and simultaneously cut production costs. Product reliability is particularly important for industries such as nuclear, aviation and petro-chemical where failure can cause a serious environmental disaster. In particular the typical life of a wind turbine is about 23 years (Luke, 2012), but there is considerable commercial pressure increase this lifespan and improve productively, both of which will require effective health monitoring of the gearbox.

Of particular note because they are so widely reported are helicopter accidents. Between 1964-1974, one fifth of UK helicopter accidents were caused by gearbox malfunction (Tan, 2005; Le Sueur, 1978). The problem of faulty gearboxes in helicopters has not been solved as witnessed by the report of the AAIB (UK Air Accidents Investigation Branch) which blamed the North Sea helicopter crash of 1 April 2009 which killed 16 people on gearbox failure (B. O. H, 2011). (McNiff, 1991) contains more reports on fatal aviation accidents caused by gearbox failures. (Kar and Mohanty, 2006) have discussed monitoring of helicopter transmission systems to avoid failure and the resulting catastrophic accidents.

The correct choice of lubricant for a gearbox is essential for smooth running and long life of gear boxes. The gear box is an important element of a wind turbine and it has been reported that the right lubricant could save a typical operator as much as $5,000 year-on-year per turbine operated (Luke, 2012). (Ashley, 2008) has reported that a survey of experts working in different plants found that on average some 23 % of gear box failures were attributed to either lack of lubricant or use of the wrong lubricant.

(Ribrant and Bertling, 2007) surveyed failures in Swedish wind power plants for the eight years from 1997 to 2004. Their data shows that gearboxes can be a major source of wind turbine breakdowns. Typically 20% of wind turbine downtime was due to gearbox failure, with gearbox repairs taking an average of about 256 hours (Ribrant and Bertling, 2007)). A recent report by the Low Carbon Innovation Coordination Group (LCICG) has emphasised the importance of energy from offshore wind turbines in the replacement of elderly fossil fuel and nuclear plants. It is claimed that there could be a resultant saving of as much as £89 billion of the UK's energy bill, and that technological spin offs could take a substantial share of a global market that could reach £1 trillion by 2050. Such a development would have the added benefits of reducing the UK's reliance on imported gas and help meet GHG renewable energy and emission targets; The LCICG predicts that UK companies could benefit from business opportunities worth up to £35bn from offshore wind power. The report also predicts that given the necessary investment offshore wind could deliver up to 50% of the UK's total electricity generation by 2050 (ClickGreen, 2012)

The surveys in the public domain as reported by (Spinato et al., 2009) have revealed that the gearbox has the longest downtime per failure for all onshore wind turbine sub-assemblies, (Various, 2008; Faulstich, 2008) have revealed that gearbox faults account for some 30% of all onshore lost wind turbine availability.

Early maintenance practices was breakdown strategy where an item was repaired only when it broke down, this was also termed run-to-failure or unplanned maintenance. A more advanced technique was preventive, or planned maintenance where the item was removed from service, inspected and any necessary repairs or upgrading carried out at set intervals, regardless of the health of the item. The relative complexity of modern products and the production lines on which they are produced has increased the cost associated with preventive maintenance until today it has become a major cost on production. Thus, more efficient maintenance practices are being used, these include condition based maintenance. For a good review of condition-based maintenance for detection and diagnosis of faults see (Jardine et al., 2006).

Effective condition monitoring should detect the onset of a fault at an early stage and provide a diagnosis of what the fault is and where it can be found. Ideally condition

monitoring should provide an all-round and detailed health assessment of the item of equipment.

Condition based methods can be used for both production quality control and maintenance planning, with the main benefits being cost savings and increased safety. For maintenance, condition based monitoring is often used as an early warning system which can be extremely useful in the process industries where unplanned shutdowns can result in severe financial consequences or possibly even an accident involving working personnel (Benbouzid, 2000). Condition based maintenance may necessitate significant initial investment but can reduce overall costs by minimizing down-time and maximizing the life time of items of equipment.

Today, condition monitoring usually means the application of advanced technology but traditionally it has included visual and aural inspection (using the human senses), oil analysis (also called wear debris analysis), temperature monitoring, airborne sound and acoustic emission analysis, vibration measurement and analysis, and motor current signature analysis. It has also included non-destructive testing.

Visual inspection although a basic form of condition monitoring can detect potential failure modes such as leaking, cracking, corrosion, etc. Visual inspection should always be carried out and other fo r.m.s of condition monitoring should augment it, (Keith, 2002)

Oil analysis is very useful for use with e.g. the gearboxes and bearings of wind turbines. The measured levels of ferrous and non-ferrous particles in the lubricant give useful information about the condition of the equipment. Trending is often used to predict faults prior to failure (Tan et al., 2007).

Thermography is a well tried and tested method of condition monitoring and is especially useful where heat is indicative of a fault as with electrical contacts, high speed bearings or where there is metal-to-metal contact (Beattie and Rumsey, 1999) .

Using the vibration signal from a machine is a widespread as a method of condition monitoring of rotating machinery as the vibration signal contains useful information concerning the running condition of the machine (Tan et al., 2007; Lebold et al., 2000; Mba and Rao, 2006).

Over the last few decades there has been a growing interest in using Acoustic Emission for monitoring the condition of gearboxes. Recently Acoustic Emission has been shown to be particularly useful in detecting and diagnosing fault formation at rolling contacts. Acoustic Emission has a high frequency content, well above normal background, and so is relatively insensitive to background noise, it is also highly sensitive to change in machine condition but it has the disadvantage that the sensors must be place in close proximity to the source(s) (Tan and Mba, 2005b; Tandon and Choudhury, 1999).

1.1 Project Aim and Objectives

The aim of this research is to use experimentally measured AE signals to identify and classify lubrication regimes at gear mesh as a function of specific film thickness (λ). This is to be achieved by measuring the AE signal as a function of lubricating oil and gear metal temperature.

To achieve the objective it was necessary:

(i) To understand the effect of variations in the test operating temperatures on oil film thickness and ability to identify the oil regime using AE technology.
(ii) To design and build a novel device to spray liquid nitrogen onto rotating gears, in-situ, to reduce lubricant temperature whilst monitoring changes in AE.
(iii) To increase understanding of AE technology and its ability to monitoring helical gears.
(iv) To investigate the condition on the AE signal produced due to a change in lubrication regime of helical gears.
(v) Understand the influence on AE from studied natural surface fatigue under various oil film regimes in real time operating gears.
(vi) To study the application of appropriate advanced signal processing techniques to enhance the diagnostic effectiveness of AE signals to ascetain the lubricant regime.
(vii) To develop a relationship between oil film thickness and AE.

1.2 Project Contribution

- The main contribution is the ability to effectively detect the oil film thickness during helical gear mesh with the AE.

- The outcomes of this research can contribute to a better and deeper understanding of lubrication film classifications and their effects on gear performance and service life efficiency.
- It encourages the use of AE technology as an effective diagnosis technique in lubrication-related failures of helical gear.
- Results from this research program will establish a relationship between AE technology and the lubrication regimes.

Chapter 2

Gears

2 Gears

2.1 Background

2.1.1 A historical Note

Gears are wheel-like elements within a machine which have teeth spaced uniformly around their outer perimeters, see Figure 1. Gears have been in use for over 3000 years (Gitin M, 1994) in rotating machines from clocks to giant transporters and vary in size from a few mm to several metres in diameter

Gears are usually used in pairs, each on its own shaft, with the teeth of one meshing with the teeth of the other which allows power to be transmitted from one shaft to the other without slippage. When the gear teeth are meshed, turning one gear causes the other to rotate. This set up allows the direction and speed of rotation of the driven shaft to be changed. The gear with fewer teeth is the pinion. Speed of rotation is decreased when the pinion drives the gear and increased when the gear drives the pinion. The speed reduction factor is the ratio: = (number of gear teeth)/ (number of pinion teeth)**.** Theoretically, when the driven gear has three times the number of teeth of the driving gear it will rotate at one-third the speed but deliver three times the torque.

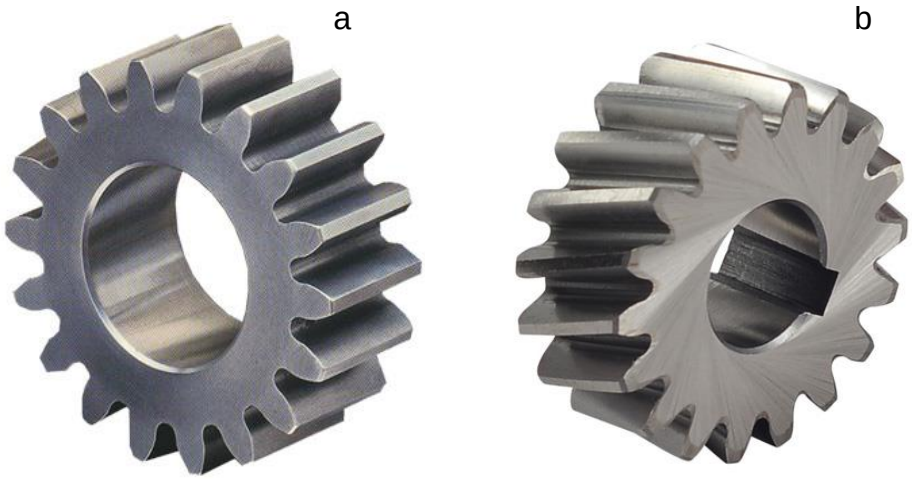

Figure 1: Illustration of (a) spur and (b) helical gears (Gitin M, 1994)

This control of speed and torque obtained by changing the relative number of teeth on the gears is invaluable in industrial design and a large proportion of the world's industry depends on gears and gearing for its functioning (Manufacturing Association American Gear, 1989).

2.1.2 Gear Types and Terminology

When considering their applications it is convenient to divide gears into one of three groups. The differentiation is based on the different relative movements of the teeth when meshing.

Figure 2 shows deferent types of gears. Spur gears have teeth which are cut parallel to the shaft and are used to transmit power with parallel shafts. Spur gears produce no axial thrust and this combined with their lower costs means spur gears are very widely used in general machine applications of moderate speeds.

Helical gears - which are the subject of this study, are described in more detail in Section 2.1.3 - have their teeth cut at an angle, see Figure 1, which has the advantage that the load is transferred progressively along the length of the tooth from one edge of the gear to the other.

Bevel gears are used when quietness of operation is important. Bevel gears transmit motion between shafts with intersecting centre lines (the intersecting angle is normally 90 deg). The teeth of bevel gears can also be cut in a curved manner to produce spiral bevel gears, which produce smoother and quieter operation than straight cut bevels.

Other type of gears is worm and hypoid gears for high gear ratio, usually operate under mixed friction conditions. Figure 3 shows some of the te r.m.s for gears (Ham et al., 1958).

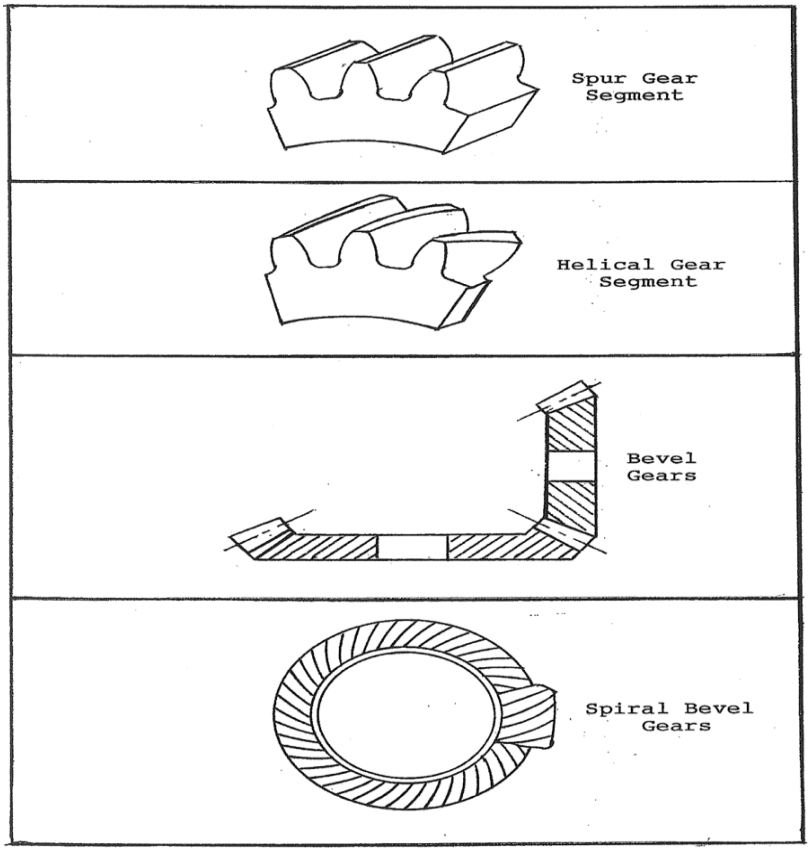

Figure 2: Gear Types (Ham et al., 1958)

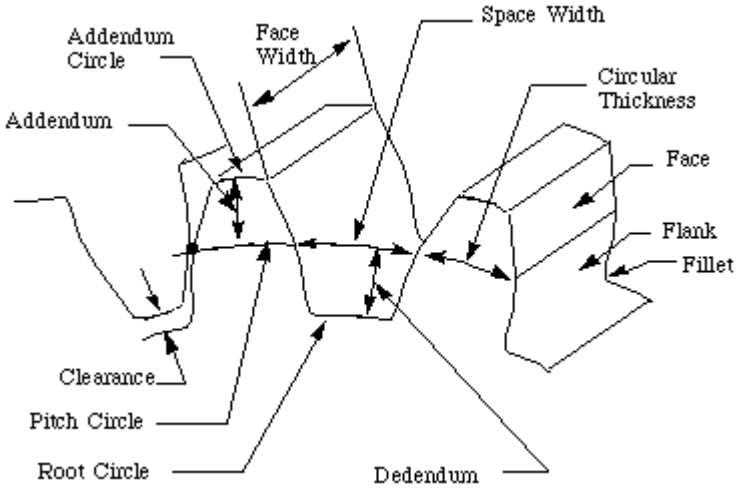

Figure 3: Gear Terminology (Ham et al., 1958)

2.1.3 Helical Gears

An alternative to the spur gear are single helical gears where the teeth run around the pitch cylinder in the form of a regular helix. Because of this helical shape the line of contact the helical tooth makes with the mating gear is not parallel to the axis, as with spur gears, but runs diagonally across the tooth face (Shigley et al., 2004). The helix angle, an important parameter for helical gears is the acute angle which this line makes with the axis, see Figure 4 and Appendix A and B. The helical gears may be viewed as an infinite number of spur gears immediately adjacent to each other but with a relative offset which in the limit combine to form a continuous smooth line, see Figure s 1 and 4 (Becker and Shipley, 2002). This slanted-line tooth contact is common to helical, hypoid and spiral bevel gears. For equal standards of manufacturing accuracy helical gears have a greater load carrying capacity and will transmit more power between parallel shafts more quietly.

Helical Gear - Tooth Contact

The helical arrangement ensures tooth engagement is smooth and gradual and the load more evenly distributed which gives quieter running and sudden shock loadings are virtually eliminated. Figure 5 shows tooth contact lines for helical, straight spur and bevel toothed gears. Of course, where single helical gears on parallel shafts are mated they must both have equal helix angles, but in opposite directions, that is, they must be opposite handed. To find the handing of a gear view the teeth on the end face looking along the axis. If the teeth slope from bottom right to top left, the thread is a left handed helix, if the teeth slope from bottom left to top right the thread is a right handed helix.

Careful selection of the helix angle ensures that the number of teeth in simultaneous contact can be arranged to give the best compromise between mechanical efficiency and smooth running. However, the helix angle means that a proportion of the force exerted by the mating teeth is transmitted as an axial thrust along the shaft, and this must be allowed for when choosing bearings to support the shaft.

The thrust on the bearings due to single helical gears can be overcome (to an extent) by using double helical gears with opposing helix angles. These are more expensive and require an increase in the width of the gears, but are widely used where quiet and smooth-

running gearing is important in the transmission of heavy loads at high speeds. They also usually need longer and heavier shafting with larger capacity bearings (Stokes, 1992).

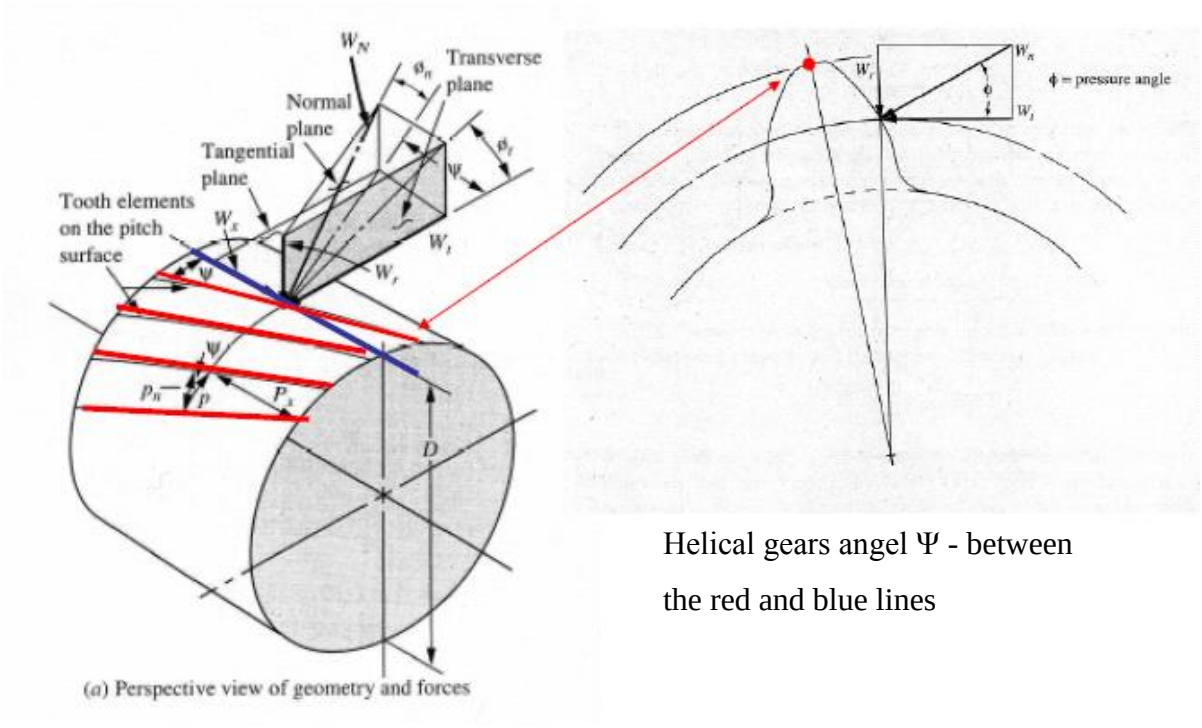

Helical gears angel Ψ - between the red and blue lines

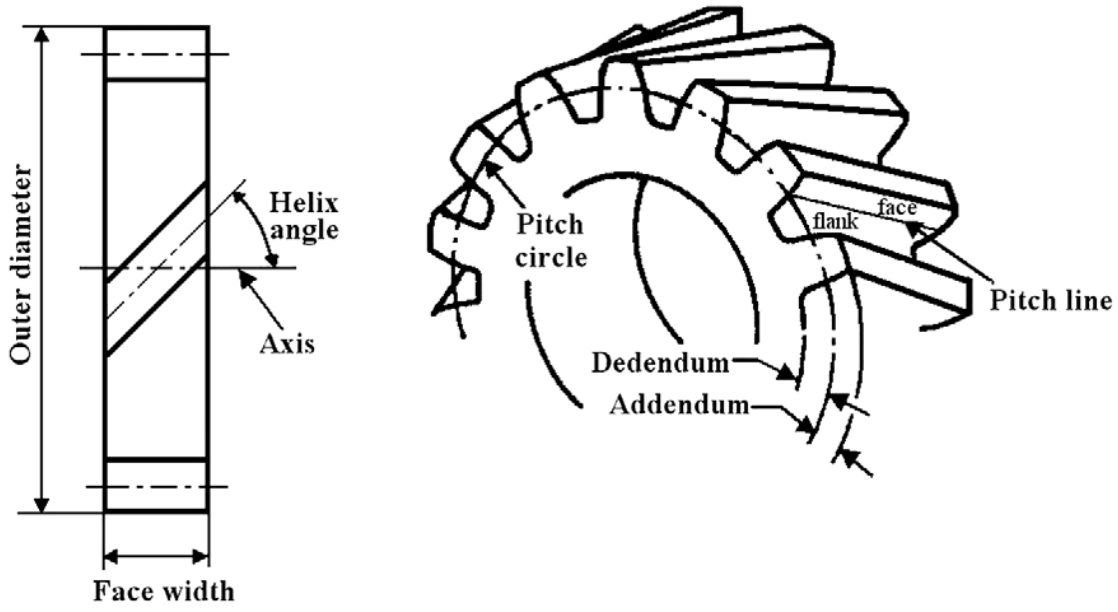

Figure 4: Helical gear geometry (Becker and Shipley, 2002)

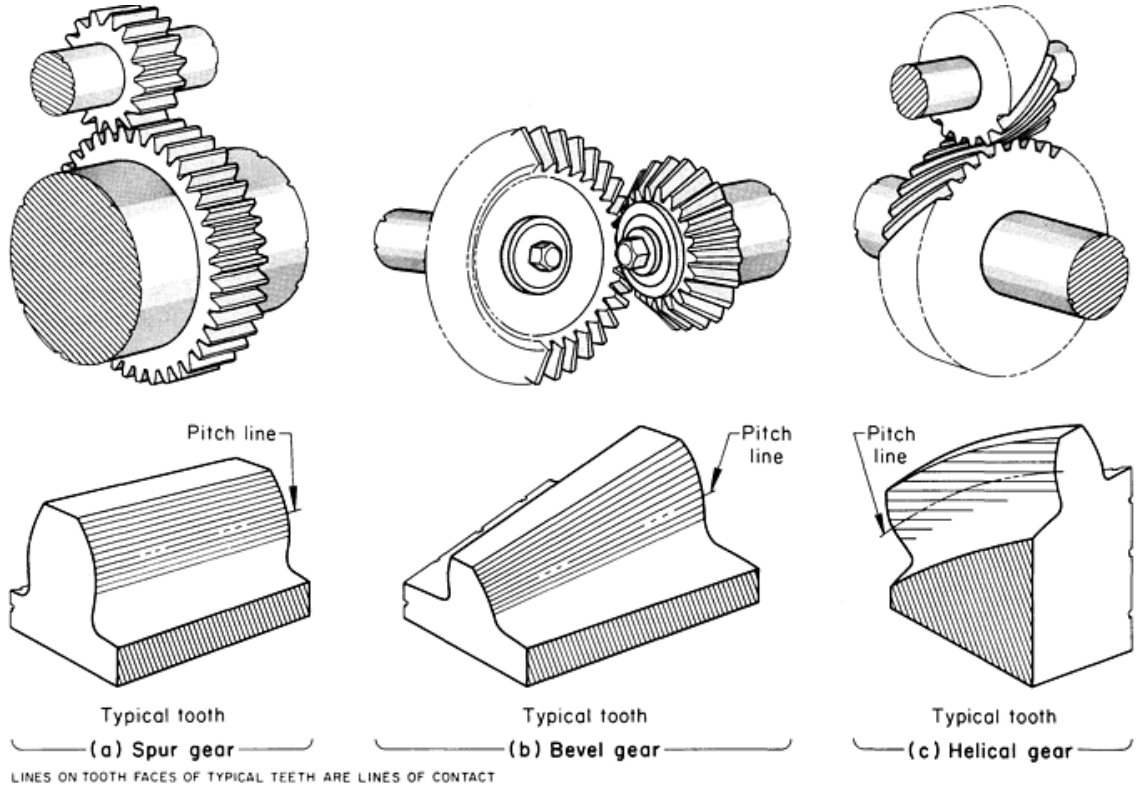

Figure 5: Tooth contact lines on a spur gear (a), a bevel gear (b), and helical gear(c). (Stokes, 1992)

2.1.4 Advantages of Helical Gear

- In a helical gear train the teeth progressively engage rather than all at once. This reduces noise generation and gives "silent" power transfer.
- Is able to transfer power between non-parallel shafts, though with some loss of efficiency.
- The teeth of the helical gear are positioned diagonally (see Figure 1) and so are effectively larger than the teeth on a spur gear. Hence, for same tooth size helical gears can carry a greater load than a spur gear.
- Suitable for high-speed, high-power transmission systems.

2.1.5 Gear Life Predictions

There are so many factors and indeterminacies that govern the life of gears (e.g. alignment, load, lubrication, operating temperature, etc.) that predicting the remaining useful life of a gear remains an inexact science. Nevertheless, based on experience it is possible to usefully estimate the life of gears. A combination of accelerated life tests and practical on-site experience is commonly used to predict the life of gears. This method tends to be used conservatively to avoid catastrophic failure and so usually underestimates the remaining life. The capability of predicting gear life more accurately would allow the process of gear design to be undertaken with greater confidence, as well as enabling greater length of working life.

Both the International Standards Organization and British Standards have developed methods for estimating a gear's strength and durability, allowing the life of the gear to be estimated. Using BS 436-3:1986 as a basis, the British Gear Association (BGA) has produced a software package (Gear Analysis Suite) which simplifies the load capacity calculation for helical and spur gears and estimates the safety factor for these gears using bending and contact stresses. It also takes into account a number of parameters such as lubricant, gear material and tooth profile, etc. (Joseph, 2005).

The lubricant and its properties are clearly of vital importance in determining the life of gears and it is now becoming increasingly clear that oil-film thickness is often over-estimated by isothermal smooth surface analyses (Olver, 2002). Consequently it is necessary to review the estimation of gear surface temperature to improve reliability of film thickness calculations. Figure 6 shows that where the lubricant has a specific film thickness greater than unity there is a rapid and substantial increase in surface fatigue life (Townsend and Shimski, 1994).

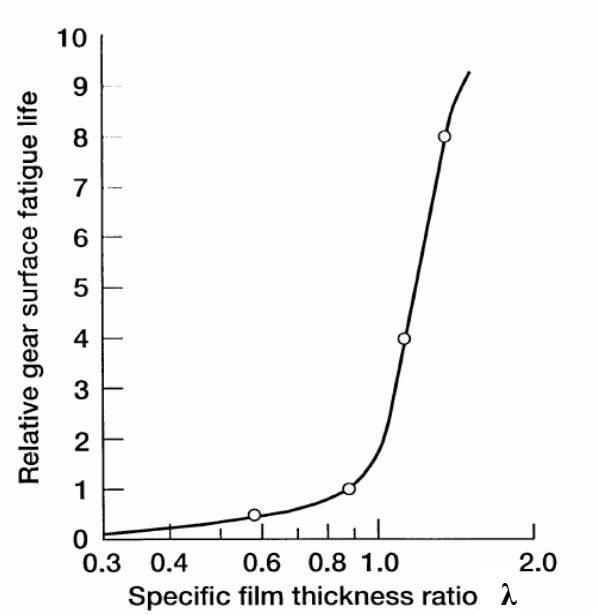

Figure 6: Relative gear surface fatigue life as a function of (λ) (Townsend and Shimski, 1994)

2.2 Gear Lubrication

An essential element of mechanical engineering is determining what takes place at the interface when two machine components meet or touch. Whenever one surface slides over another there is a frictional force. The common explanation for this is that the peaks of the surface roughness (asperities) of the one surface interact with those of the other surface, increasing the friction and possibly causing cause surface damage. Lubricants are used to maintain separation of the surfaces and so reduce friction and wear. Lubricants can also act to remove heat and protect against corrosion. To maintain the operation of helical gears at the required power and speed appropriate lubrication and cooling are necessary (Gitin M, 1994).

The duration of the working life of a gear is largely determined by the specific film thickness (λ) of the lubricant. The specific film thickness is the ratio of the thickness of the oil film to the composite surface roughness of the two gears in contact. It has been shown that for elastohydrodynamic lubrication (EHL – see Section 2.4.2) λ is strongly influenced by gear loading, speed and temperature (Dowson, 1977); Dowson and Higginson, 1977).

2.2.1 Gear Tooth Temperature

When gear trains are continuously operated important surface failure problems (e.g. pitting, cracking and scoring) can occur due to thermal effects. High transient temperatures can be generated by tooth contact and these heat up the surface of the gear, sometimes at start-up when the layer of lubricant is thin the rate of temperature increase is so great as to generate a thermal shock and thermo-cracking of the tooth surface and break up (desorption) the layer of lubricant. Seireg (2001) has reported that transient temperatures on the surface of the tooth and in the lubrication film have a significant influence on surface pitting and wear.

Each cycle of heating and cooling generates microscopic changes in the structure of the gear surface material which accumulate and eventually a network of microscopic cracks appears on the gear surface. Thus, the monitoring and evaluation of the temperature of the gear surface is important and a large number of reports and publications concerning the prediction and evaluation of transient temperatures due to heat generation during meshing are now available. For example, John et al., (1985) reviewed gear lubricant selection and methods for tooth temperature prediction, and more recently Handschuh and Kilmain (2002) reported on the thermal behavior of helical gear trains operated at high-speed.

(J and Quin˜o´nez, 2004) concluded from their experimental research that the thermocouple is a very practical and reliable means of surface temperature measurement for online monitoring of gear conditions.

2.2.2 Purposes of Lubrication

Lubrication is primarily to reduce heat generation and wear between surfaces in contact and with relative motion. Heat and wear can never be completely eliminated but they can be reduced to acceptable or even negligible levels. Both heat generation and wear are due to frictional forces and can be minimized by lowering the coefficient of friction between the surfaces in contact.

(Pirro and Wessol, 2001) have described how lubrication is also used to prevent the formation of rust by reducing oxidation and to seal the system against the ingress of dust

and water. With transformers it also provides insulation and with hydraulic fluid power applications it can transmit mechanical power.

2.2.3 Lubricant Selection

Published standards are available to assist in the selection of lubricant for gear systems. These take into account gear type, gear speed, operating sump temperature and lubricant viscosity index to determine the lubricant that is the best for the given application (ASM., 1992). The properties of the lubricant are listed in Section 2.2.4 and each needs to be considered in the selection.

2.2.4 Lubrication Properties

The most important properties of lubricants for gears operating under typical or conventional conditions are (Pirro and Wessol, 2001):

- *Viscosity.* This is a measure of the lubricant's resistance to flow. When the gear is operational the viscosity is key in determining and maintaining the optimal lubricant film thickness between moving surfaces (teeth). The viscosity will often be different for different types of gearbox. Manufacturers will state the appropriate viscosity limits which will be a compromise for the various operating conditions for the unit.
- *Adherence* is a measure of how well the lubricant sticks to the teeth of the gear. It is very important because it ensures the maintenance of the lubricant layer between the meshing teeth.
- *Resistance to Oxidation.* The lubricant must resist oxidization. Large gear units can contain several thousand litres of oil which is expensive to replace so the lubricant must be remain serviceable as long as possible.
- *Resistance to Corrosion*. Corrosion inhibitors are included in good quality gear lubricants to prevent surface oxidation should the lubricant become contaminated with water due to, for example, condensation.

- *High Film Strength and Oiliness.* Modern lubricants often use additives to increase the oil's natural film strength which maintains separation of the meshing surfaces, Oiliness is important, especially in the case of worm gears, to reduce the very high tooth friction.
- *Demulsibility* is the property of rapid separation should the gear lubricant be contaminated with water.
- *Extreme Pressure Properties* are important to prevent possible welding and consequent tearing of tooth surfaces when in contact under high pressure.
- *Prevent scuffing* by using anti-scuff additives; Anti-scuff additives reduce scuffing by forming thick films of high melting point metal salts on the surface which prevent metal to metal contact which, when extensive, may cause scuffing.

2.3 Lubrication Methods

The lubrication conditions for spur and helical gear are basically same. The magnitudes of the loads and sliding speeds are similar, and requirements for viscosity and anti-scuff properties are virtually identical. As has been stated above, viscosity is one of the most important lubricant properties, and the higher the viscosity, the greater the protection against gear tooth failure. For critical applications, the specific film thickness, λ, should be calculated using Dowson and Higginson equation (Dowson, 1995).

The method of applying the lubricant to the gear teeth depends primarily on the pitch line velocity and there are three methods in general use:

1. Spray lubrication (forced oil circulation lubrication),
2. Splash lubrication (oil bath method), and
3. Grease lubrication.

The selection depends upon tangential speed (m/s) of gear teeth and shaft rotational speed. Grease is a good lubricant to use at low speeds but splash and forced circulation lubrication are more appropriate for medium and high speeds. Table 1 shows the three basic lubrication methods with applicable speed ranges.

Table 1: Ranges of tangential speed for gears (Handbook of metric gears,).

No.	Lubrication	Range of Tangential Speed (m/s) 0 5 10 15 20 25
1	Grease Lubrication	
2	Splash Lubrication	
3	Forced Circulation Lubrication	

2.3.1 Spray Lubrication (Forced oil circulation lubrication).

The lubricant (oil) is supplied through jets placed on the incoming side of the gear mesh for high pitch line velocities and for gears equipped with plain bearings. This method can be used for even the fastest peripheral speeds met in gear systems (about 250 m/s). Oil is sprayed through perforated or slotted nozzles onto the tooth flanks and contact zone either at the initial or the final meshing zone, see Figure 7. It is assumed that it is more beneficial for lubrication for oil to be sprayed onto the initial meshing zone, but cooling is enhanced by oil sprayed onto the final meshing zone. ASM recommend the amount of sprayed oil to be between 0.5 and 1.0 l/min per cm width of tooth depending on the heat to be dissipated (ASM., 1992).

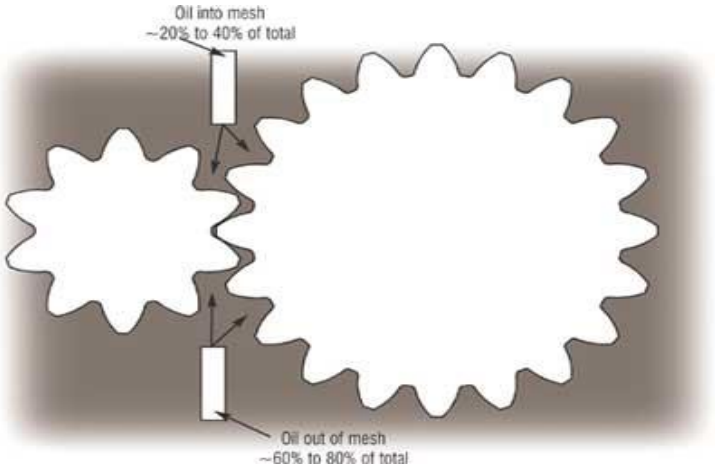

Figure 7: Lubricant spray arrangement (ASM., 1992)

2.3.2 Splash Lubrication Systems

Splash lubrication gear systems are considered the easiest to use but are limited to a low pitch line velocities, up to about 5 m/sec for helical, spur and bevel gears, but less than about 4 m/sec for worm gears. To avoid excessive churning with unwanted loss of power the lubricant level should not be too high, see Figure 8. The bottom wheel, see Figure 8, should dip into the lubricant to about twice the tooth length, possibly between 2 cm and 4 cm depending upon the diameter of the gear. (Pirro and Wessol, 2001) have suggested that high speed, high power gear sets should use pressure circulating systems with oil coolers to reduce churning.

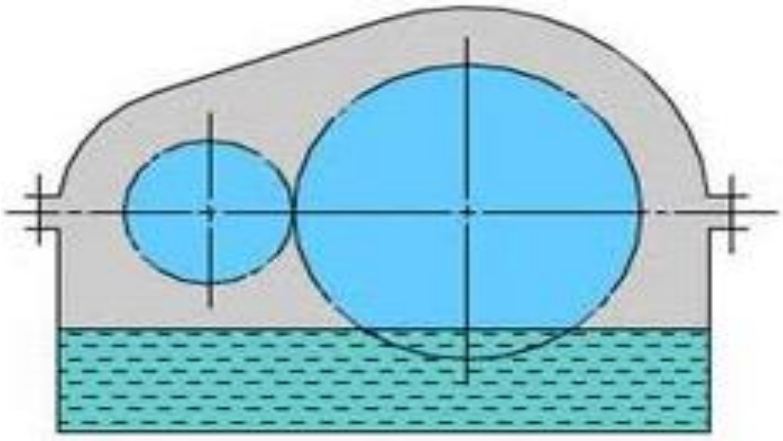

Figure 8: Splash (Bath) Lubrication System (Pirro and Wessol, 2001)

2.3.3 Grease Lubrication

The third type is grease lubrication; is suitable for any low speed gear system.

2.4 Lubrication Regimes in Gears

Most gear failure mechanisms occur because the lubricant layer breaks down and the surfaces of the teeth come into intimate contact. Lubrication minimizes or eliminates this contact by ensuring the presence of a thin film between the components which supports the necessary load. The lubrication must be such that the motion of the surfaces does not remove the lubricant film. Any lubricant that is "used up", i.e. removed from the system must be replaced so the load between the components will remain supported. Table 2 lists the three lubrication regimes which are described by the specific film thickness ratio (λ, lambda) and the mechanisms by which the film is formed (E. Richard Booser, 1983)

(Dwyer Joyce, 1995). (Copper, 1983; Kutz, 2006; Martin, 1978; Neale, 1995) all studied specific film thickness (λ) and their findings regarding values of lambda were almost compatible with those shown in Table 2.

Table 2: Film thickness regimes, mechanisms and applications (Dowson, 1995; Dowson and Ehret, 1999)

Regime	Specific film thickness or Lambda ratio (λ)	Typical Friction Coefficient	Mechanism of Film Formation	Typical Applications
Boundary Lubrication (BL)	**λ<1**	**0.1-0.3**	**Surfaces not fully separated. Thin chemical layers reduce the tendency of the asperities to adhere.**	**metal cutting, bearing start-up or shutdown**
Elasto-hydrodynamic Lubrication (EHL)	**1< λ<10**	**0.001-0.01**	**As hydrodynamic, but high local pressure causes increase in viscosity and elastic deformation**	**rolling element bearings, gears, cams and tappets**
Hydrodynamic Lubrication (HL)	**λ>10**	**0.01-0.03**	**Lubricant is dragged into wedge between components. The lubricant pressure increase supports the applied load**	**journal bearings, machine slideways, piston ring/liner.**

2.4.1 Boundary Lubrication (BL)

Much research is being conducted to gain a better understanding of boundary lubrication, where the lubricant acts as a protective barrier and the oil film thickness is greater than the sum of surface roughness of both surfaces. However, most boundary lubricants are a sacrificial film – in the sense that must be continually renewed - that only delays the onset of friction and wear. A number of factors exist that can prevent a lubricant film from forming. (Krantz and Kahraman, 2004) list these as: misalignment, interruption of lubricant supply, lubricant with too low a viscosity, too high local temperatures, loads too great for the lubricant to support, shock loads and low speeds.

Boundary lubrication exists when the lubricant film between sliding surfaces breaks down and the gears meshing surfaces come into contact. This occurs at low speeds and high loads, when the surfaces slide over each other, see Figure 9. The absence of an oil film means the load is transferred to those areas of the sliding surfaces in direct contact, which is only a small a fraction of the apparent area. At the microscopic level it is the

surface asperities which meet and create numerous micro scale grooves in the opposing surface. In these circumstances the asperities are constantly being crushed and restructured and in the process release bursts of energy in the form of Acoustic Emission (AE) and local flash temperatures (Macconochie and Newman, 1961). The exact nature of the surface interactions is not fully understood but in such a regime the properties of the lubricant film are assumed to be unimportant.

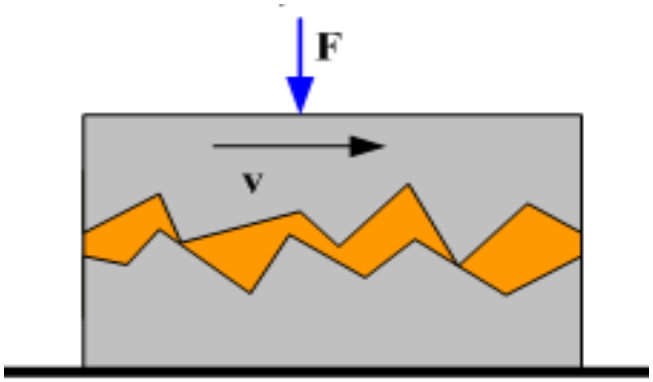

Figure 9: Boundary lubrication. (Richard Booser, P. D. (1983)

2.4.2 Elastohydrodynamic Lubrication (EHL)

Figure 10 shows pressure and temperature distributions and film thickness for Elastohydrodynamic Lubrication (EHL). Dowson (Dowson, 1995; Dowson and Ehret, 1999) has provided a wide-ranging history of the research into EHL during the 20th century. Operating experience accumulated over many years of gearbox operation where suitable lubrication was used, clearly pointed to metal-to-metal contact as a rare event even in highly loaded gears. The conclusion was that a protective film of oil separated the surfaces of the meshing gear teeth, thus EHL is considered the dominant mode of lubrication for meshing surfaces such as bearings and gears.

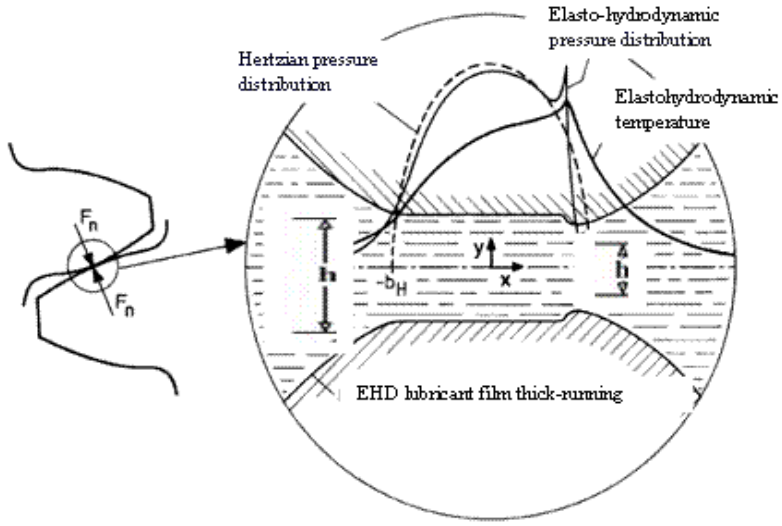

Figure 10: Distribution of pressure, temperature, pressure path in Hertz and film thickness in an EHL contact (Dowson, 1977).

(Dowson, 1977) has described how, initially, the minimum thickness of the lubricating oil film between gear teeth was calculated on the basis of hydrodynamic theory alone but this was found to be much less than the measured surface roughness of the gear teeth. By the 1950s it was realised that the analysis had to include lubricant viscosity and local elastic deformation. Dowson explains how this breakthrough resulted in a number of empirical dimensionless expressions for minimum oil film thickness, in each of which the minimum oil film thickness was strongly influenced by the properties of both the lubricant and the gear teeth, and the speed of rotation. In practice the range of materials involved is small so the lubricant film thickness is dominated by the speed of rotation so much so that an increase in load has negligible effect, what happens is that the size of the effective loading carrying region is increased.

Figure 11 shows typical features of EHL contact in te r.m.s of the surface contact friction model. For continuity of mass flow of the oil film between the two meshing surfaces, the product of film thickness and lubricant density must be constant. Over most of the Hertzian contact zone (between the meshing surfaces, refer to Figure 7) the film layer is assumed to be of constant thickness, though the fluid pressure can rise to large values. As the oil flows out of the contact zone the fluid pressure quickly returns to that in the body of the lubricant. This sudden drop in pressure creates a restriction or choke point. In order to maintain the continuity of mass flow of the film, the mass flow at the

entraining end has to increase. Coupling this phenomenon and the geometrical form, a secondary pressure peak arises at the exit end. This feature characterises EHL. The magnitude of the secondary pressure peak always far exceeds the maximum Hertzian pressure. It is also at this exit where the minimum film thickness is located. Minimum film thickness usually is 80% of the central film thickness (Dowson, 1995; Johnson, 2012).

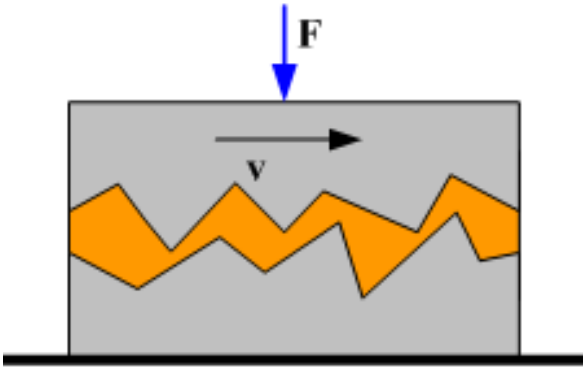

Figure 11: Elastohydrodynamic Lubrication (EHL) (. Richard Booser, P. D. (1983)

2.4.3 Hydrodynamic Lubrication (HL)

Hydrodynamic Lubrication (HL) is the regime where a continuous film of lubricant fully supports the sliding surface hydrodynamically. In HL, a fluid layer of thickness, h, as shown in Figure 12 is formed by the relative motion of the gear teeth, this film decreases friction between sliding surfaces by separating the solid surfaces and replacing mechanical friction with fluid friction, see Figure 9. Factors effecting HL formation include oil film viscosity and temperature, and speed of the fluid flow. When applied correctly, HL can substantially reduce friction with high speeds and loads, reduce vibration, and substantially extend service life. Most industrial equipment such as turbines, compressors, transmissions and bearings operates under this regime (William, 1992).

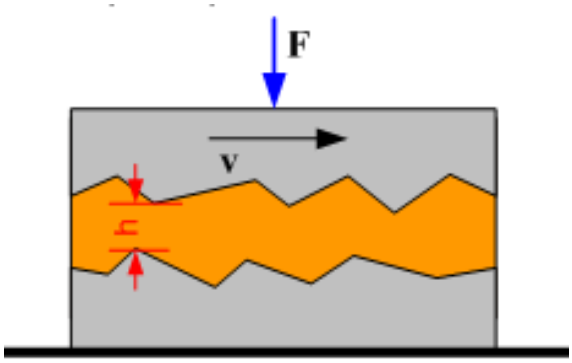

Figure 12: Hydrodynamic lubrication (HL) (. Richard Booser, P. D. (1983)

2.4.4 The Stribeck Curve

(Stribeck, 1902) performed a series of experiments on bearing friction and derived a relationship between the applied load, the coefficient of friction (μ), dynamic viscosity of the lubricating oil (η) and rotational speed (*v*), which is presented as the Stribeck curve in Figure 13. The Stribeck curve confi r.m.s that the lubrication process can be divided into the three regions (regimes): boundary lubrication h (film thickness) < R (surface roughness), elastohydrodynamic lubrication h ≈ R and hydrodynamic lubrication h >> R.

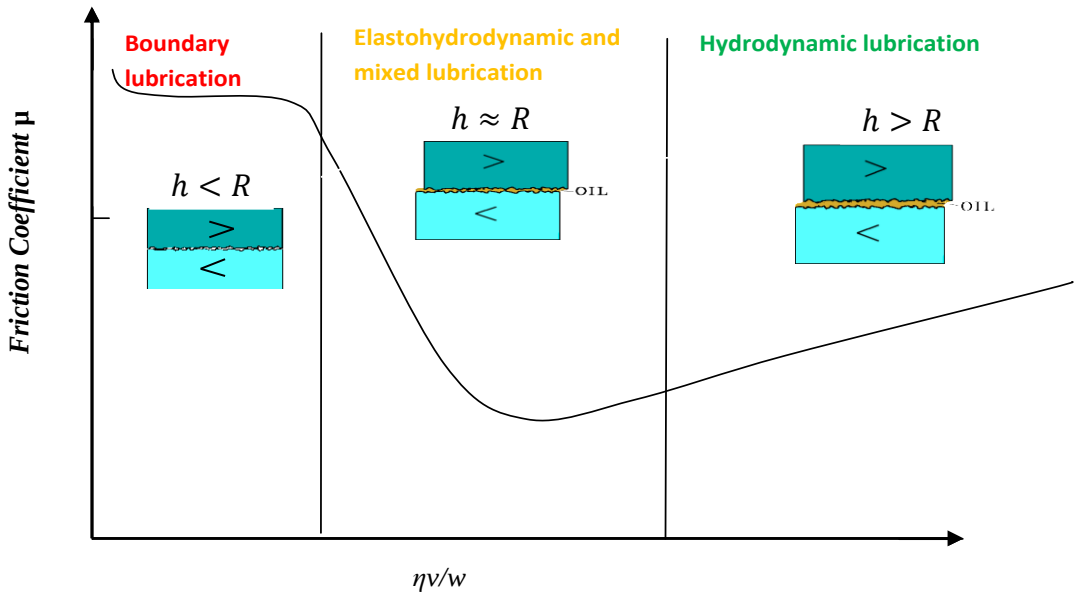

Figure 13: Stribeck Curve (Stribeck, 1902)

With HL, the lubricant totally separates the two friction surfaces and lubricant viscosity is the major factor determining the tribological characteristics. With EHL lubrication, three factors dominate the tribological characteristics: the coefficient of elasticity between the solid surfaces, the viscosity of the lubricant, and the relation between viscosity and applied pressure. BL tribology is largely determined by frictional forces between the surfaces in asperity contact and the action on those frictional forces of the lubricant (including any additives) present between the friction surfaces. Because the determining characteristic of BL is the actual contact made between the surfaces the hydrodynamic properties of any lubricating oil are not a significant influence on the tribological characteristics (Hamrock J et al., 2004).

(Macconochie and Newman, 1961) showed that the thickness of the lubricant film formed between gear teeth is of the same order of magnitude as the surface roughness or the diameter of foreign particles in the lubricant. Thus the film regime may be considered to act hydrodynamically at the pitch line for all but the heaviest loads. If the gears are heavily loaded, the lubrication will be quasi-hydrodynamic. The film regime conditions depends upon the load, speed, tooth contour, surface finish, impurities in the lubricant and lubricant viscosity. For a hydrodynamic film to be retained between two rolling surfaces in contact strongly suggests additional mechanisms are at work – e.g. in high speed rollers the transit time of the lubricant may be of the same order of magnitude as the molecular relaxation time which determines the value of the viscosity and may cause the lubricant to exhibit symptoms of shear rigidity. To calculate oil film thickness the pressure viscosity may be used but pressure viscosity may not be used to calculate the friction coefficient because the results obtained are far higher than found experimentally.

(Krantz and Kahraman, 2004) experimentally investigated the average wear rate of spur gear pairs made from AISI 9310 steel, with lubricant viscosity and additives. Seven lubricants with a range of viscosities were used to test gear tooth wear for gears that were heat treated and case carburised. The measured wear was related to the elasto-hydrodynamic film thickness, the contact fatigue lives of the specimens as determined in the experiments, and the as-manufactured surface roughness. Typically, the rate of wear was inversely proportional to the lubricant viscosity and specific film thickness (see below). An exponential relationship was found between surface fatigue life and average

wear rates. The addition of different additives to lubricants with similar viscosities produced different gear surface wear rates and fatigue lives.

2.5 Specific Oil Film Thickness (λ)

Specific film thickness (λ - lambda ratio) is strongly related to the lubricant viscosity, temperature and surface roughness. Increasing λ can help to improve contact fatigue life and a lambda ratio (λ) greater than 1 is usual for gears (Dowson, 1995);

$$\lambda = \frac{h}{\sigma_{rms}} \qquad \text{.....1}$$

Where *h* is the thickness of the film of oil and $\sigma_{r.m.s}$ is a measure of the composite r.m.s roughness of the two surfaces in frictional contact.

$$\sigma_{rms} = \sqrt{(\sigma 1^2 + \sigma 2^2)} \text{.....2}$$

Where *σ1* and *σ2* are the r.m.s . *surface* roughnesses of the *two surfaces* in *contact*.

The problem can be simplified by assuming the two areas in frictional contact are infinitely stiff, so that any wedging effect will depend only on the relative velocity of the two surfaces and the lubricant. Such an assumption is valid only for low pressures. At high pressures there will be deformation in the contact zone, and the increase in working temperature will cause changes in the viscosity of the film. Both these need to be included in any working model (Dwyer-Joyce, 1995). In fact, the viscosity of all lubricants will generally increase as pressure increases and decrease as temperature increases. These changes will be important for gears and rolling bearings which have highly contact loads.

Viscosity will vary with temperature as given by the MacCoull equation (Alexander, 1992), and reference tables normally provide values of the lubricant viscosity at 40^{o}C and 100^{o}C (104^{o}F and 212^{o}F):

$$\ln(\mathrm{In}(\nu + 0.7)) = A + B\ln(T) \text{.....3}$$

Where

ν= Kinematic viscosity = η/ρ, (η = dynamic viscosity, ρ= density)

T= Absolute temperature, and

A and B = Constants for any given lubricant.

Re-arranging we obtain:

$$\nu = e^{e^{(A-BlnT)}} - 0.7 \ldots\ldots\ldots\ldots 4$$

The manufacturer of lubricant provided values for the viscosity of Mobilegear type 636 used in these experiments at 40°C (680 cSt) and at 100°C (39.2 cSt), see Appendix C. By substituting these values into the equation for viscosity it was possible to solve for A and B.

Mobilegear Type 636	A=20.58	$\boldsymbol{\nu = (e^{e^{(20.58-3.26\,lnT)}}) - 0.7}$
	B=-3.26	

Using results obtained by other workers and simplifying the physics of the situation by assuming the load factor could be neglected and that for small temperature changes the change in viscosity could also be neglected, Dowson and Higginson (Dowson, 1977) obtained the following equation for oil film thickness:

$$h = 1.6(\eta o u R)^{0.5} \ldots\ldots\ldots\ldots\ldots\ldots\ldots\ldots\ldots\ldots 5$$

Where: *h*= oil film thickness in µm,

η_o= dynamic viscosity in Pas,

u= entraining velocity in m/s, and

R= Equivalent radius in m.

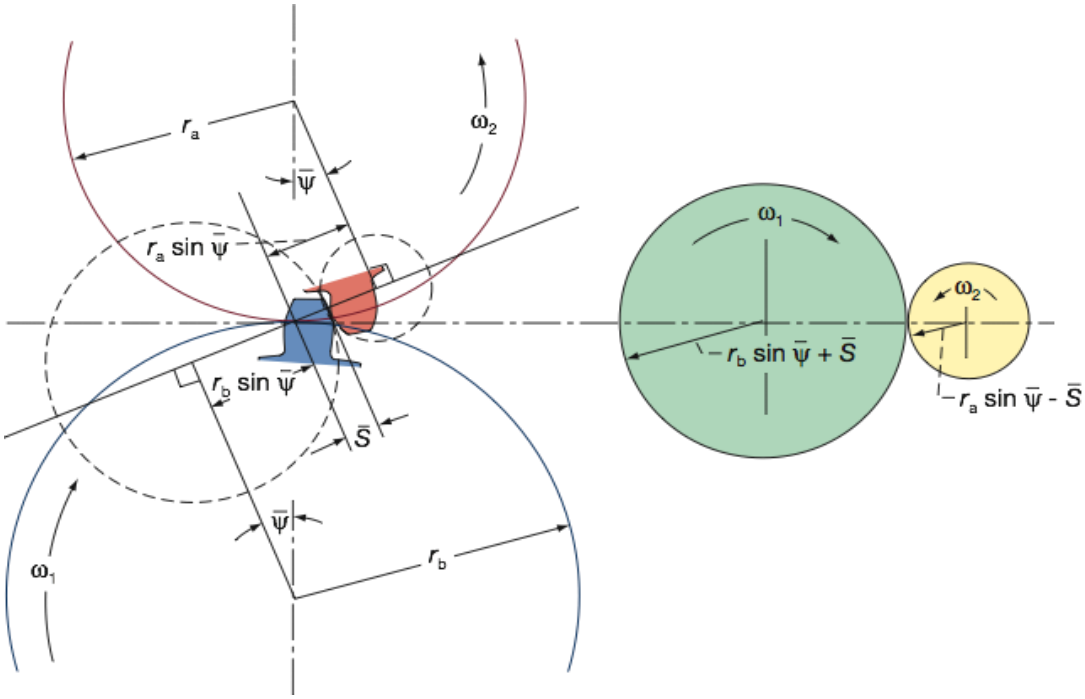

Figure 14 : Diagram of gear pair

R can be obtained from:

$$R = \frac{(R_1 sin\,\Phi + S)\,(R_2 sin\Phi - S)}{(R_1 + R_2) sin\Phi} \text{.....6}$$

u, entraining velocity, can be obtained from:

$$u = \frac{\pi N_1}{30}(R_1 sin\,\Phi - \frac{S}{2} + (r-1)) \text{..... 7}$$

Where gear ratio,

$$\boldsymbol{r} = \frac{R_2}{R_1} \text{.....8}$$

r always expressed as a number larger than 1.

S= the distance between pitch line and contact point

R_1 = pitch radius of the pinion

R_2= pitch radius of the wheel

Ψ =Φ= pressure angle in Figure 14

N_1 = rotational speed of pinion

To simplify the derivation, the contact between the meshing teeth will be assumed to be on the pitch line, which implies S = 0, so Equations 6 and 7 simplify to:

$$\text{R} = R1(\frac{r}{r+1})\sin\emptyset \quad \text{.....9}$$

$$u = V_1 \sin\emptyset$$

Where

V_1 is the pitch line velocity of pinion

Dynamic viscosity (*cP*) = Kinematics viscosity (*cSt*) * density(*g/ml*)

Or

Dynamic viscosity (Pas) = Kinematics viscosity (cSt) * $(\frac{\text{density}(g/ml)}{1000})$

$$h = \frac{k(\eta 0 u)^{0.7} R^{0.43}}{w^{0.13}} \text{ µm} \quad \text{.....10}$$

Where *h* is in µm

$k = 1.6\alpha^{0.6} E^{0.03}$

E= modulus of elasticity (Pa)

w = load per unit length of cylinder (N/m)

α = pressure exponent of viscosity (Pa^{-1})

Since: $W = \frac{F}{lc}$ and

$$F = \frac{T}{d1}$$

F = Total load applied on the tooth/teeth (N),

d1 , *d2* = Diameter of wheel and pinion (m),

T = Torque applied on the wheel shaft (Nm), and

l c = Line of contact length (m) (Appendix A and B).

The λ which used in this research was calculated as:

$$\lambda = h_{min} = \frac{h}{\sigma_{rms}} \text{.....11}$$

2.6 Gear Failures

Gearbox failures usually result from wear in the primary load carrying elements such as gears, bearings and shafts. When gears fail there may be an increase in noise and vibration levels but no further indication until total failure. However, each type of failure imparts certain characteristics to the gear teeth, and (Peter Lynwander, 1983) has

described how a detailed examination can provide sufficient information to determine the specific failure.

Figure 15 shows how the various gear failure modes can be classified into lubrication related and non-lubrication (material strength) related failures. The most common gear failures are associated with the lubricant or lack of it. The commercial pressures for increased speed and efficiency of production have resulted in significant increases in the speed of machinery to increase production rates, but the price has been a substantial increase in damage to machines, often due to problems of inadequate lubrication. These lubrication problems has been assessed as costing somewhere between UK £5 billion and UK £8 billion per year. Thus industry has been active for at least a decade researching into condition monitoring to predict and identify possible gear failures (Stokes, 1992; ASM., 1992; ASM., 1992).

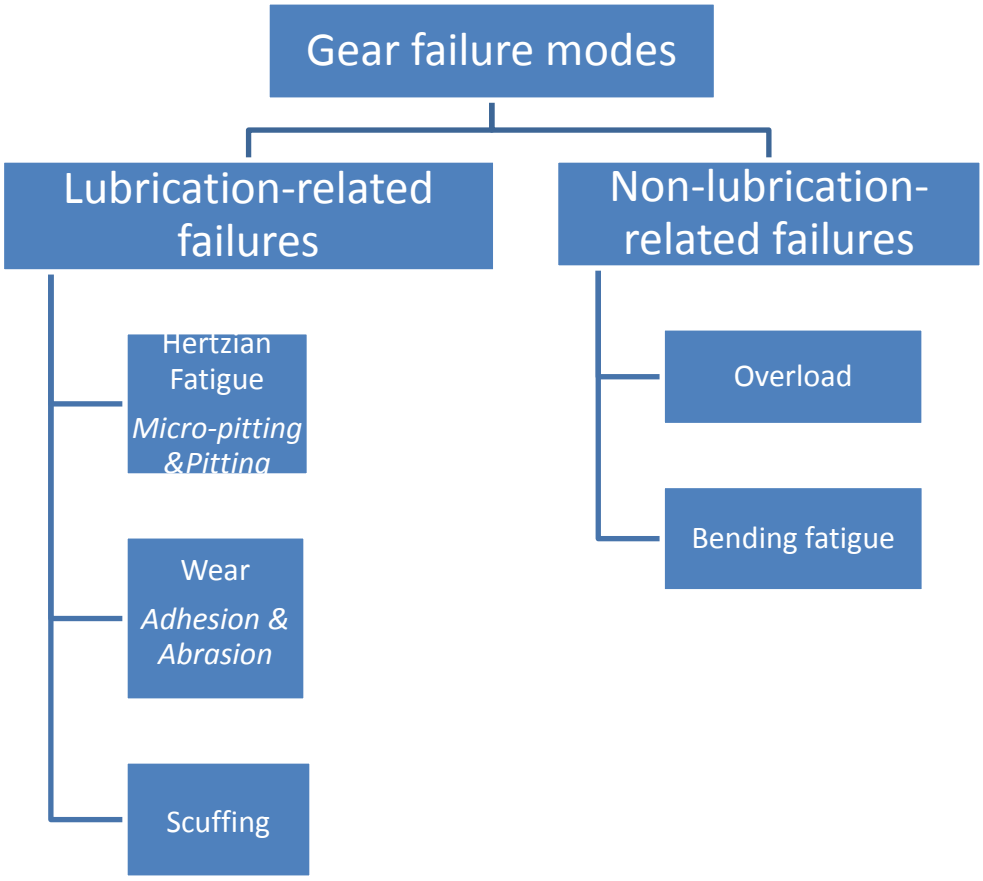

Figure 15: Gear failure modes

2.6.1 Lubrication Related Failures

Lubrication and cooling are necessary for the successful and efficient operation of helical gear transmission systems. As helical gear teeth mesh the surfaces both roll and slide against each other, see Figure 16, actions which can cause numerous failures.

Direct contact of tooth surfaces due to a lubrication related failure will generate stress at and/or beneath the surface which can lead to tooth/gear failure. This has two fo r.m.s :

a- Micro-pitting along the pitch-line of gear teeth due to rolling contact fatigue.

b- Sliding-rolling contact fatigue which occurs in the gear teeth below the pitch-line where negative sliding conditions exist. This can lead to surface pits which can then act as the starting points for other failure modes.

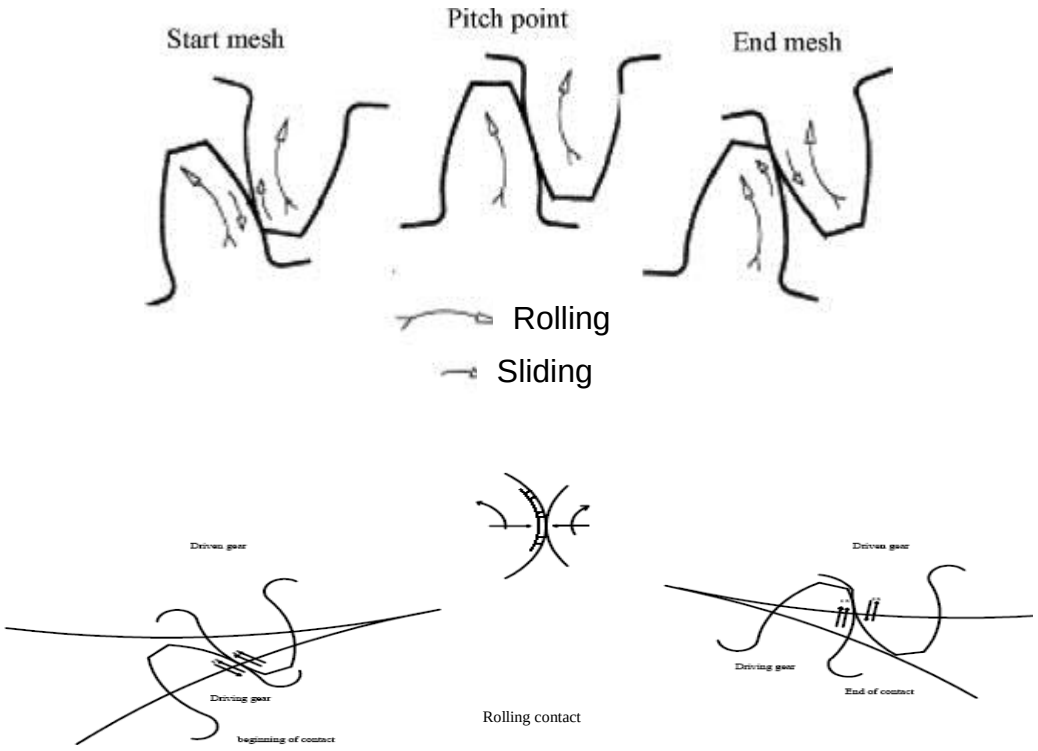

Figure 16: Combination of sliding and rolling in gear teeth (Walton and Goodwin, 1998)

The lack or loss of lubricant between the gear teeth causes the teeth to rub against each other and small particles of metal break loose. The areas in contact take on a roughened appearance due to the consequent abrasive effects (sometimes called fretting corrosion)

and red oxide debris may be seen. A badly worn surface is often produced very quickly if the operation of a gear with the lubrication problem is not stopped. Unless remedial action is taken the tooth will bend or break and the mesh disengages.

Lack of lubricant in gearboxes can usually be ascribed to damaged gaskets or seals, a lubrication plug not re-inserted, oil leakage through inadequately sealed shaft keyways, or an insufficient amount of lubrication used. There are no significant differences in the lubrication problems which occur for spur gears as occur for helical gears.

Not only an adequate volume but the right lubricant must be used. That is, the lubricant must have the correct viscosity to be thin enough to flow into the tooth mesh contact area when cold but at operating temperatures and speeds is not too thin to support the tooth mesh load. These conditions impose tight restrictions on the choice of lubricant and thus an extreme pressure (EP) lubricant should be used (Fernandes and McDuling, 1997).

Pitting takes place due to metal fatigue and when the surface cannot withstand the high Hertzian contact stresses. Small crack opens either on the tooth's surface or just below the surface. For sub-surface cracks, repeated cycling causes the crack to propagate nearly parallel to the surface of the tooth for short distances before branching up to the tooth surface, see Figure 17. Individual cracks can grow sufficiently long and in such a pattern that small pieces of the surface layer are separated off and a pit is formed, see Figure 17. Of course, adjacent cracks can have the same effect.

Spalling is when several small pits coalesce into a single large pit. Chemicals (particularly hydrogen) contained in the water in lubricants can accelerate pitting of metal surfaces, and metal particles carried with the lubricant can scratch the surface of the tooth which enhances pitting by interrupting the continuity of the lubricant film as well as causing stress concentrations, see Figure 18. Crack generation and pitting problems can be reduced and even avoided by reducing the load to minimise contact stresses, ensuring the surfaces of the gear teeth were carefully ground to be smooth, and properly heat-treated.

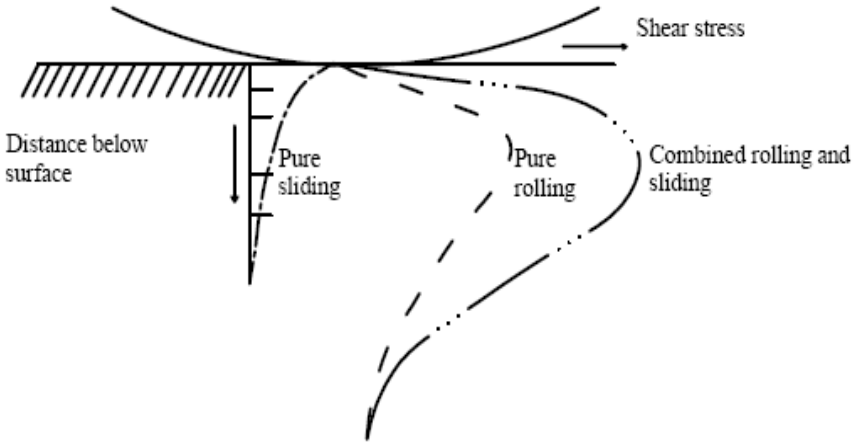

Figure 17: Stress distribution at and near contacting surfaces under rolling contact

Micropitting: even when gears teeth have been surface hardened pitting can still take place, though to a smaller depth, typically 10μm. Surfaces which have suffered micropitting have a so-called frosted appearance, see Figure 18.

***Adhesive*:** adhesive wear takes place when two surfaces rub together and material transfer occurs. Mild adhesive wear does no more than disrupt the thin oxide layers on the surfaces of the gear teeth. Severe adhesive wear is where the oxide layer is stripped away and the bare metal of the gear tooth is exposed. Scuffing is severe adhesive wear, see below.

Special care must be taken with gears operating at high loads and low speeds. Here increasing the viscosity of the lubricant will significantly decrease adhesive wear, but lubricants with chemically active extreme pressure additives should be avoided as they are likely to be cause a high wear rate at low speeds and high loads.

Scuffing: occurs if the lubricant conditions are such that there are relatively large areas of metal-to metal contact. The oxide films that protect the tooth surfaces are stripped away and the bare metal revealed, which results in roughened surfaces and metal transfer from one surface to the other. This can result in catastrophic damage if the teeth weld together due to the frictional heat generated. New gear teeth are most vulnerable because their surfaces have not been smoothed by running-in. The lubricants used in this situation should contain anti-scuff additives which form a protective oxide layer at any local point

of high temperature by chemically reacting with the gear tooth's surface. The oxide layer once formed has a high melting point and remains as a solid on the surface of the tooth even at high contact temperatures.

Scuffing is reduced by good alignment, rigid gear mounting and accurate machining of the gear teeth. Scuffing will also be reduced if the temperature of the lubricant is prevented from rising too high. This can be done by a heat exchanger in circulating-oil systems. The materials used in the manufacture of the gears needs consideration, and aluminium and stainless steel should be avoided. If there is any risk of scuffing, use nitrided steel instead. Scoring of a gear tooth is similar effect to scuffing.

Abrasion: abrasive wear of gear teeth is invariably (and often) caused by particulate contamination of the lubricant: spalled particles, sand or dirt particles taken in through breathers, or particles that become added during maintenance. The spalled particles can become work hardened when they pass between the gear teeth and are then especially abrasive, so the use of oil filters in circulating-oil systems is essential. The use of filtered breather vents and oil tight seals should minimize ingestion of contaminants. With abrasive wear, inspection of gear teeth surfaces will reveal surface scratches.

Plastic flow: heavy loads combined with rolling and sliding action between gear teeth can stress the material of the gear tooth beyond its elastic limit and deformation occurs resulting in "fins" along the tops of the teeth.

2.6.2 Non Lubrication Related Failure

Non-lubrication-related failures tend to be tooth breakages which usually occur as result of high levels of residual stress (e.g. due to an inclusion or cavity) in the region of the root of the gear tooth, see Figure 18. Another cause of fracture or breakage of gear teeth is the propagation of cracks due to overloading, impact or fatigue. With thin rims the crack will start at the tooth root and travel through the gear resulting in catastrophic failure (Joseph, 2005).

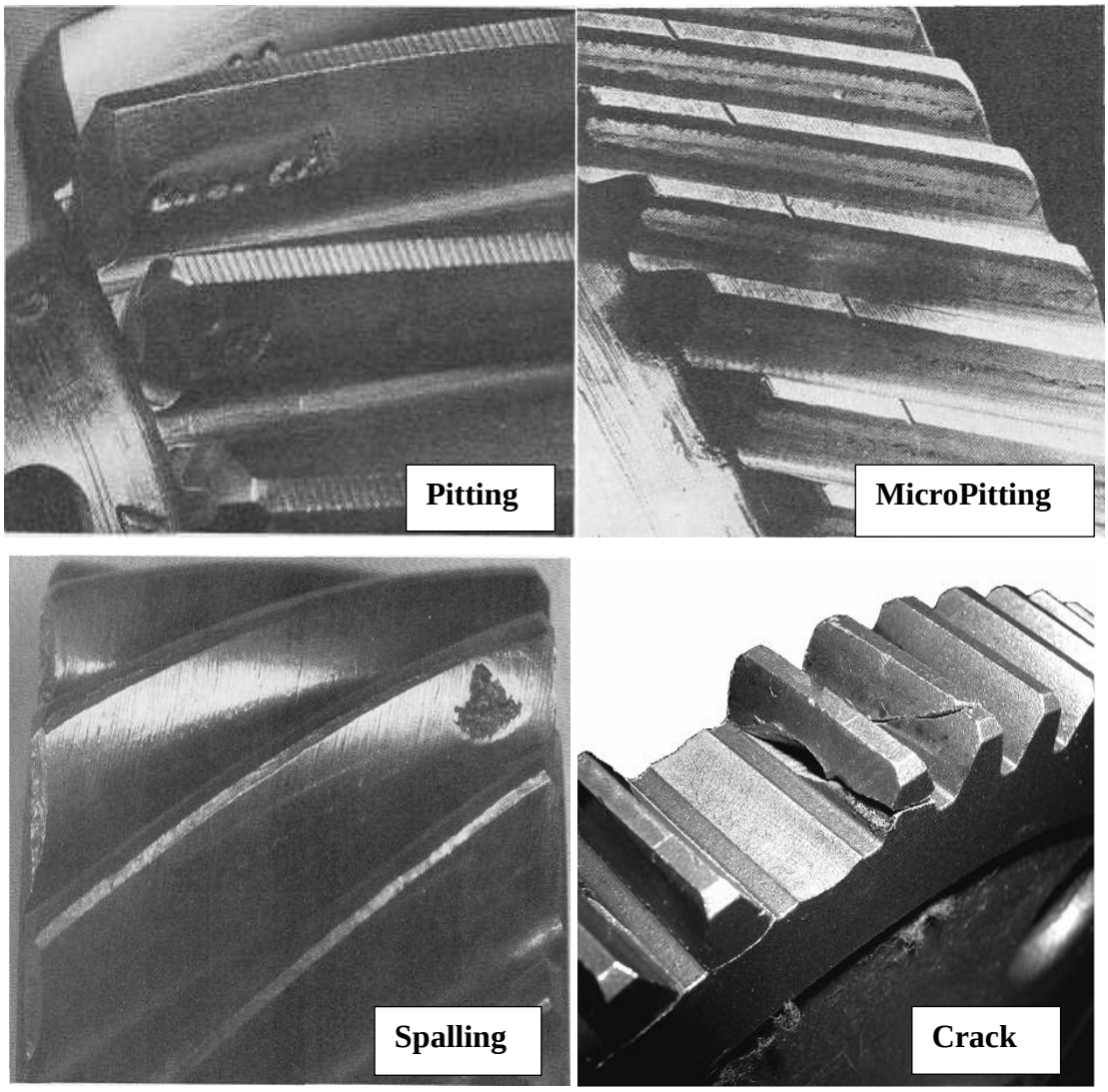

Figure 18: Modes of gear failures (Boyer, 1975)

Chapter 3

Gearbox Condition Monitoring Review

3 Gearbox Condition Monitoring Review:

When monitoring the condition of gearboxes it is important to have the ability to detect faults early, but the reliability of such detection must be high or there could be unwarranted and costly shut downs of plant and production lines. Faults which progress at a slow rate, if detected early, do not require immediate action. On the other hand, it is essential not to confuse e.g. bending fatigue which can rapidly lead to catastrophic failure, with pitting on gear teeth, which progresses at a slow rate and may even heal over. In some industries such as the aircraft industry prevention of catastrophic failure is put at a premium.

(Forrester, 1996) suggested catastrophic failure and can be prevented by;

1. Early detection at the beginning of the failure mode and rapid replacement of the component well before catastrophic failure occurs, and
2. Reduction of the probability of failure, either by redesign of the component and/or monitoring the component's usage and replacing it when the probability of failure exceeds a set threshold limit.

To detect and correctly diagnosis an imminent failure, suitable methods for collecting and quantitatively analysing and assessing the necessary data, and a good understanding of the failure mode are all necessary. Many faults are easily detectable if the component in question can be removed and subjected to a series of tests: microscopy, X-ray, etc. Such methods have an important place during manufacture, assembly and overhaul, but they are often impractical in an operational system such as a plant production line or helicopter transmission. In such circumstances non-intrusive methods need to be used for routine condition monitoring.

Where the signal to be monitored is generated by the gear(s) any failure mode of the rotating elements will cause changes in the vibration signature. They may also increase the local temperature or produce material debris in the lubricant. Unlike industrial plant and machinery where vibration monitoring is widely used and is often the system of choice, few helicopters used temperature and oil debris monitoring (Forrester, 1996). Figure 19 illustrate a diagram for types of condition monitoring techniques.

Figure 19: condition based monitoring techniques

3.1 Signal Processing Techniques

Gearbox fault detection was traditionally carried out by monitoring the vibration signal and extracting certain statistical parameters. The extracted features were correlated with particular faults within the gearbox. The most common of these parameters was the r.m.s value of the time domain signal which was taken as a direct measure of the vibration energy. (Samuel and Pines, 2005) have described other statistical parameters of interest for condition monitoring, these included Kurtosis and Crest Factor. These parameters and the associated theory are presented by (Samuel and Pines, 2005). The basis of the technique was (Samuel and Pines, 2005) work reviewed a report by Stewart describing how changes in the gearbox vibration signal were produced by damage to the gear(s) and McFadden's mathematical model for generation of gearbox vibration signals (McFadden, 1986).

Until the mid-1970s the statistical indices were invariably extracted from the time domain signal (Drouillard, 1988; Miller and McIntire, 1987b). However, with increased memory and more rapid processing it has been possible to transform the time domain signal into the frequency domain using, for example, the Fast Fourier Transform (FFT). With the

time domain signal the energy at all frequencies is summed by the r.m.s value thus, to be detected, a fault must have developed to an extent that the "fault energy" is of sufficient magnitude to be detectable over the general background. In the frequency domain, on the other hand, the energy of each frequency component can be seen. By trending the growth in vibrational energy at a particular frequency a fault can be detected well before would be detected in the time domain signal (Jardine et al., 2005). The vibration spectrum of a gearbox contains a range of characteristic frequencies and their side bands, e,g, the tooth mesh frequency, its harmonics and sidebands. It has been found both experimentally and from theoretical analysis that when gearbox faults occur they have their own characteristic frequencies. When these frequencies are detected in the spectrum they can be used to classify gearbox faults (Henning, 1988).

Both time and frequency domain signals can be characterised using the same statistical parameters, e.g. r.m.s , Crest Factor and Kurtosis. Creast Factor CF is the measure of the relative energy above and below the mean signal level. Those parametres of interest to this project are described in more detail below.

The techniques for analysing Acoustic Emission (AE) signals may be considered simply as an extension of those used with vibration signals. The essential difference is that the frequency range for AE is much higher than for vibration.

Time domain analysis: The most common statistical parameters extracted from the time domain vibration signal for fault detection are the peak value, r.m.s (measure of signal energy), Crest Factor, Kurtosis and the duration of specific events.

The mean value, $\overline{x} = \frac{1}{T}\int_0^T x(t)dt$ **……..12**

Root mean square (r.m.s): is a measure of the power content of the signal and is defined as follows (Broch, 1973):

$$r.m.s = \sqrt{(\frac{1}{T}\int_{-\infty}^{\infty} x^2(t)dt)} \text{……..13}$$

Where *x(t)* is the instantaneous value of the time signal being analysed and *T* is the period of measurement.

Crest factor: is a measure of the number and sharpness of the peaks in the signal. The higher the crest factor the more "peaky" the signal. A high value for the vibration signal from a bearing would normally be taken as an indication of the presence of a fault (Yesilyurt, 1997; AlKazzaz et al., 2003).

Crest Factor, Fc = Peak value / r.m.s $= \frac{P}{rms} \ldots\ldots\ldots 14$

Where *P* is the peak value of the signal: P = max(x) – min(x)

Kurtosis for a signal which is digitally sampled is given by:

$$K = \frac{\sum_{i=1}^{N}(x_i - \bar{x})^4 / N}{(\sigma^2)^2} - 3 \ldots\ldots 15$$

Where x_i is the value of the ith sample, N is the total number of samples, $\bar{x}$ is the mean of the samples and σ is the standard deviation of the samples. The "-3" is a normalisation factor included so that the Gaussian/Normal distribution has K=0. A "peaky" signal will have K > 0 and, conversely, a high value of K usually means the signal includes a number of extreme peaks.

Kurtosis has been successfully used to detect and discriminate between different faults but it has a significant weakness. If the fault is allowed to grow, the signal gradually loses its "peakiness" and the K value decreases and ceases to be useful in detecting the fault (Naid et al., 2009)

Consider two signals $S_1 = x_1(t)$ and $S_2 = x_2(t)$. Suppose S_1 contains the greater energy; then the r.m.s $_{S1}$ > r.m.s $_{S2}$. It is also possible for S_1 and S_2 to simultaneously have the same

peak values but the time-domain of S_2 to be spikier than that of S_1. In this situation we the K value (and crest factor) for S_2 would be larger than for S_1.

Frequency domain analysis: The Fourier transform produces a frequency spectrum which is the average of the input signal over the sampling period. It does not show how a signal spectrum changes with time (Ruqiang, 2007) Today, the Discrete Fast Fourier Transform (DFFT) is the most popular method of deriving it (Mathew, 1989). Decades of practical application have confirmed frequency-domain analysis can reliably identify frequency components within the signal indicative of a faulty condition of one or more components. In practice the frequency components identifying the presence of a fault may show themselves not as peaks in their own right but as sidebands to particular frequencies in the spectrum and it is the change in the amplitude of these sidebands that indicates the presence of mechanical problems in, say, a gear. Indeed, condition monitoring of gearboxes invariably uses frequency domain analysis precisely because the failure modes associated with each component have their own characteristic frequencies (Muller and Errichello, 2001).

Where the signal is stationary the FFT is very useful, but many signals contain transient phenomena including step changes, and these cannot be adequately analysed by FFT. The Short-Time Fourier Transform (STFT) which analyzes only a small section of the signal at a time was developed to overcome this problem. The STFT is able to map the signal into both time and frequency providing useful information about both. The precision is limited and determined by the window's width (Da Silva, 1997) and (Liu et al., 1997).

Time-frequency domain analysis: Despite their usefulness there are occasions when time domain and frequency domain analyses cannot characterise a fault. In such circumstances to extract useful condition information from the vibration signal time-frequency domain analysis is widely used**.**

Time-frequency domain (wavelet) analysis: is a procedure which contains variable-sized windowing; using longer duration windows when accurate frequency information is required, and shorter duration windows when accurate time information is needed. Wavelets do not use the term "frequency" nor do we refer to time-frequency domains,

rather we speak about time-scale depiction where scale is an inverse function of frequency. Wavelet analysis has attracted significant attention as a diagnostic tool for condition monitoring and is recommended as an effective tool for detecting faults in gears and bearing faults which are difficult to detect by the other frequency analysis methods (Tse et al., 2004; Gaberson, 2002).

The Fourier transfo r.m.s the time-domain signal in te r.m.s of trigonometric functions (sine and cosine); the wavelet transform expresses a signal in te r.m.s of known standard "mother" wavelet functions which makes it more useful for the extraction of transient features contained in a signal. Because these wavelets are of variable scale - the scale can be varied by contraction/expansion and translation of the mother wavelet (window function) - wavelet analysis can scrutinise the entire spectrum when extracting a fault signal.

Wavelet analysis has the major advantage that it can characterise a signal localised in time (non-stationary signals). This property is valuable for extracting information on small magnitude changes in the signal and separates the wavelet transform from other signal analysis methods.

Spectral Kurtosis: spectral kurtosis was introduced by (Dwyer, 1983) as a technique able to distinguish between stationary signals and impulses and other transients in a background of Gaussian noise. Spectral kurtosis has a high value for a frequency band where the signal is dominated by impulses, and a low value for a frequency band where the signal is dominated by stationary periodic components or Gaussian noise.

Recently, however, spectral kurtosis has also been applied for this purpose. Spectral kurtosis was first introduced some twenty years ago but recently has it been applied to fault detection in rotating machines (Antoni, 2004).

Spectral kurtosis was originally used to detect randomly occurring signals. Equally it can be used to detect non-Gaussian components in a signal, e.g. structural vibrations in a machine generated by a gear fault such as a cracked tooth. (Antoni, 2006) provides the theoretical background to spectral kurtosis together with many references and examples of its application to machine diagnostics including determining the frequency of the excited component. (Antoni and Randall, 2006) and (Sawahli and Randall, 2004) present

the application of spectral kurtosis to the detection and diagnosis of faults in gears and bearings.

(Sawahli and Randall 2004) concluded "spectral kurtosis is an exciting new analysis technique for use in the diagnostics of rolling element bearing faults". They claim it can identify the frequency band that will provide most information on the presence of a fault without the necessity of comparison of the "faulty" spectrum with the baseline healthy spectrum. In this way the spectral kurtosis can aid fault detection and diagnosis by providing information on what filters to use to isolate the most impulsive sections of a signal spectrum from stationary masking (stationary components).

With spectral kurtosis it is useful to consider the vibration signal (say) to be stationary Gaussian white noise modulated by a time and frequency varying complex envelope function H(t,f) (Antoni, 2006). If signal Y(t) is defined as the system response at frequency f, then

$$Y(t) = \int_{-\infty}^{\infty} e^{2\pi f t}\, H(t,f) dH(f) \text{.....16}$$

With real machine vibration H(t,f) should be presented as H(t,f,w) because it is a stochastic process. Here w is introduced as a random variable which represents time variations. When *H* is time stationary and independent of the process X, we obtain a conditionally non-stationary process (CNS).

Spectral kurtosis is a fourth-order spectral cumulant of a conditionally non-stationary process:

$$(C_{4Y}) = S_{4Y}(f) - 2{S_{2Y}}^2(f) \text{.....17}$$

Where $S^2_{nY}(t,f)$ is second-order instantaneous moment and a measure of the energy of the complex envelope:

$$\frac{S_{2nY(t,f)=E\{|H(t,f)dx\,(f)|^{2n\omega}\}}}{df} = |H(t,f)|^{2n}\, S_{2nX} \ldots\ldots\ldots 18$$

Thus, the spectral kurtosis is defined as the energy normalized cumulant (Antoni, 2004) which is a measure of the peakiness of the probability density function H:

$$K_Y(f) = \frac{C_{4Y(f)}}{S_{2y(f)}{}^2} = \frac{S_{4Y(f)}}{S_{2y(f)}{}^2} - 2 \quad \ldots\ldots\ldots\ldots\ldots\ldots 19$$

The kurtogram was suggested by (Antoni and Randall, 2006) as a means of designing a band-pass filter which can be applied to increase the signal–to-noise ratio. The kurtogram is a 2-D map of the values of the spectral kurtosis calculated for various baqndwidths and frequencies. Originally the kurtogram was based on the STFT but now it uses a filter bank approach which gives the same quality of result but requires less calculation time – this is the fast kurtogram which will be used here (Antoni, 2007).

The method will thus include following main steps (Antoni, 2007):

1. “Calculate the fast kurtogram of the vibration signal”.

2. “Design the bandpass filter based on the results of the kurtogram”.

3. “Analyse the filtered signal”.

Since a cracked tooth should generate impulses at a characteristic gear frequency, analysis will focus on identifying the presence of such a signal.

3.2 Temperature Monitoring:

(Townsend and Akin, 1981) have shown that tooth load and tooth modification are the most important factors in determining the temperature attained by the gearbox oil, and toothed gears meshing under EHL produce a considerably higher temperature in the lubricant than for direct contact of the tooth surfaces. Secondary factors include oil viscosity and gear rotational speed. Further investigation of such factors as tooth shape

should help in determining optimum temperatures of lubricants under EHL conditions (Wiśniewski and Janczak, 1981).

Present methods of temperature monitoring are not sufficiently sophisticated to determine the temperatures of specific components and are used to indicate overheating due to such problems as insufficient cooling and/or loss of lubricant. The effects of rotational speed, load and meshing point on the gear tooth surface temperature have been investigated for a spur gear using miniature type-K thermocouples. Maximum surface temperature was found to occur on the dedendum. It was also shown that thermocouples are a practical and reliable means of on-line CM of gears (J and Quin˜o´nez, 2004).

Temperature measurements of the tooth flanks has been achieved using thermocouples which were glued as closely as possible to the areas of interest. The electronic evaluation unit that was used provided a digital output to a PC for subsequent analyses. (Peter. J and Stefan, 2001) claim that this his method produced accurate measurement of the temperature for gearbox surface and lubricating oil temperatures. These results were then used to estimate viscosity of the lubricant, wear, etc.

During continuous operation the gearbox temperature will arise until it reaches a stable temperature, when heat generated within the gearbox equals the heat lost. The heat generation is due to friction between the gears, hydrodynamic friction between the lubricant and the moving components (during gear meshing, in the bearings and at the seals) and overcoming viscous forces in the lubricant. These heat sources are, typically are less than the heat generated when a fault or malfunction is present and this is offers a method of monitoring the condition of gearboxes. Temperature can be measured by a variety of thermal sensors such as thermometers, thermocouples, thermographic paints, and thermal cameras (Pekka, 2006); (Cairns, 1991).

3.3 Oil Debris Monitoring:

Oil debris analysis is a widely used condition monitoring technique, from the technician who rubs the oil debris between finger and thumb to spectrometric oil analysis and

scanning electron microscopy. The fault must have progressed sufficiently for enough debris to be carried by the oil to the collection site for the fault to be detected. Careful and detailed monitoring can indicate the type of component (e.g., gear teeth), type of failure (e.g., spalling) and rate of degeneration. Unfortunately, while oil debris monitoring cannot differentiate between two components of the same material, spectrometric oil analysis has proved to be second only to acoustic emission techniques in detecting pitting rates (Tan et al., 2007).

Trending is a common practice with wear debris analysis. Figure 20 shows the classic Bath-tub curve for wear over the life of a gear. During running-in wear is high which produces a lot of debris. Once the system has "settled in" and is properly lubricated the rate of wear reduces to a low level. With time the gear shows signs of fatigue and the rate of wear increases rapidly (Neale, 1995)(Evans and Hunt, 2008; Hamzah and Mba, 2009).

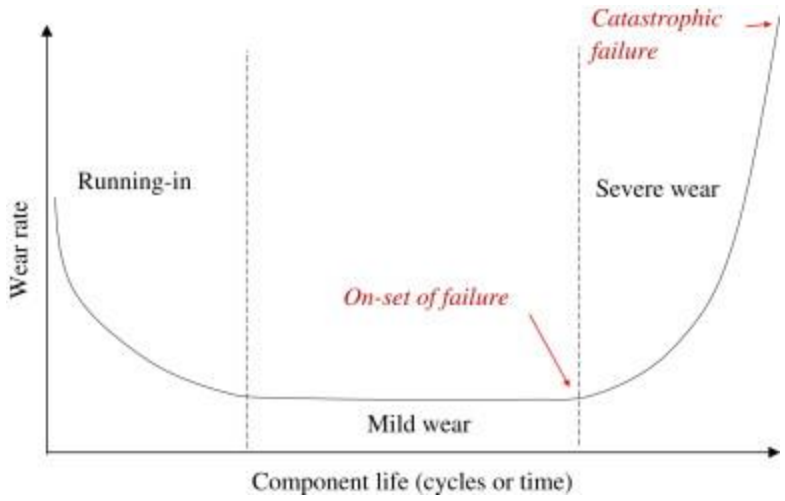

Figure 20: Classical Bath-tub curve for wear (Roylance and Hunt, 1999)

Wear occurs if two surfaces rub against one another with sufficient normal force. However, adequate lubrication between the surfaces prevents the occurrence of wear when the lubricant is clean, there is no overloading, temperature remains within acceptable limits, etc. Excessive loading will cause the gear teeth to come into contact and the material removed from contacting surfaces (wear debris) will contaminate the

lubricant and can be detected by lubricant monitoring. The analysis of the lubricant to determine its condition can be off-line or continuously working (on-line). Both methods usually use representative samples of the oil, though sometimes with the on-line method all the oil flow passes through the measuring devices. Wear particles can be sorted and collected by means of magnetic chip detectors (MCD). Most measurements concentrate of detecting and analysing the solid debris to determine wear and need for oil additives.

Many techniques are used for wear metal analysis, for example spectrometric oil analysis (SOA). Before analysis of oil samples using spectroscopic methods pre-treatment is usually required. In SOA, an inductively coupled plasma (ICP) technique is used with an Atomic Emission spectrometer. The oil sample is subjected to a high-voltage plasma which energises the atomic structure of metallic elements present and the emitted light can then be analysed. The wavelengths and intensity of this light determine the elements present in the debris and their concentration.

However, oil analysis methods cannot identify faults such as fatigue cracks because such as these failures may not generate metal particles (Tan et al., 2007; Pekka, 2006).

Debris analysis is, of course, intimately linked to EHL film thickness for lubricants. Thus debris wear detection and analysis has also been used successfully for the detection adequate lubricant thickness able to provide a protective film and control surface distress in lubricated highly stressed components such as gears.

Some researchers have detailed the influence of load, speed and material properties on the Elastohydrodynamic pressure distribution between solids and the thickness of the oil film separating them (Bankim and Bernard, 1882). Speed and material of gears tend to be the most important factors influencing the behaviour of the secondary pressure peak; which is the result of the local pressure peak far in excess of the Hertzain maximum which effectively reduces the film thickness at that position by approximately a further 25%(Dowson, 1977). However, as the range of materials is very small in practice, the speed factor is the dominant variable.

In evaluating the EHL, (Tan et al., 2007) assumed the contacting surfaces were flat. However in practice, particularly in gears, the contacting surfaces may be rough, leading to asperity contact between the meshing surfaces even with the presence of a lubricant

film. The ratio of the minimum lubricant thickness to surface roughness will determine the rapidity with which surface fatigue failures such as pitting and wear occur.

(Czichos, 1977) was performed experimental work with two different types of equipment; line contact conditions were realised with a disc-on-flat tribometer, point contact conditions were obtained using a ball-flat contact or ball-ball contact tribometer. Experimental evidence indicates that the changeover from partial EHD to full asperity contact is accompanied by only a small increase in the friction coefficient and may therefore be overlooked if friction is not continuously recorded (with high resolution) during the whole failure test. With full asperity contact, the onset of incipient scuffing is determined by the stability of the asperity surface films, which in turn are affected by the metal-lubricant interactions and the existence of the initial surface oxide films. It was concluded that a criterion predicting the failure of sliding concentrated contacts should take into account the physical and chemical nature of protecting surface layers as well as the EHD and asperity contact conditions.

The FZG gear test rig system was used to study and observe the affect of oil temperature on gear failures such as wear, pitting, micropitting and scuffing. High temperatures lead to low viscosities, thin lubricant films and high chemical activity with good tribological layer formation in the gear mesh which generally has a detrimental influence on failure performance. At higher temperatures and thus lower viscosities and film formation decreases, adhesive forces decrease and chemical activity is increased (Höhn and Michaelis, 2004).

(Guangteng et al., 2000) used the spacer layer imaging method (SLIM) to study the relationships between lubricant film thickness, rough surface and rolling EHD contact. It was observed that there was a reverse proportionality between the elastic deformation of the asperities and the rolling speed, suggesting that the fluid film contributes to a lowering of asperity pressure. Effectiveness of asperity on increasing mean EHD film thickness depends on the relative orientations of transverse and rolling directions. A small EHD film thickness is produced at the asperity tip at slow speeds, increase in rolling speed results in an increase in micro-EHD film thickness in the classical mode.

(Dempsey et al., 2004)and (Paula. J, 2001) used the spur gear test rig at the NASA Glenn Research Centre to test 8 spur gears without damage and 8 spur gears with pitting

damage. The data collected was analysed using a fuzzy logic technique and it was concluded that while the accumulated mass of debris cannot discriminate between gear and bearing damage it can be a good predictor of pitting damage on spur gears.

3.4 Vibration analysis:

There have been many investigations carried out to monitor and evaluate of industrial gearboxes using different techniques. Among these techniques vibration signal processing technique is well known. Measuring vibration gearbox with the help of accelerometer fixed on the gearbox case is one of the best procedures for gear damage evaluation. Thus, condition monitoring of the gearbox system during its operation is essential to prevent the system from failure that could cause system shutdown (de Kraker and Stakenborg, 1986).

(Cairns, 1991; Vayionas, 1991) have both reported results from purpose built back-to-back gearbox test rigs for condition monitoring, and showed that vibration signal analysis was able to detect an eccentricity on just one of the gears. (Reimche and Südmersen, 2003)used purpose designed back-to-back gearbox test rigs and demonstrated that analysis of the vibration signal analysis is able to detect the eccentricity on one of the gears.

The competence of a gearbox depends on the state of the internal components; load carrying elements such as shafts, gears and bearings cause wear and fail. These failures increase noise and vibration in the gearbox. Thus vibration monitoring is a method used on a large range of equipment and provides the most information (Yesilyurt, 1997; Hasan, 2006). Vibration monitoring can be used to detect a variety of faults; bent or eccentric shaft, misaligned components, unbalanced components, faulty bearings and gears, inappropriate clearances, and many more. Vibration monitoring is well able to detect, locate, and distinguish between the different failures in a machine. Today time domain, frequency domain and time-frequency domain analyses are all well established.

Time domain analysis uses statistical analysis techniques on direct or filtered time signals to detect parametric or pattern changes as transmission components wear. Statistical parameters such as r.m.s , Kurtosis and Crest Factor are used to qualify general wear from tooth specific damage. In the frequency domain the change in amplitude of the peaks in the vibration spectrum are used to detect and diagnose faults (Stokes, 1992; ASM., 1992). Moreover, Time-frequency analysis has been found to be effective in monitoring the transient or time varying characteristics of machinery vibration signals, and therefore its use in machine condition monitoring is increasing (Peng et al., 2005).

(Choy et al., 1994) developed a signature analysis scheme to study and identify the characteristics of vibration signal of a gear system using time averaging and spectrum analysis. Simulating varying degrees of wear and pitting damage, could provide a comprehensive database of gear fault detection to study and characterise the vibration signal of the gear system.

To detect defects in rolling elements and gears the piezoelectric accelerometer is the vibration transducer of choice for very nearly all situations. As consequence the peak ratio was more reliable than r.m.s , Kurtosis or Crest Factor as an indicator of the presence of localised defects, and also demonstrated a good correlation with defect size. While the frequency-based peak ratio is excellent for localised defect detection, a time domain method such as r.m.s is more suited for non-localised defect detection such as debris denting (Shiroishi et al., 1997). However, results reported by (Tandon and Choudhury, 1999) claim that Kurtosis is the most effective measure for fault detection but identifying the initial stages of a bearing fault directly from the vibration spectrum was not possible. This is confirmed by (Hasan, 2006) who found variation of Kurtosis values for the raw vibration data provides a better basis than r.m.s for understanding fault progression.

(Yesilyurt et al., 2003) studied vibration behaviour of roller bearings with different viscosity lubricants using vibration monitoring and were able to detect changes in lubrication regime resulting from change in oil viscosity. It was found that the viscosity could modulate the r.m.s value of specific frequency bands in the vibration signals because the film thickness of the oil changed. For gear systems the gear mesh and gear transmission errors were the main contributors to r.m.s vibration level in the time-averaging method.

During wear detection tests using vibration analysis, early stage faults on spur gear teeth were identified and an approximately linear decreasing relationship between tooth mesh stiffness and time was found (Serrato et al., 2007; Smith, 1993).

In gearbox health monitoring and fault detection the scalogram based parameter (mean frequency variation) provides the most useful basis for monitoring of localised pitting gear damage (Hasan, 2006).

In the wind power industry, vibration monitoring is used routinely to detect faults in bearings and gears. Sensors are mounted on the bearing housing to detect the unique characteristic vibration signatures for each gear mesh or bearing, which depends on the geometry, load, and speed of the components (Lucente, 2008).

Other research extracted that the overall condition of the tested gearbox is well represented by the r.m.s of the time domain vibration signal. The Kurtosis did not reflect any explicit trend. The Crest Factor reflected the trends of the r.m.s and peak values both of which increased slightly during the test. Narrow band filtering techniques enable easier detection of fatigue cracks in gear teeth, largely due to the occurrence of a phase lag in the vibration produced by the affected teeth (Shiroishi et al., 1997; Vecer et al., 2005).

Continuous wavelet transfo r.m.s applied to the vibration signal have been successfully used for the detection of localised and distributed pitting damages in a helical gearbox. Time and frequency domain techniques and cepstrum analysis did not provide any significant diagnostic information about the presence and advancement of pitting fault until the fault severity was substantial (Hasan, 2006).

Chapter 4

Acoustic Emission

4 Acoustic Emission

4.1 Brief history of Acoustic Emission

The application of acoustic emission was used as early as 6500 BC in the manufacture of pottery. The potters would listen to the cooling clay vessels in the kiln. Cracking sounds were taken as an indication of structural instabilities indication. More recently (Kaiser, 1950) used tensile tests to determine the AE characteristics of engineering materials. He demonstrated the irreversibility phenomenon that now bears his name, the Kaiser Effect. The Kaiser effect is defined by (Holroyd, 2000); 'Material does not start to re-emit AE activity until the applied stress exceeds that which it has previously experienced'.

Schofield realised the potential of Kaiser's work and began the first wide-ranging research programme in the USA into AE phenomena, in particular the identification of AE sources and applications of AE to materials science. Schofield's work encouraged many subsequent researchers to become active in AE research and development which then progressed rapidly particularly in the nuclear industries.

(Miller and McIntire, 1987b) have described how applying AE to the detection of coolant loss in nuclear reactors. This work was to develop a novel non-destructive test that was faster than the then conventional methods. Also by 1965 the Space Division of Boeing began research on applications of AE to (i) detection of the early stages of bearing failure, (ii) detection of leaks in hydraulic systems (iii) cavitation in fluid flow and consequent erosion of flow valves and (iv) analysis of AE signals produced within rotating machinery. (Balderston, 1969) reported on a response from a transducer with high signal, as compared to a background noise compared to vibration signals. Balderston understood that the response with its associated high resonance frequency was potentially useful as a diagnostic tool. Soon afterwards (Board, 1975) explored the potential benefits of AE diagnostics over conventional vibration techniques for the detection of incipient machine failures.

The interest in the applications of AE for condition monitoring of rotating machinery can be seen to be relatively new and has grown significantly in the last decade accompanied by the development of new more advanced signal analysis techniques particularly for the detection of incipient failure in bearings and gears. Defect growth was often characterised

by the slow growth of the AE signal, but with the advances in signal processing this method has become a reliable technique for health monitoring of machinery (Mba and Rao, 2006; Holroyd, 2000; Vahaviolos, 1999). The recent progress in industrial applications of acoustic emission testing AET to the formation of several organizations including, acoustic emission Working Group (AEWG) aims to support the research and development of AET in the field of non-destructive testing NDT.

4.2 Acoustic Emission Sources

Acoustic Emission Technology and Application AE can be defined as the transient elastic wave generated when strain energy is released suddenly within or on the surface of a material under stress; e.g. initiation and extension of fatigue cracks or plastic deformation and the associated dislocations. Other sources of AE can be thermal stress, cracking during rapid cooling and the failure of fibres composite materials. The elastic waves generated cover a broad frequency range between about 100 KHz and 1 MHz (Miller and McIntire, 1987b). The wave travels through the body of the material to the surface where it is "picked-up" by an AE detector. The detector converts the AE signal into an electric voltage which characterises the wave and can be used for fault detection and diagnosis, see Figure 21.

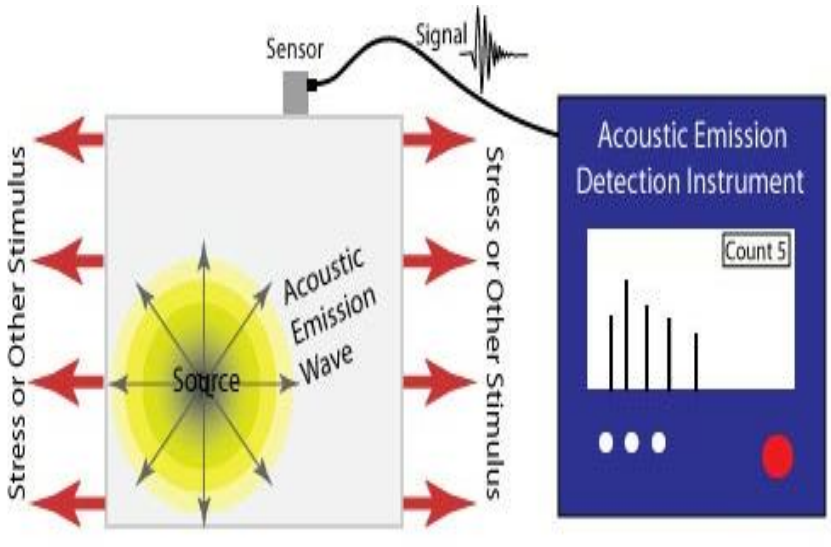

Figure 21: Schematic of the Acoustic Emission principle (NDT, 2013)

Condition Monitoring of rotating machinery based on AE uses time, frequency and time-frequency domain analyses of the signals for fault detection and identification. However, whether the signal being monitored is AE or vibration there will always be a common factor - the rotational speed of the machine. For example, in gears, the main factors would be shaft rotational speed and subsequent interactions between gears within the gearbox; transducer location may also be a factor. The major frequency of gear induced vibrations, for example, would be the gear meshing frequency, $m = N*rpm/60$ = Hz. Where, N is the number of teeth, and rpm is the rotational speed of the gear in revolutions per minute (Miller and McIntire, 1987a).

Factors affecting the amplitude of the AE will include applied load, see Figure 22 which also shows the Kaiser effect (NDT, 2013). In Figure 22 the applied load is first increased (A to B) with the result that the number of AE counts increases. At B the load is decreased (B to C) and then increased back to its original level (C to B). There is no more AE until the load again reached the level B when the AE signal recommences (the Kaiser Effect, occurs when there are few or no flaws in the material). There is a further increase in the AE signal as the load is increased form B to D) but the signal ceases as the load is reduced for a second time (D to E). However on this occasion as the load is increased (E to D) the AE signal recommences just prior to the load reaching the level at D. This is known as the Felicity Effect, and is due to flaws present in the material. The AE signal then continues to increase as the load is further increased (F to G).

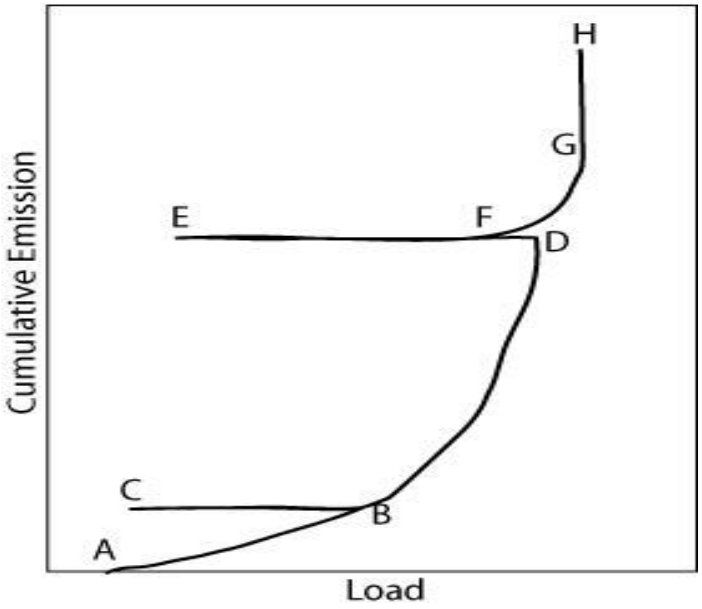

Figure 22: Example of Kaiser Effect (NDT, 2013)

4.3 Acoustic Emission Applications

A classification of the functional categories of AE applications according to (Capgo Pty Ltd., 2009; Envirocoustics S. A., 2007) is given below:

1. Material; and mechanical property testing and characterisation;
2. Pre-service proof testing;
3. In-service testing (requalification);
4. On-line process monitoring;
5. In-process weld monitoring;
6. Mechanical signature analysis;
7. Leak detection and location;
8. Geological applications; and
9. Other application: drought stress monitoring of crops and woods, wear and friction engine status monitoring and crack detection of steel rollers.

AE technique has been applied in a wide variety of research, civil and industrial fields. These applications include ((Capgo Pty Ltd., 2009; Envirocoustics S. A., 2007):

1. Chemical and petroleum industries,

2. Electric and power plant industries,
3. Aircraft and aerospace industries,
4. Metalworking industries,
5. Civil engineering, and
6. Transportation application.

Successful application of AE to gearboxes has included detection of crack initiation and crack propagation in gear teeth, pitting and wear of specific gear teeth, lack of adequate lubrication. The AE signal provides sufficient information to detect and diagnose the presence of faults before vibration or wear debris analysis (Robinson, 2001). The AE signal generally increases as the fault progresses.

4.4 Acoustic Emission's, Advantages and Disadvantages

For condition monitoring, AE offers a number of advantages over most commonly used technique (Miller and McIntire, 1987b; Holroyd and Randall, 1993):

- AE signals are omnidirectional so that an AE sensor can be placed anywhere in the vicinity of the AE source(s),
- Because of its frequency range AE is less affected by mechanical background noise, and offers a high signal to noise ratio giving a clearer indication of the presence of a fault,
- AE is a more effective measure than vibration at low rotational speed because the latter can have difficulty due to the low frequencies of the signals generated at low speeds.
- AE sources are usually generated at the microscopic level which makes AE more capable of detecting incipient faults,
- AE is a non-destructive technique,
- Sensitive to activity from faults, and
- The AE signal is independent of structural resonances.

The main drawbacks associated with acoustic emission are (Miller and McIntire, 1987b; Holroyd and Randall, 1993):

- Because AE signals tend to be low amplitude and of high frequency (which is rapidly attenuated) AE must be placed closed to the source(s),
- AE signals tend to require considerable amplification,
- AE signals are usually limited to faults produced by/within solid materials such as cracking, asperity contact, etc.,
- AE can have difficulty in detecting unsafe situations related to imbalance and misalignment, and
- AE can suffer from interference from high frequency noise such as turbulence.

4.5 Acoustic Emission Sensors

Before use AE sensors are checked for sensitivity and frequency response. Normally sensors are resonant (narrow frequency range) or broadband piezoelectric transducers (typically 20 kHz to 1 MHz) used with an impedance matching couplant which can be silicon epoxy or even a mechanical clamp (Physical Acoustic Co., 2007). The former type of sensor has the advantage of that the low frequency signals from machine vibration have minimal influence on its output. When more than one sensor is used, the location of the AE source is determined by measuring the signal's arrival time at each sensor and source distance calculated, see Figure s 21and 23.

The sensor voltage is generated by the variation in strain in a very thin wafer of piezoelectric ceramic (e.g. lead zirconate titanate (PZT) or polyvinylidene fluoride (PVDF)). These sensors can "detect various combinations of waves (compressional, shear, surface and plate) coming from any direction" (BS EN 13477-1:2001., 2001). With AE transducers as with most other types of transducer the three major considerations are (1) sensitivity, (2) operating frequency and (3) physical characteristics such as operating temperature range, repeatability, robustness and reliability.

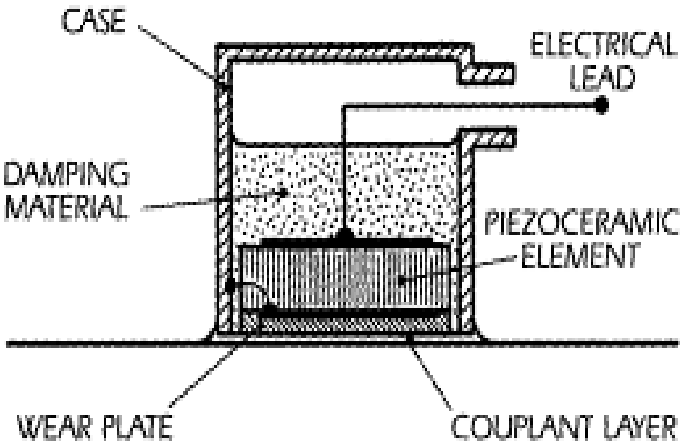

Figure 23: Schematic diagram of typical AE sensor(Miller and McIntire, 1987b)

4.6 Sensor Couplant

Sensor Couplant because AE signals are usually of low amplitude it is essential that there is good mechanical coupling between the surface to which the transducer is attached and the transducer itself. To eliminate air gaps between the two surfaces a layer of couplant is used, though this should be as thin as possible. Proprietary couplants are available to match the impedance of the moving surface to that of the transducer and maximise transmission of signal energy. As with accelerometers and other measuring transducers the surface should be cleaned with a wire brush or similar to remove debris and any layers of loose paint, and then wiped down with an appropriate solvent. The surface where the transducer is to be positioned should be flat and smooth to maximise adhesion. To ensure the couplant layer is thin it is usual to firmly press the transducer onto the test surface.

The optimum characteristics of a couplant are (i) good matching of transducer and surface impedances (highly viscous), (ii) low attenuation at AE frequencies, (iii) high wettability, (iv) corrosion resistant and (iv) easy removable. If the sensor is disposable then an excellent couplant is ethyl cyanoacrylate based super glue.

After attaching the sensor(s), the quality of the coupling(s) should be tested and calibrated and the simplest way of doing this is to use the pencil lead break, or Hsu-

Nielsen pulse calibration, test (BS EN 1330-9:2009 Non-destructive testing (HMSO, London). This simple, easy and direct test also provides a check on whether the AE data acquisition system is functioning properly.

Figure 24 shows the calibration device which consists of a graphite pin ("pencil lead") of hardness 2H and 0.5 mm diameter. The test is made repeatable by pulling the lead out a distance of 3 mm to give the same break angle for each test. The lead is broken by pressing it against surface of the workpiece, and this generates a sudden intense AE signal (Boczar and Lorenc, 2004). Because it is so simple this test is very popular and has been standardised (BS EN 1330-9:2009 Non-destructive testing (HMSO, London).

The emitted AE signal from the pencil lead break test is shown in 25. Signal intensity shows whether the location of the sensor is close enough to the source to detect the required AE signals strong signal and there exist no saturation due to setting the sensitivity of the sensor too high and whether it may saturate during grinding (single grit grinding).

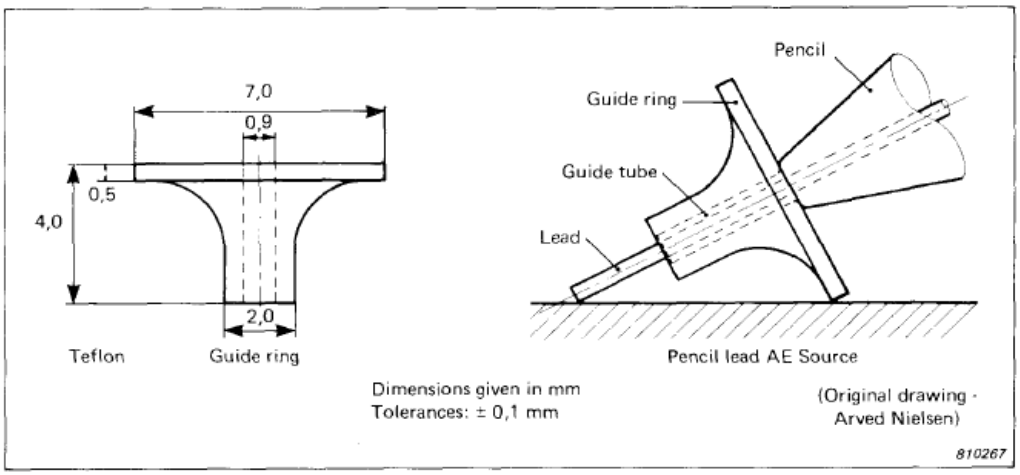

Figure 24: Hsu-Nielsen calibration head (Brüel and Kjaer., 1981)

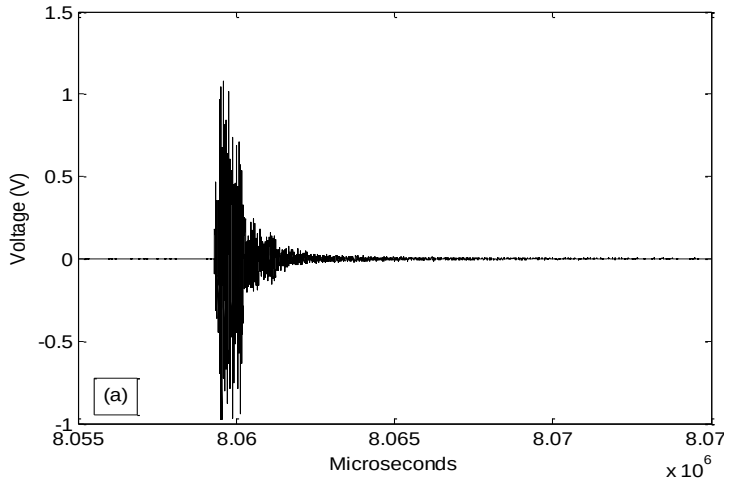

Figure 25: Pencil lead break test raw signal, (Brüel and Kjaer., 1981)

4.7 AE Measuring

(Holroyd, 2000) has described AE signals as being of three types, see Figure 26. Burst type signals are generally emitted by static structures. The Individual events can be seen quite clearly and can be recorded and analysed separately. However, for rotating machinery it is possible for individual events to have much the same amplitude and occur sufficiently frequently that the signal appears "continuous". However a more common type of signal with rotating machinery is where the "continuous" signal appears as background with more energetic events appearing as peaks.

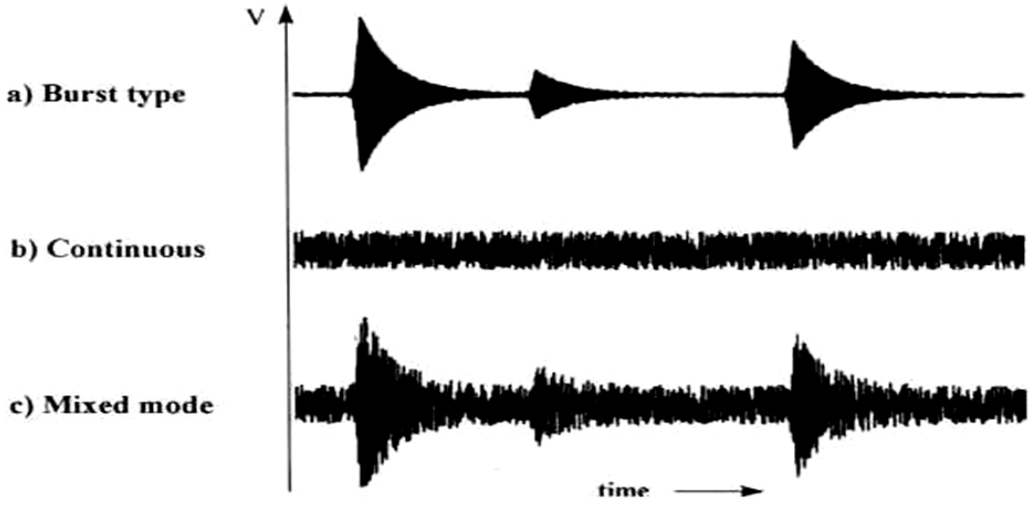

Figure 26: Different AE signal types (Holroyd, 2000)

AE signals are often described as a series of events (Physical Acoustic Co., 2007). An event required several parameters to describe it, see Figure 27:

- Maximum amplitude of the pulse.
- Determination of threshold level; AE signals are processed after the amplitude becomes larger than the threshold level. This might be the r.m.s value of the background noise in the absence of the event.
- Rise-time (duration between first threshold crossing and peak amplitude).
- Number of times the threshold is crossed (counts) in an "upward" direction.
- Signal duration (time between first and last threshold crossings).
- Energy (integral of the square of the amplitude over duration of signal.

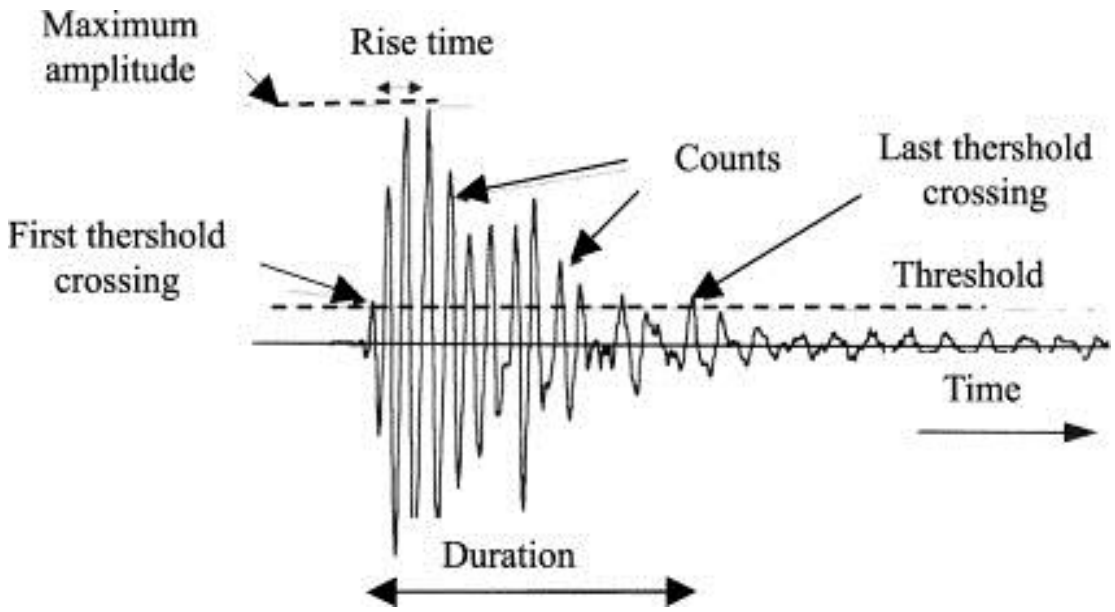

Figure 27: The typical AE signal features (Physical Acoustic Co., 2007)

4.8 Wear Conditions and Acoustic Emission

Various methods have been used to detect and diagnose fatigue in rolling contact in bearings, and AE is the latest. However, the results still have not been completely successful because the AE measurement techniques developed thus far have dealt only with the AE emission generated by rolling contact with time. (Tekeo and Takashi, 1982) have shown that by employing of acoustic emission technology it could be explored defects of rolling bearings before the start of accelerated vibration . There is needed to further clarify the type of relationship between AE and wear failure (Halme and Andersson, 2010; Mba, 2003). After studying the relation between AE and failure detection in rolling contact fatigue processes it was clear that the AE was related to bearing fatigue failure and can precisely locate the defect position.

(Sarychev and Shchavelin, 1991) investigated the relationship between cumulative AE counts and frictional work, it was found that the real area of contact between surfaces comprised a number of discrete asperity contacts and the deformations of these are associated with the AE output with only larger asperities generating AE above the threshold level. In dry sliding metals it was easy to detect the AE signals which were varied more or less consistently with process conditions (speed and load) and material

combination used. (Lingard and Ng, 1989)found there was an increase in the cumulative AE counts with total friction work. Also the rate of AE was directly proportional to the contact area in the direction of sliding.

A ball and cylinder test rig give conditions of pure sliding if a stationary ball is held against a rotating cylinder. (Boness et al., 1990) postulated that the first peak in the r.m.s value of the signal was associated with the initial removal and gross deformation of the original surface asperities. A special test using a polished cylinder established that when a full elastohydrodynamic film existed between the specimens no r.m.s signal above the noise level of the instrument could be detected, inferring that asperity contact was the prime source of the AE signal.

A scanning electron microscope (SEM) examination of the rubbing surfaces showed that the gradual increase to the second peak in the r.m.s value of the signal was related to transference of debris from the rotating cylinder to the smoother stationary ball. For the unlubricated situation the erratic behaviour of the r.m.s signal after 120 s was observed to be predominantly due to abrasive wear. It was demonstrated that r.m.s measurements of the AE signals provide a valuable tool in the study of wear between dry and lubricated sliding contacts. The time-dependent nature of the r.m.s signal is able to distinguish between different wear mechanisms. A direct empirical relationship between integrated r.m.s signal and the wear volume removed from the test ball in a ball on cylinder test rig was obtained (Boness et al., 1990).

(Mechefske et al., 2002) studies the mild-to-severe wear transition using sapphire sliding over steel sliding disks using AE to measure changes in test conditions. AE signals generated during the wear process were analysed in both time domain and frequency domain. Experiments demonstrated that AE has the possibility to be a useful wear rate monitoring technique. In the time domain the increase of AE r.m.s and peak level values were in direct proportion to the sliding speed and inversely proportional to the applied load conditions and so are useful measures of the wear surface strain rate.

Boness et al [60] indicated that the asperity contact, micro-crack initiation and growth, plastic deformation are the basic wear mechanisms. Also, Boness et al stated that the AE signature was mostly continuous with superimposed AE burst attributed by the rapid high-amplitude at events the rubbing surfaces. Boness at al [60] experienced AE under

dry and lubricated contacts under pure sliding conditions. Tests with a full elastohydrodynamic film between highly polished surfaces did not generate any AE activity above the electronic noise of the acquisition system, inferring that asperity contact was the prime source for AE. Also found AE r.m.s signal varied directly with wear Volume. In general, the occurrence of severe wear results in high AE activity as evidenced by a high AE count rate in the time domain and high spectral variation in the frequency domain (Boness et al., 1990; Jiaa and Dornfeld, 1990).

(Tan and Mba, 2005b) investigated the use of AE detection of pitting damages on gear teeth surfaces. They noticed that the lubricant oil temperature is relatively higher at higher operating torques generating a higher r.m.s value in the AE signal, of course at this higher temperature the oil film is thinner resulting in more asperity contact so long as the lubricating regime is under partial EHL. They concluded that a linear relationship existed between measured AE levels generated by pitting of a gear pinion and area of pitting and that detection of pitting began when only 8% of the area was pitted. This strongly suggests that AE techniques can be used for health monitoring and pit progression. It was also found that AE offered better sensitivity to pitting progression from the bearing casing than the vibration method, depending on load conditions (Vincent, 2007).

Detection of incipient faults in rolling element bearings at low speeds was evaluated experimentally **by** (Eric Y et al., 2007) it was found the time domain r.m.s value was the best parameter to clearly show the difference between normal and defective bearings regardless of speed and type of the defect.

Preliminary fatigue testing of a complete landing gear has demonstrated the applicability of the AE signal using resonant sensors attached to the outer surface of the landing gear assembly. Fatigue crack monitoring of compact test specimens has confirmed that AE can detect the initial stages of crack growth in typical landing gear materials (Matthew G et al., 2004). The study examined AE from fatigue cracks in compact tension specimens using a broadband transducer and a resonant sensor to assess their effectiveness in monitoring fatigue crack growth in aerospace grade steel. It was shown that detection of fatigue crack growth in aerospace grade steel compact tension specimens using appropriate AE techniques is possible. Furthermore a quick and efficient way to

distinguish between emissions from a hydraulic actuator and fatigue crack growth in the laboratory has been identified (Matthew G et al., 2004).

4.9 Gear faults monitoring using acoustic emission.

(Boness et al., 1990; Boness and McBride, 1991) investigated the application of AE to both sliding and rolling conditions and found that asperity contact generated AE. This research was an attempt to better the understanding of how the operation of both helical and spur gears generate AE. That work was extended by (Tan and Mba, 2005b; Toutountzakis et al., 2005) who found that the principal AE sources are interactions between the surface roughnesses of the two gears due to their relative motion. Helical and spur gears undergo combined rolling and sliding on both sides of the pitch point, and pure rolling at the pitch point. However, due to the geometry of the helical gears, the pitch point during gear mesh does not pass along the width of the gear at the same time as with meshing of spur gears mesh, instead pitch point contact for the helical gear mesh is progressive.

The operating life of gears is determined by the lambda ratio which is vital for maintaining mechanical integrity. Recommended values for λ have been published but the actual value is difficult to determine during operation. EHL studies have shown that λ is predominantly determined by temperature, load, surface roughness and speed of the meshing gears (Dowson, 1977; Dowson, 1995). Because λ changes with change in any or all these parameters, the level of contact between the surface asperities during gear meshing will also vary.

(Hamzah and Mba, 2009) observed that AE was more sensitive to changes in specific film thickness under combined rolling and sliding (spur gear) compared to pure rolling (helical gear).and established a relationship between load, speed and AE for both spur and helical gears; the increase in speed increases the AE r.m.s and the reduction in load conditions, has reduced the AE r.m.s . levels. Further the variation in AE levels during helical gear mesh is suggested as attributable to not only the asperity levels but also to the variation in contact length during meshing.

4.10 Acoustic Emission Activities Constraints

(Loutas and Kalaitzoglou, 2007) compared the abilities of monitoring techniques to differentiate between different load and defect states in a single stage gearbox. It was observed that the AE r.m.s changed with increasing oil temperature and these findings confirm the conclusions of (Tan et al., 2007) and (Toutountzakis et al., 2005) that oil temperature significantly affected AE and should always be taken into account.

Pitting in gear tooth progresses from of micro-cracks initiation and crack growth to the separation of tiny particles from the gear surface. Simultaneously, these particles and other debris resulting from wear create abrasions between teeth surfaces. All these stages emit AE.

The detection of defects seeded into gearboxes using AE is fraught with difficulties. The biggest burst of the AE signals were not always present in the centre region of the window at the same location as the artificial fault (pit) on gear tooth. However, some researchers claim to have shown the contrary; that the AE energy as measured by the time domain r.m.s clearly distinguished a simulated pit, micro-cracks initiation and crack growth up to removal of tiny particles from the gear surface (Tandon and Choudhury, 1999; Toutountzakis and Mba, 2003). In addition third-body abrasions will be created by wear particles removed from gear surfaces and will have their own AE activity and further complicate observations (Matthew G et al., 2004). As stated earlier AE levels are inversely proportional to oil film thickness and directly proportional to asperity contact and are influenced by surface roughness (Tan and Mba, 2005b; Ebersbach et al., 2006).

4.11 Acoustic Emission and lubricant

(Benabdallah and Aguilar, 2008) investigate how the AE depended on friction and wear properties using a ball-on-cylinder lubrication test machine with a fixed, stationary ball sliding over a flat ring around a rotating cylinder. Included in the investigation was dry sliding contact lubricated with pure grease and contamination simulated by the introduction of small glass particles. The speed of the cylinder (sliding speed of the ball) was the parameter of major interest and it was found that for dry contact: sliding contact

generated a continuous AE waveform, the r.m.s voltage of the AE signal produced by the ball sliding over the ring was a good measure of the coefficient of friction (μ).

(Jie and Drinkwater, 2006) used an ultrasonic technique to measure the thickness of lubricating films for the rolling element of a ball bearing steel type 6016. The results obtained were in good agreement with those produced by EHL theory over the range 0.3–1.0 μm for radial loads greater than 2.5 kN but shaft speeds were limited to less than 200 rpm (3.3 Hz). Ultrasonic measurements suffer from a number of limitations, including: the pulse repetition rate limits the number of measurement points, the ultrasonic beam does not focus at a point but over a small area and so gives an average value over that area. However it was clearly demonstrated that ultrasonic measurement has the potential for monitoring the thickness of lubricant films in industrial applications.

(Toutountzakis et al., 2005; Toutountzakis and Mba, 2003) used AE for an experimental investigation of gear defects and their diagnosis. They showed that AE monitoring of the health of gears was a useful tool that would allow monitoring for developing defects in gears externally, from a sensor on the bearing casing. (Tan and Mba, 2005a) noted that for isothermal conditions the imposed load had a minimal effect on the r.m.s level of the AE signal, but that speed had a significant effect. They confirmed that for rolling contact the level of the AE signals depended on the speed of rotation of the gears and that AE transients were found at the gear mesh frequency. The r.m.s value of the AE signal also depended on film thickness. The relative proportions of rolling and sliding contact strongly affected the overall level of the AE signal.

(Hamzah and Mba, 2007) extended previous work into the generation of AE as a function of λ using helical and spur gears made of 045M15 steel without any heat treatment, in a standard back-to-back oil bath lubricated gearbox, powered by a 1.1 kW motor. It was found that the value of λ clearly and directly influenced the level of the AE signal for both types of gears **(**inversely proportional**)**.

(Eftekharnejad and Mba, 2008; Eftekharnejad and Mba, 2009) assessed the ability of AE to identify specific defects seeded into helical (214M15) steel test gears. The gearbox test rig used was the same back-to-back arrangement as used by (Hamzah and Mba, 2007). It was operated at a speed of 11.5 Hz (690 rpm). Mobilgear 636 oil was the lubricant used. They concluded that the AE waveform could be used to identify the seeded defects. They

also concluded that the measured AE r.m.s levels were more useful for identifying the seeded faults than vibration measurement made with an accelerometer situated on the bearing pedestal. However (Toutountzakis and Mba, 2003; Hamzah et al., 2008) using a similar test procedure found this was not the case for spur gears.

In most of the studies conducted earlier, the impact of specific film thickness (λ) or rather lubrication regime on the AE generation has at gear contact area not been investigated in detail. And the main focus of previously published work was on the use of the AE technology for the detection of defects on gear tooth surface, and understanding the influence of the operation parameters such as applied load, speed, and surface roughness on the AE signal.

Thus the aim of this project work is to understand how three different lubricating conditions, hydrodynamic (HL), elastohydrodynamic (EHL) and boundary (BL) lubrication influenced the generation of AE at the meshing gears. Gear operating temperature will be changed while whilst AE activity in monitored during the whole test. The main objective of this research programme is to assess the potential of AE technology as a monitoring tool capable not only to detect the failure onset but as an effective preventive maintenance tool. Knowing the lubrication regime at gear meshing is responsible on lubrication-related-failures. So, in this research programme, the capability of AE in quantifying the lubrication regime of the operational helical gears will be evaluated.

Chapter 5

Experimental Setup and procedure

5 Experimental Setup and procedure

5.1 Experimental Gearbox

The test programme used a back-to-back type gearbox designed and fabricated at Cranfield University comprising slave gears driving the test gears via a flexible coupling, see Figure s 28 and 29. This type of gearbox is typical of those used for gear fatigue tests (Vayionas, 1991). AC 3 phase 1KW electric motor was used to drive the gearbox. A flexible coupling connected the motor input to the slave gears, two loaded plates on the power return shaft were used to dissipate the energy of the motor. The loading coupling consists of couple of half flanges bolted to each other; through a threaded hole on one of the flanges. The applied torque rotated the loaded plates against each other (Vayionas, 1991). The idea of applying the back-to-back arrangement is to allow the torque to be maintained within a closed loop so that the power requirement overcomes frictional losses only. In other words, when the gearbox is operating at a steady speed, even when the test gears are operated under very high load, the energy supplied by the drive driving only has to compensate for power losses in the system.

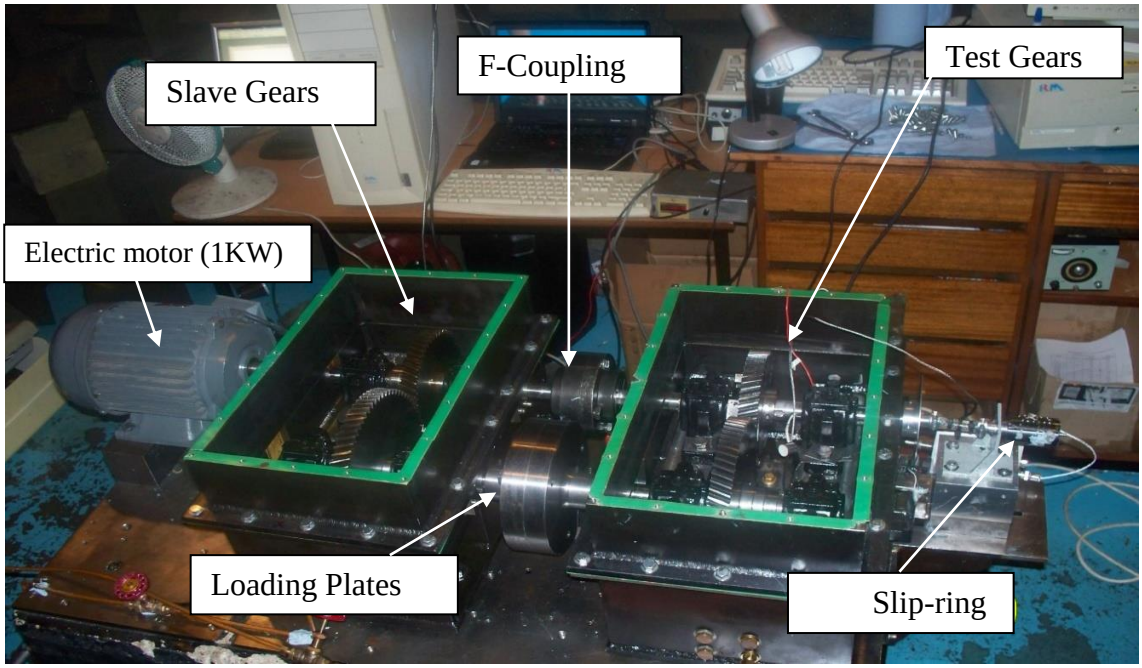

Figure 28: Back-to-back gearbox

The details of the gearbox design are presented schematically in Figure 29.

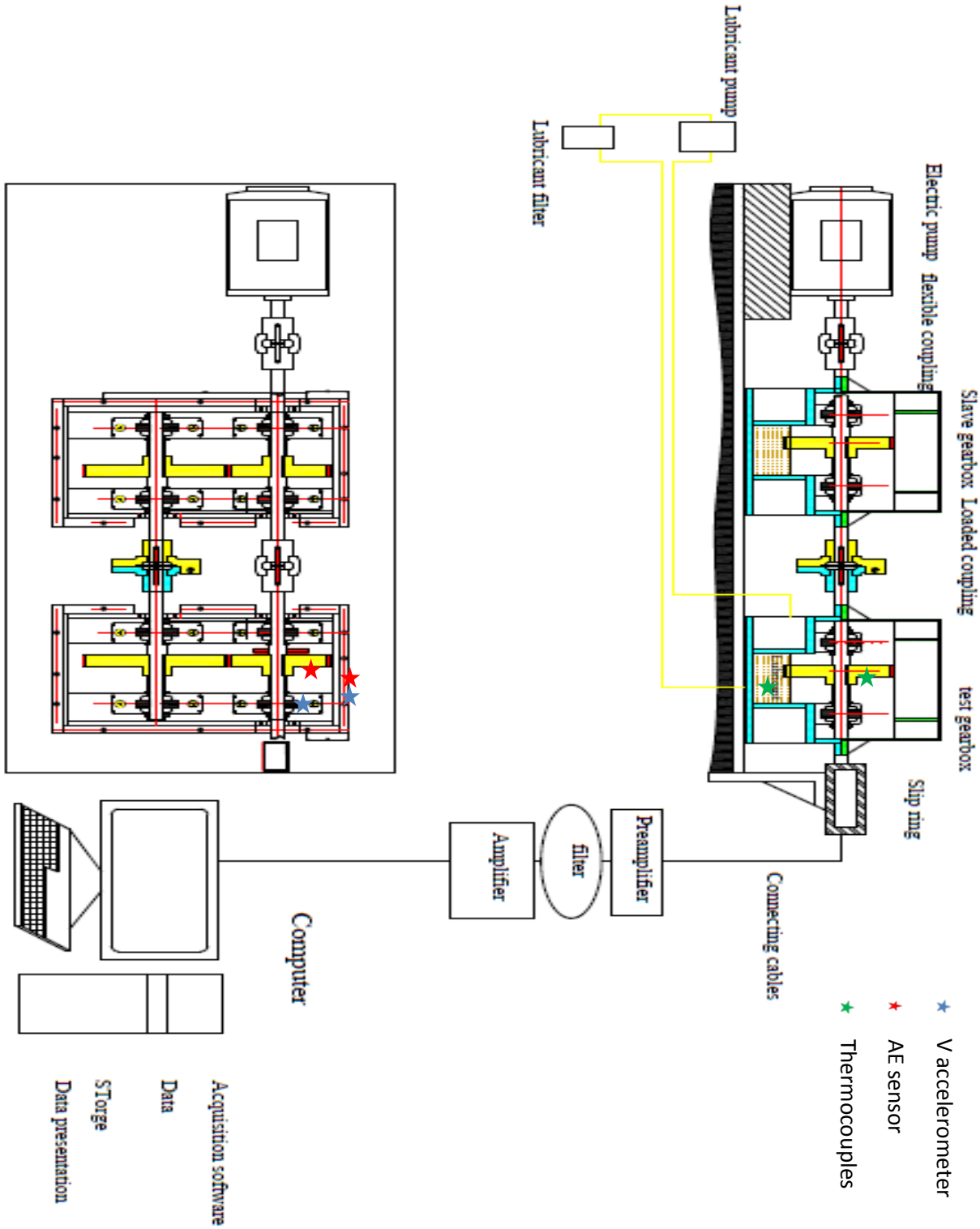

Figure 29: Schematic diagram of the test arrangement

5.1.1 Gears

The helical gears from HPC Gears Limited were used for the experiment. These were 045M15 steel supplied without any heat or surface treatment. The pinion (or driver gear) had 51 teeth and wheel (or driven gear) had 70 teeth. The contact ratio was 1.7 mm and center distance between the pinion and wheel was 171 mm. A 25 mm face width was used for both pinion and wheel during the tests. Table 3 shows the gear specifications.

Table 3: Specifications of helical gears used in the experimental work (Appendix A)

Specification of test gears	Pinion	Wheel
Number of teeth	51	70
Module	3 mm	3 mm
Pressure angle	20	20
Helix angle	17.5	17.5
Contact ratio	1.7	1.7
Face width	25 mm	25 mm
Direction	Right Hand	Left Hand
Hardness	137 Hv30	137 Hv30
Surface roughness	1.327 μm	1.327 μm
Pitch circle diameter	160 mm	220 mm
Size of Addendum	3 mm	3 mm
Size of Dedendum	3.75 mm	3.75 mm

5.1.2 Electrical Motor

A 1 kW AC electrical motor of operating speed 690 rpm was used to power the back-to-back gearbox. The operating speed was measured using a tachometer at the input shaft; the accuracy of the measurements was ±1 rpm.

5.1.3 Lubrication

Splash lubrication was used for the gears during the tests. This is supported by (Drago, 1988.) who claims that splash lubrication is well suited to applications with pitch line velocity less than 25.4 m/s. The pitch line velocity used in these tests was approximately 5.4 m/s which is well below the Drago limit. Mobilegear 636, a high performance oil intended for splash lubrication in gearboxes was used, see Table 4.

Table 4: Specification of the lubricant (Appendix C)

Lubricant properties	Mobil gear 632
Kinematics viscosity at 40 C°	664 (cSt)
Kinematics viscosity at 100 C°	62.8 (cSt)
Viscosity index ASTM D2270	165
Density at 15_ ASTM D4052	0.87

5.1.4 Loading Plates

The back-to-back gearbox arrangement is to contain the torque inside a closed loop system so that ay a steady operating speed the power requirement overcomes frictional losses only (Vayionas, 1991) and (Hamzah and Mba, 2007). The maximum applied torque in this system is 370Nm with an accuracy of + 5Nm. Twisting the loading plates against each other by tightening or loosening a bolt into or out of the threaded hole. This procedure will allow a static torque to be applied across the gearbox, see Figure 30. The loading plate consists of two half flanges bolted to each other; one of the flanges has a threaded hole. The loading plates were calibrated using an optical strain gauge with rosette arrangement mounted at the opposite shaft connecting slave and test pinions together.

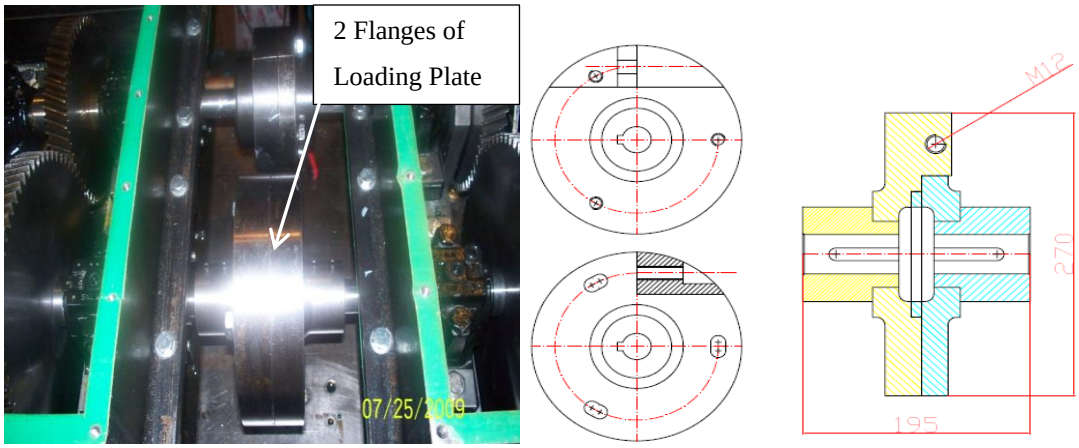

Figure 30: Loading plates

5.1.5 AE Sensors

Physical Acoustic Corporation (PAC) Acoustic Emission wideband (WD, Physical Acoustic Corporation) sensors (with operating frequency range from 100 KHz to 1 MHz were used for the test work. The AE sensors were mounted on the pinion and held in place with superglue.

5.1.6 Thermocouples

K-type (Iron-Constantan) thermocouples - see Table 5 for brief specifications - were used to measure gear metal and lubricant temperatures. Five thermocouples were mounted on the test pinion and one dipped into the lubricant (RS Components Ltd, UK). J-type thermocouple was used and placed inside the oil bath for monitoring oil temperature.

Table 5: K&J-type Thermocouple Specification (Appendix D for data sheet)

Maximum Temperature Sensed	+200°C
Minimum Temperature Sensed	0°C
Probe Diameter	6.35mm
Probe Length	1000mm

5.1.7 Slip Ring

A Moog Components PM-12 80039-950 slip ring with 12 contact channels was used - see Appendix E for specifications. The slip ring was used to transmit the signals from the AE sensor mounted on the pinion to the data acquisition board. Figure s 28, 29 and 31 show the slip ring connected in-line with the input shaft of the gearboxes at the end of the test gearbox.

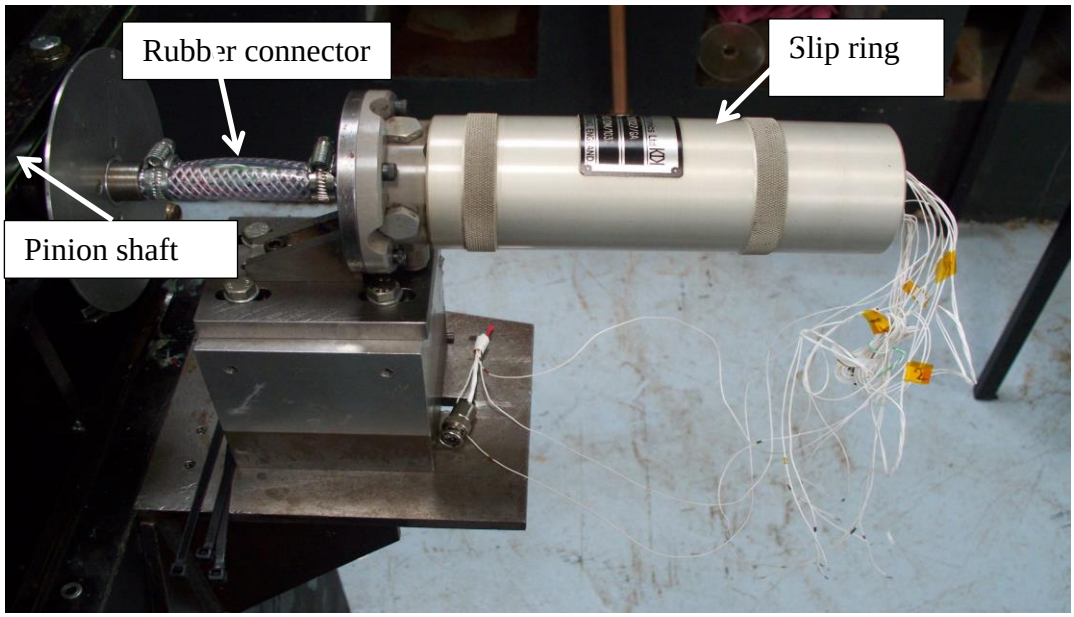

Figure 31: Slip ring

5.1.8 Pre-Amplifier

AE piezoelectric transducers are high impedance sources producing low voltage signals and so require both pre-amplifier and amplifier. A PAC preamplifier made by the 'Physical Acoustics Corporation) was used this has gain settings of 20, 40 and 60 dB. It also has a plug-in filter and single-ended and differential sensor inputs. The AE output signal was fed directly from the pre-amplifier to the data acquisition card using BNC connectors on coaxial cable.

5.1.9 Accelerometers

The accelerometer used for vibration measurement in this experimental work was an Endevco Dynamic Instrument Division ISOBASE Model 236 piezoelectric transducer with operating frequency between 10 and 8000 Hz. One of the accelerometers was mounted on the pinion shaft bearing pedestal and the second was mounted on gear casing, see Figure 39, to record the vibration of the gear system at that point.

.

5.2 Data Acquisition (DAQ) Cards

A Physical Acoustics Corporation PAC PCI-2 16-bit, two channel card was used to continuously acquire the AE signal, from which such parameters as the r.m.s level, Absolute Energy and Absolute Signal Level (ASL) were obtained. The card has a maximum sampling rate of 5 MHz. The system has anti-aliasing filters prior to the Analogue to Digital Converter (ADC) which can be controlled directly from the software. For higher speed data capture a Physical Acoustics Corporation MISTRAS AE DSP-32/16 16 bit 2 channel card with a maximum sampling rate of 10 MHz was used.

5.2.1 Data Acquisition (DAQ) Software

AE-win

AE-win Version E1.62 software developed by the Physical Acoustics Corporation was used to calculate and record the r.m.s , Absolute Energy and ASL of the AE signal. With this package real time calculation of the AE parameters is possible. Each value from the ADC was squared and added into the accumulator by a “hardware accelerator” for the programmed time interval. The r.m.s value was found by taking the square root of the accumulated squared ADC readings. For real time calculations the software has the minimum time driven rate of 10 milliseconds and minimum time constant of 10 milliseconds. The accumulator was cleared at the end of each time interval and then the same process was repeated. The software is capable of recording the waveform at a maximum sampling rate of 5 MHz.

Mi-Tra

With the MISTRAS AE DSP-32/16 card the software used acquire the AE raw waveform data was Mi-Tra Mistras 2001 E1.73. This package has a digital filter of between 10 kHz to 1200 kHz. The pre-amplifier range that the software can accommodate is between 0 dB and 60 dB. The test arrangements are shown schematically in Figure 33.

Lab-view 7.5 software script was used for temperature measurements and display.

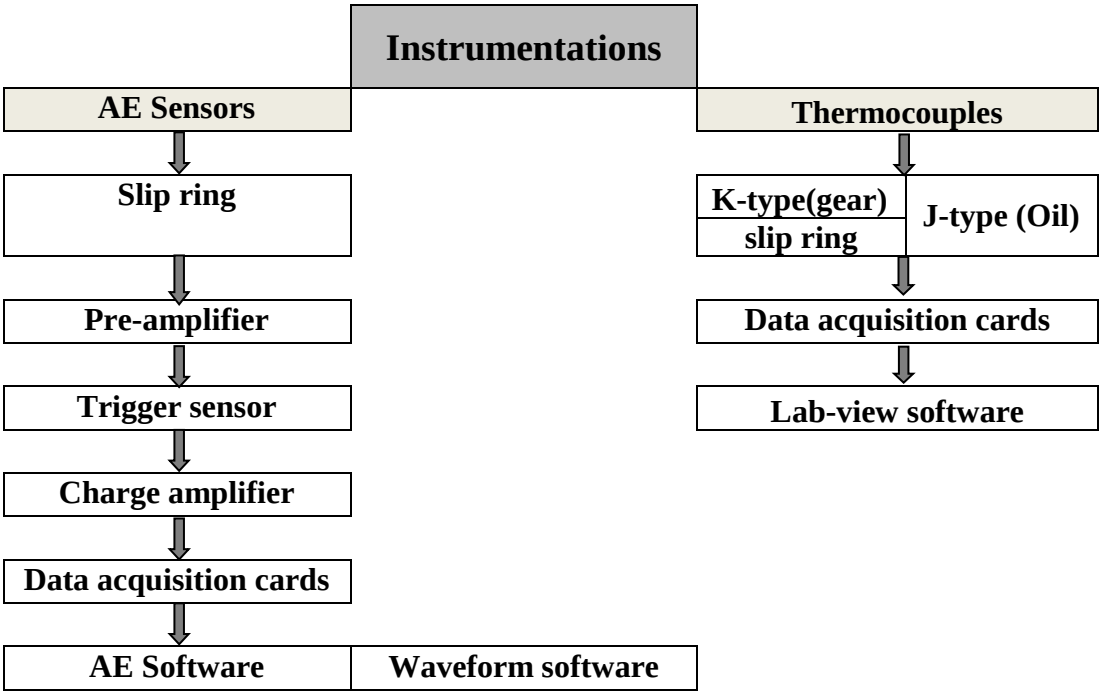

Figure 32: Schematic diagram of the Data Acquisition Systems

5.3 Experimental Procedure

The research was undertaken with Mobilgear 636 lubrication on the helical gear. A load of 370 Nm was used at this stage of the test procedure. Gear data, lubricant properties and operating conditions were as shown in tables 3 and 4.

5.3.1 Capability of AE Technology for Gearbox Diagnosis

5.3.1.1 Comparative Study on Monitoring Methods

This test compares the relative effectiveness of AE and vibration methods for monitoring helical gears defect free and with seeded defects at various operating temperatures. Firstly, a defect free test was conducted to investigate the effect of temperature on the level of the AE and vibration signals and to allow identification of AE features. Secondly, a simulated defect was used to assess the damage detection capability of the AE method.

An initial attenuation test was performed to better understand the AE signal transmission characteristics of the test gearbox. The aim of this test is to ensure transmission of AE signatures from the source to the AE sensor. Furthermore, the Hsu - Nielsen also verify that AE sensors was well connected with being monitored part.

5.3.1.2 Attenuation Test

To establish the attenuation of the AE signal using the well-established Hsu-Nielsen pencil lead break source (BS EN, 2009) was used. Here a 2H lead pencil of 0.5 mm diameter and 3 mm length was snapped in a controlled manner at the different positions shown in Figure 33. The reference signal was taken as that measured for a lead break next to the AE sensor on the pinion gear. Five measurements were made for each test position and then averaged.

The greatest attenuation (exceeding 19dB) was observed when the pencil lead break was on the wheel. This would be expected because of contact losses between teeth surfaces. Relatively high attenuation (about 11dB) was obtained for lead breaks on the bearing pedestal. This would be expected due to the number of interfaces that the AE signature needed to propagate across on its way from source to sensor. The position of the bearing balls in the loaded zone affects attenuation of the AE signal. Better transmissibility can be expected if a ball is in the loaded zone while the AE waves were travelling through. The attenuation values for lead breaks on the pinion were low due to close proximity to the sensor.

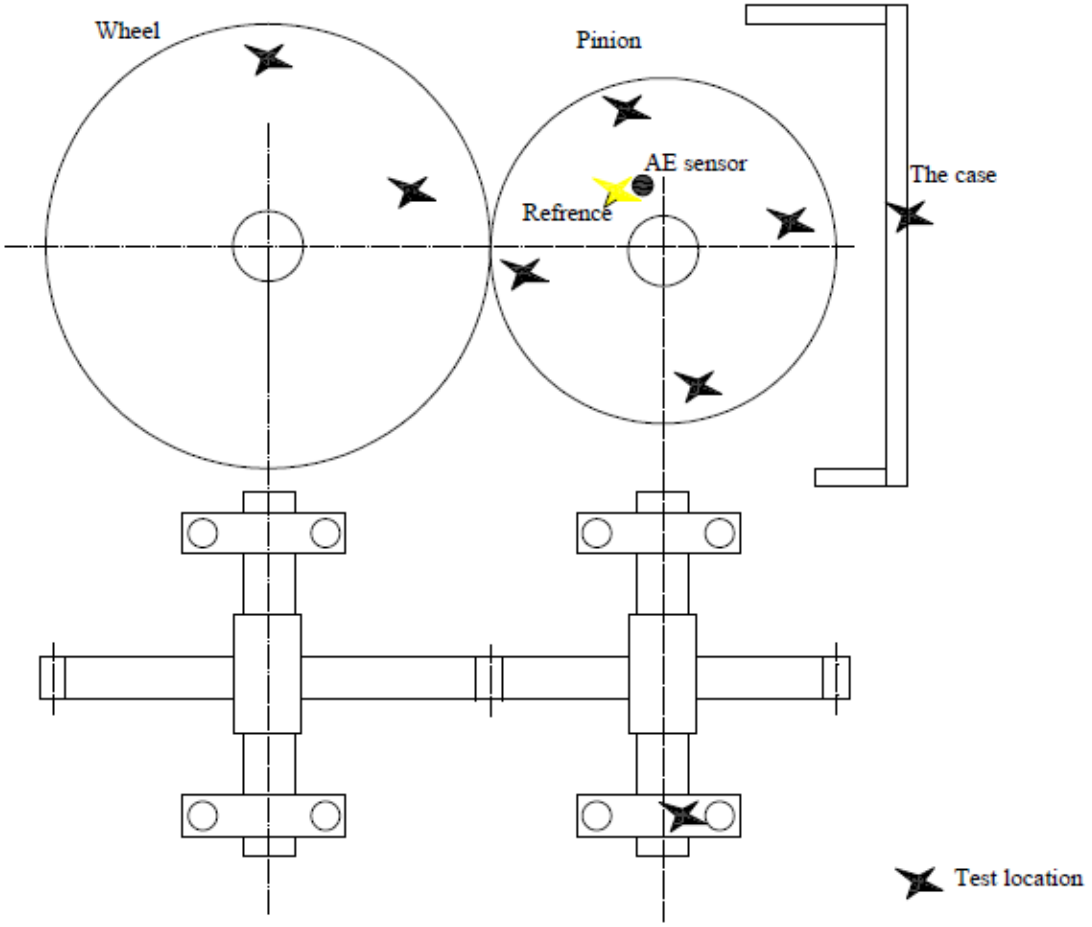

Figure 33: Schematic diagram showing the different test positions at which the Nielsen source was located

5.3.1.3 Seeded Defect for First Test

For the seeded defect test, a pitch line defect was introduced onto a single tooth as a deep rectangular scratch (8 mm long x 3 mm wide x 2 mm deep) as shown in Figure 34. The gearbox was then restarted and the same measurement procedure followed as for the defect free test.

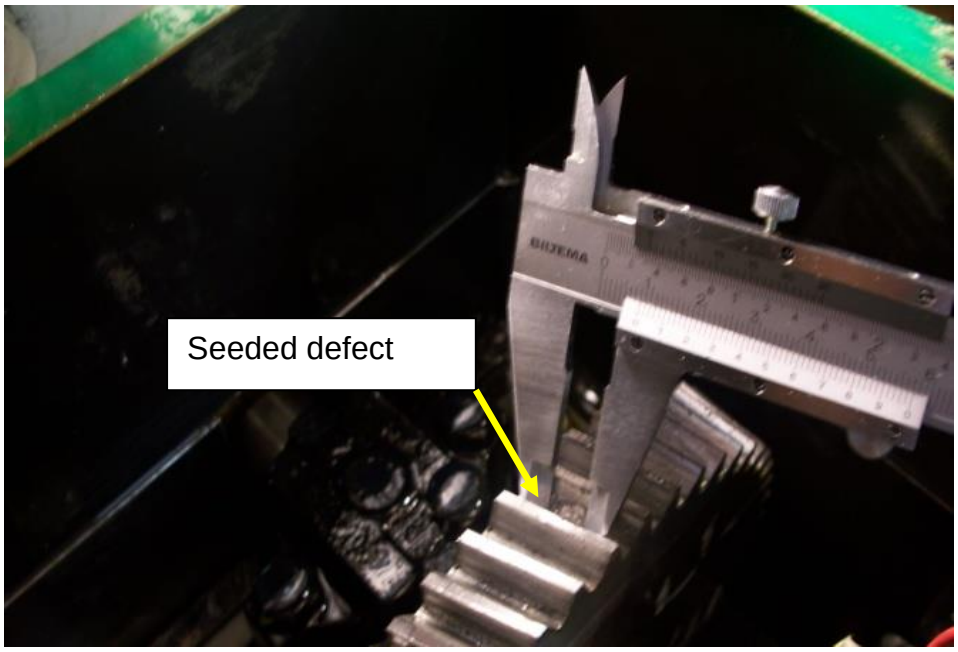

Figure 34: Seeded defect on single tooth

5.3.2 Influence of Lubrication Film Conditions on AE Signal

The purpose of this test was to study the effect of temperature of the lubrication on the AE signal. This could be achieved only using wide range of temperatures, which required the use of liquid nitrogen to cool gear system and thus give a wide range of lubrication film thickness.

This test was performed to better understand the influence of temperature variation on the behaviour of specific film thickness (λ) and resulting generation of AE activities. The assumption is that lubricant viscosity is affected by temperature which thus has a direct influence on type of lubrication regime and specific film thickness (λ) generated during gear meshing (Dowson, 1977).

Liquid nitrogen was used to obtain a large temperature drop (up to 10C per minute). Figure s 35 and 36 show the location and manner in which the liquid nitrogen was sprayed onto the gear wheel. The wheel was chosen as the location because AE signals generated here suffered maximum attenuation and so any macro- and/or micro-structural activity of the gear material due to rapid reduction in temperature during the test would

be minimal at the sensor. Gear temperatures were reduced by spraying liquid nitrogen at the cylider pressure of 2 bars through the nitrogen gun made an angle of 45^{o} with the wheel surface. The tip was placed as close as possible to the wheel (approximately 5 mm), see Figure 36. (Hamzah et al., 2008) has demonstrated this is necessary to avoid freezing the oil mist and forming oil crystals which generates unwanted AE activity when crushed inside the gear mesh.

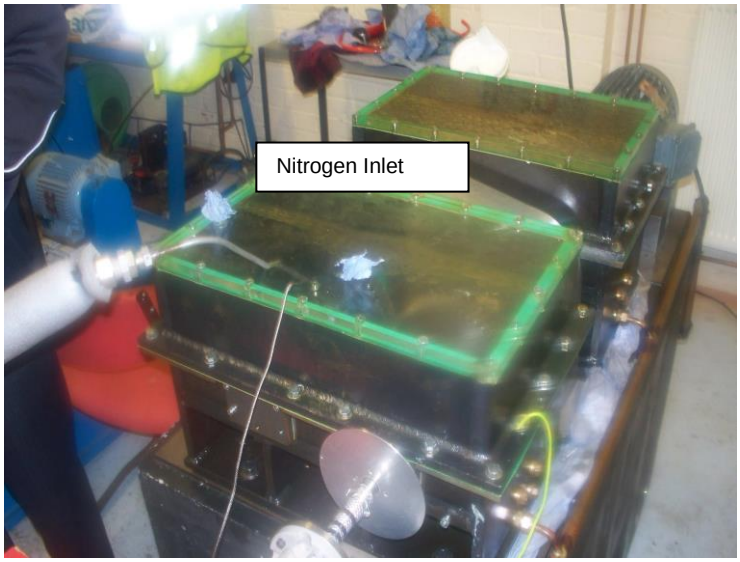

Figure 35: Cooling arrangement showing nitrogen gun nozzle

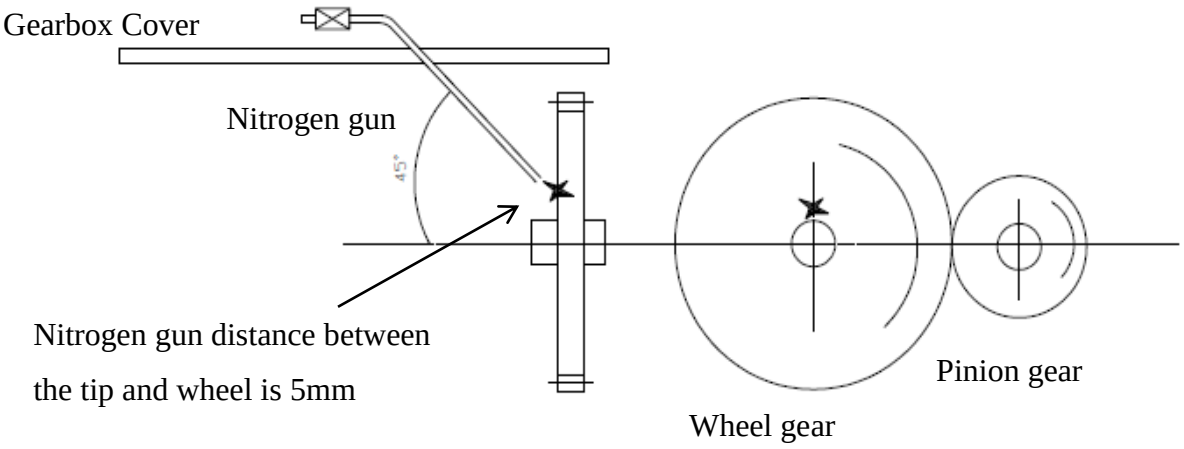

Figure 36: Liquid nitrogen gun location and gear wheel

And this is the brief View of testing methods:

5.3.2.1 Influence of Temperature Variation on AE Activity

The gearbox was run until the temperature stabilized at about 43°C (with a change of no more than ±1°C over an hour). The gearbox ran for a total time of about 4 hours at 370Nm load and speed 690 rpm. To remove heat and reduce the temperature, liquid nitrogen was spraying, approximately at rate of 10˚C per minute, onto the wheel through a 5 mm diameter steel pipe, see Figure 37. After about 10 minutes and when the thermocouple on the pinion recorded a temperature of 0^{o}C, the supply of nitrogen was stopped. The gearbox was then run continuously during which time the temperature increased until it was at about the same level as when the nitrogen flow commenced. This procedure was repeated three times to reduce random errors and ensure more accurate results.

5.3.2.2 Diagnosis During Dry and Lubricated Contact

To obtain dry contact for the start of the test the lubricating oil was sucked out of the gearbox using suctions pump, and it was run dry for about five minutes. Oil was then injected into the gearbox, the gearbox was running, which continued to run until both the gear and lubricant oil reached a steady temperature (40°C), After that test followed same procedure as described in previous test.

5.3.2.3 Defective Gear Diagnosis During Dry and Lubricated Contact

To investigate the effect of oil regimes on defect detection using AE signals a defective gear was used, see Figure 37. The test followed same procedure as described above.

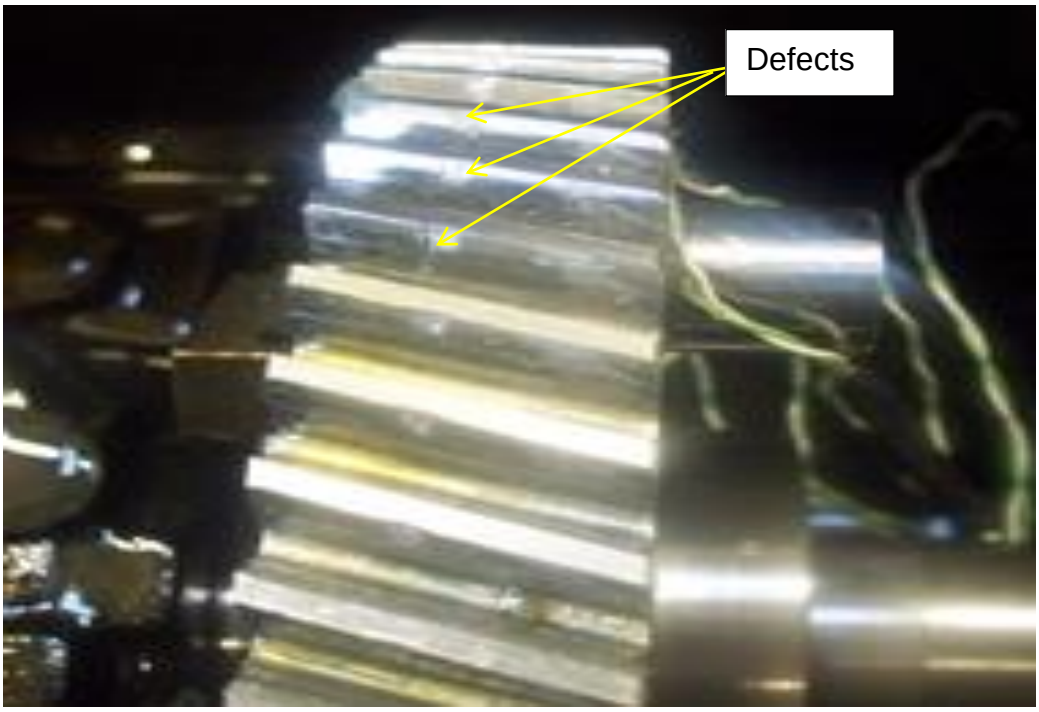

Figure 37: Defective gear

Figure 38 shows a schematic diagram of the experimental procedure and Table 6 shows the tests carried out in this project.

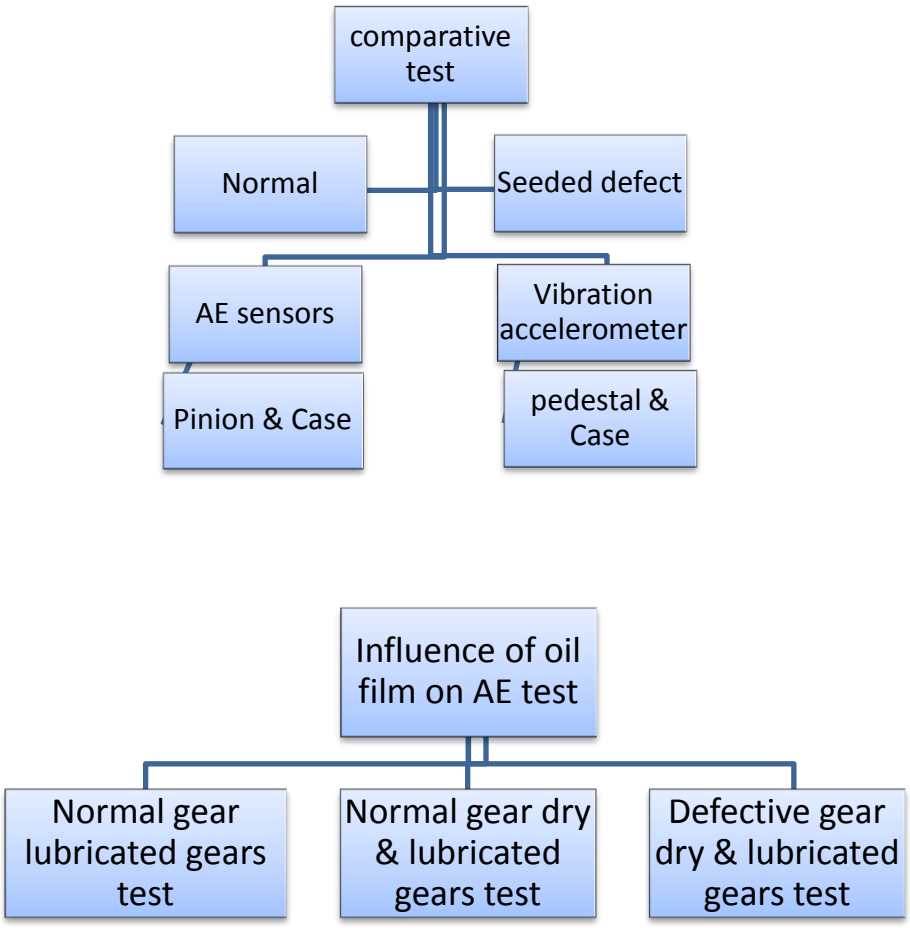

Figure 38: Schematic diagram of the experimental procedure

Table 6: Experimental stages

Process	Dry run	Oiling run Till stabilization of temperature	Cooling run using nitrogen till 0°C	Warming up
1		Comparative test First test		
3	Influence of oil film on AE Second test, Third test and Fourth test			

Chapter 6

Results and Discussion

6 Results and Discussion

6.1 Capability of AE Technology for Gearbox Diagnosis

Comparing AE activity from defect free and simulated defect conditions under varying loads and/or speeds can be very misleading if the effect of oil temperature is not considered. Previous studies related to gearbox diagnosis with AE have shown that the oil temperature affects the AE signal because lubricant temperature is an influential factor in AE generation (Tan and Mba, 2005a; Hamzah et al., 2008). These changes in the AE activity due to change in oil temperature have significant consequences that require more research work to develop AE as a robust diagnosis tool that includes temperature effects and so reduce errors.

6.1.1 Test Instrumentation and Procedure

Two wide-band AE sensors were used throughout the tests. One sensor was placed on the pinion (first channel) and the other on the gearbox casing (second channel) as shown in Figure 39. The cable connecting the sensor placed on the pinion with the pre-amplifier was fed into the shaft and connected to a slip ring placed at the end of test gearbox. This arrangement allowed the AE sensor to be placed as close as possible to the gear teeth. Both sensors were held in place using super glue. AE signals were pre-amplified at 60 dB for both sensors. A PH-12 slip rig manufactured by 'IDM Electronics Ltd' was used. The slip ring used silver contacts and could accommodate up to 12 channels. AE sensors were of differential type with a relative flat response of between 100 kHz and 1 MHz. AE was recorded with MISTRAS AE DSP-32/16 data acquisition card at a sampling rate of 5 MHz. Accelerometers (ISOBASE 236 Endevco) used had an operating range of between 10 Hz and 8 kHz.

Figure 39 shows the way the accelerometers were mounted, one mounted on the bearing pedestal of test gear and the other on the gearbox casing. All vibration data was recorded at a sampling rate of 10 kHz. J-type thermocouple, rated from -60 C° to +850 C° was placed inside the oil bath to monitor the temperature during the experiment see Figure 37. It was important that any data recorded was taken from a well-defined

circumferential point at every revolution because this experiment focused on assessing the applicability of AE for identifying seeded defects on helical gears. For this reason, an optical triggering mechanism was used. The triggering system consisted of metal disk with 2 mm diameter hole and an optical sensor. Each time the hole passed through the optical sensor the AE and vibration acquisition systems were triggered.

An Analogue-to-digital converter (ADC) controlling software was used to calculate continuous AE r.m.s values in real time. The hardware accelerator used by the software enabled the calculations of the AE r.m.s in real time. Each value from the ADC was squared and added into the accumulator by the hardware accelerator for a programmable time interval, 90ms in this case which corresponds to very slightly below one complete revolution of the pinion at the rotational speed (690 rpm). To calculate the r.m.s , the square root of the accumulated squared ADC readings was used. The accumulator was reset at the start of each new time interval and the same process was repeated. The time interval for the acquisition was set at 90 ms.

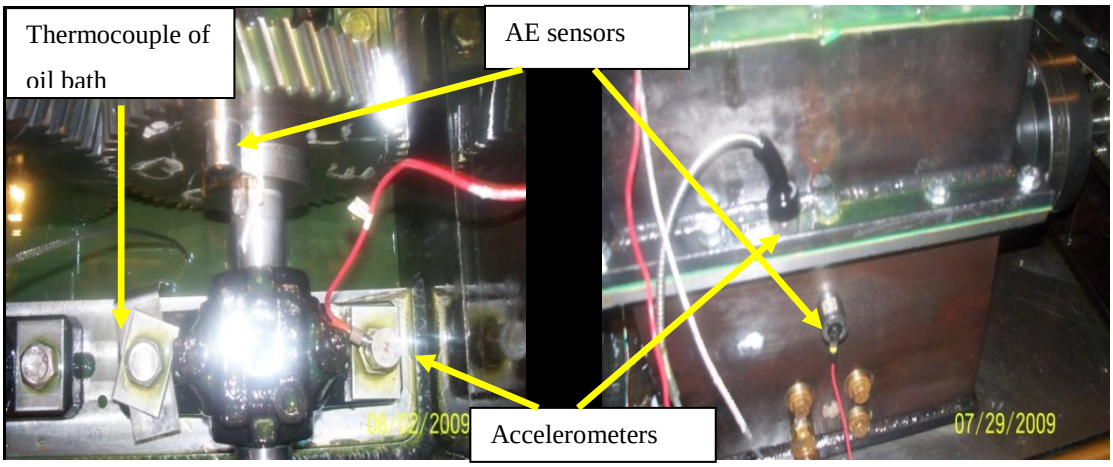

Figure 39: AE and vibration sensors locations

The defect free gearbox was run at a given load and speed (370 Nm and 690 rpm respectively) for a period of 5 hours so that the gearbox reached a stable temperature. The acquisition time window of 16 teeth was set for which the trigger mechanism allowed an acquisition duration of 0.0256-s, which corresponds to 16 teeth at 690 rpm for each set of

data. At the beginning of the test, when the oil was still at room temperature, a defect free recording of AE and vibration was undertaken. The instantaneous recording was made to allow the influence of temperature on the levels of AE and vibration to be investigated. The AE and vibration signals were then recorded with the gearbox running at each 3^{o}C rise in temperature of the oil bath until the temperature stabilized at 54^{o}C. To check repeatability, the tests were carried out twice. In order to introduce the seeded defect, the test rig was stopped and the defect introduced, see Figure 34. The gearbox was then restarted and the same procedure was followed for the seeded defect run.

6.1.2 Results Based on Acoustic Emission AE Monitoring

The AE sensors on the pinion and gearbox casing were synchronized, so that when the data acquisition system was triggered, both AE sensors captured data simultaneously. Figure 40 shows typical waveforms for the defect free condition at 370 Nm. Continuous type AE waveform is dominant although transient AE bursts whose amplitude considerably exceeds the underlying continuous wave can be seen (Don't forget a "continuous" AE waveform is a series of bursts of similar amplitudes so close together that they cannot be separated). The frequency of the periodicity of these AE bursts represents the number of meshing teeth within the acquisition window. This is similar to the observations of (Tan and Mba, 2005a) who studied AE waveforms in spur gear meshing in which both continuous and transient type fo r.m.s of AE activity were apparent. Tan and Mba concluded that rolling contact on the pitch line of the spur gear mesh was responsible for generating high amplitude AE transient bursts, whilst sliding contact generated a large portion of the continuous waveform. In the case of the helical gears, contact between a specific gear pair begins as a minute contact point which increases in contact length as the pair engage while decreasing contact length occurs as the pair disengage. The contact length varies along the pitch line of the helical gears but in spur gears the contact length remains constant. Furthermore, the continued variation in the contact length during meshing of helical gears directly influences the load conditions experienced by the gear and leads to instantaneous changes in oil film thickness (Hamzah and Mba, 2007). Thus, AE waveforms associated with helical gear meshing are expected to be of the continuous type with amplitude variations attributed to the gear mesh length, see Figure 40.

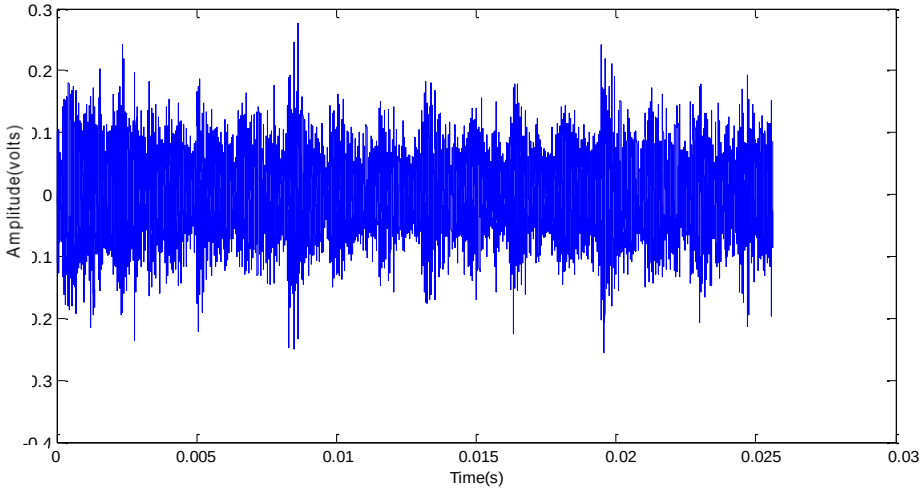

Figure 40: AE waveform associated with a defect free condition

Typical AE waveform associated with defected tooth is shown in Figure 41. The relatively large transient AE bursts associated with tooth meshing are clearly seen over the continuous AE levels. The transient AE bursts were observed to originate in the region of the tooth where the defect was seeded. Such observations were not observed in a similar test with spur gears; that means the seeded defects were not evident in the waveforms (Toutountzakis and Mba, 2003; Tan and Mba, 2005)

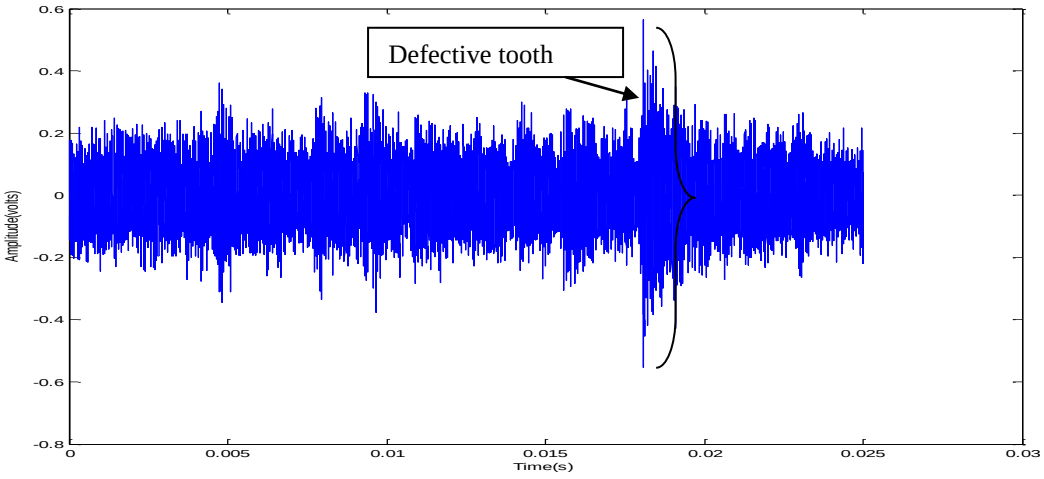

Figure 41: AE waveform associated with a tooth defect

The variation in the oil temperature with the operating time is shown in Figure 42. It is clear that there was no significant difference in oil temperature between the fault free and seeded defect conditions. Thus AE data was for the two conditions was acquired at the same temperatures.

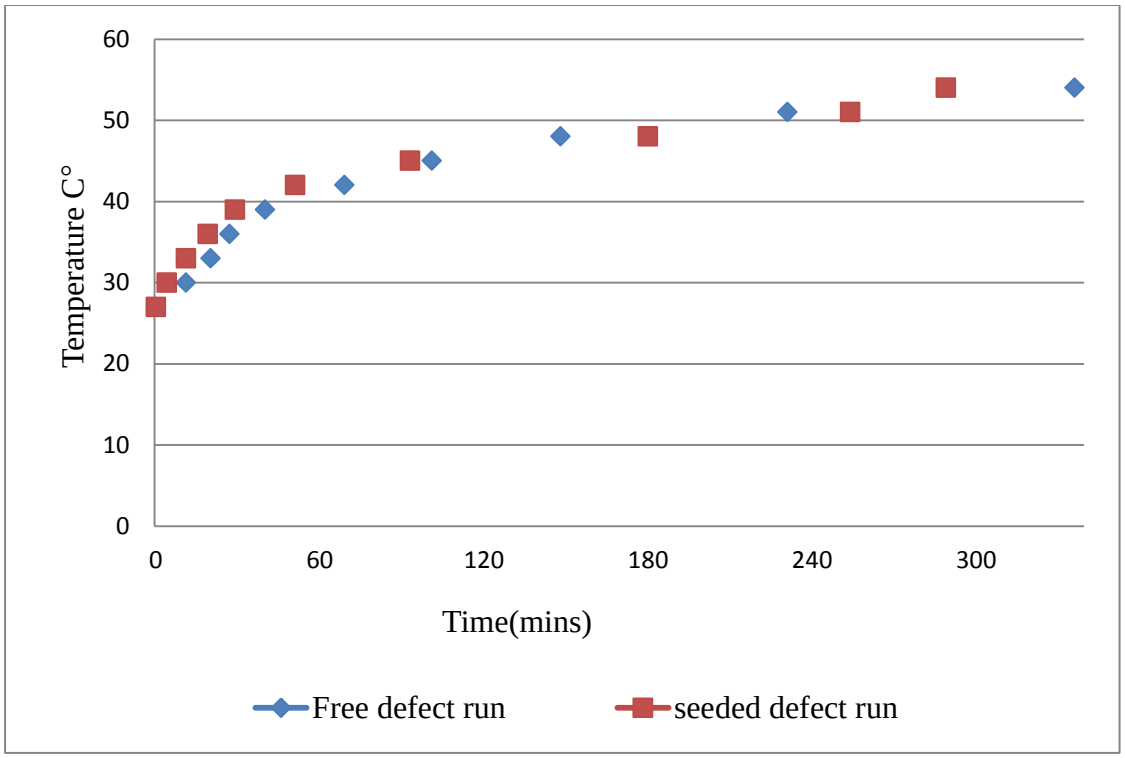

Figure 42: Oil temperature with time; defect free and with seeded defect

In both the cases, the oil temperature increased at a faster rate in the first hour after which the rate of increase reduced. Note that it took the gearbox system at least 5 hours of continuous running to reach a stable temperature.

Figure 43 shows the r.m.s value of the AE signals with temperature for both channels. For the AE sensor placed on the pinion (first channel) it can be seen that the AE r.m.s levels with the seeded defect increased as the oil temperature increased. In the defect free test it was noted that the AE r.m.s value for the sensor on the opinion grew at the start of test resulted to increase in oil temperature, this increase enabled the increase in asperities contact, and when oil thermal stabilised led to the stability in AE r.m.s .

The increase in AE r.m.s was progressive in seeded-defect case. This trend of AE r.m.s with oil temperature shows the presence of the simulated defect in the gear tooth. This increase in AE r.m.s was attributed to pinion tooth defect contact with wheel teeth due to decrease in oil film thickness in the contact area.

The AE r.m.s levels measured by the sensor on the gearbox casing (second channel) did not vary with temperature in the same manner as noted with the sensor on the pinion. This is due to dissipation and attenuation of the signal during transmission before it was received by this sensor.

The relation between AE absolute energy and oil temperature for both AE signals channels for both free/seeded defect tests are shown in Figure 44. As expected the AE energy for the first channel increased with the oil temperature in the case where the seeded defect was present and, again, no specific trend was seen with the second channel.

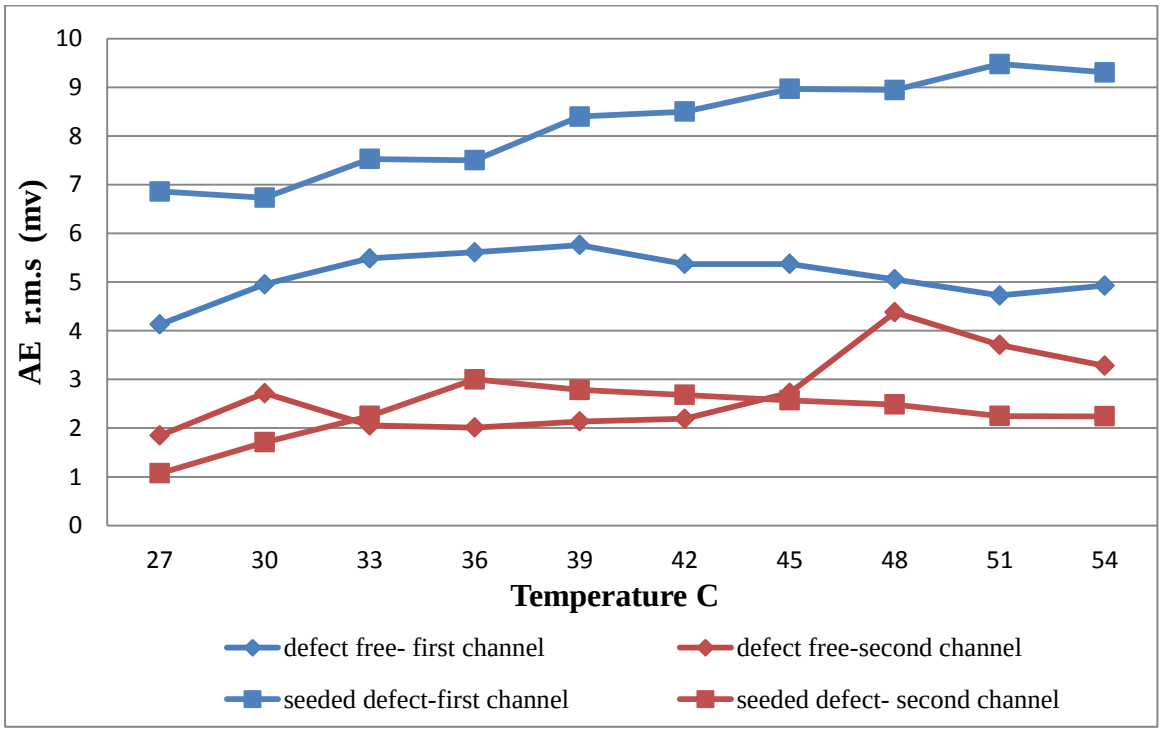

Figure 43: AE r.m.s values at each sensor with oil temperature

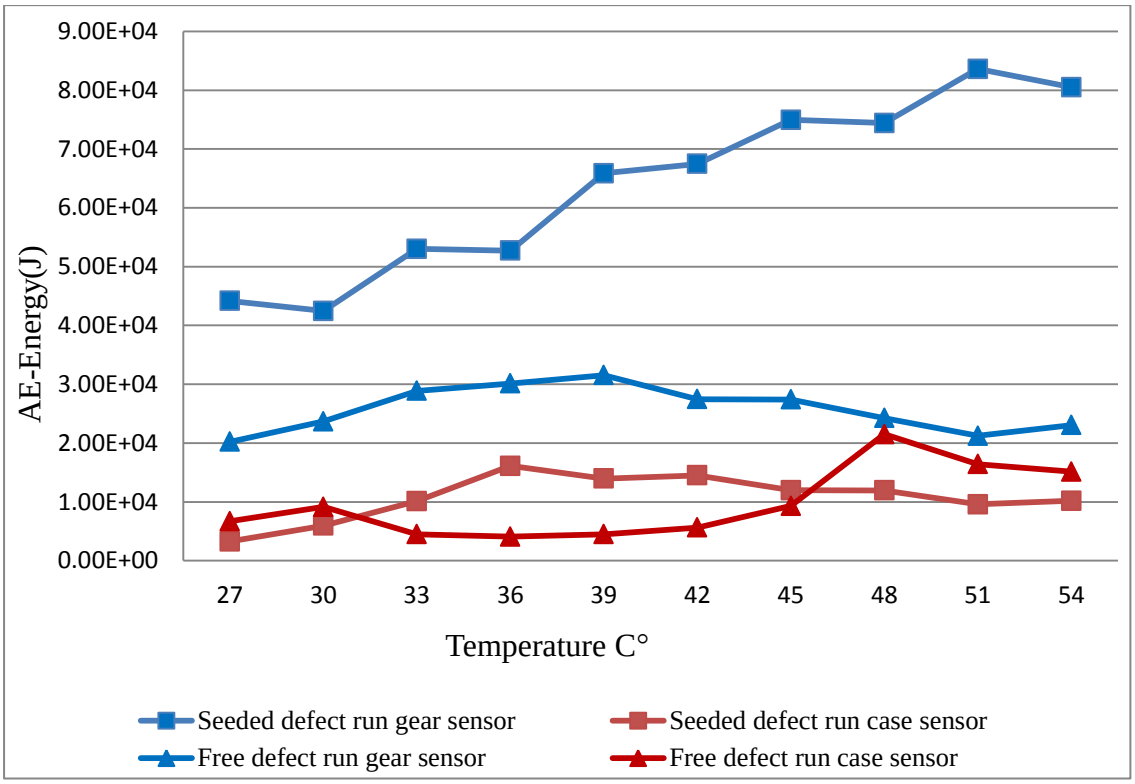

Figure 44: AE Energy values at each sensor with oil temperature

The Kurtosis (KURT) and Crest Factor (CF) of the AE signals are shown in Figure 46a and 46b, respectively with and without the seeded fault and with change in oil temperature (first channel). Both K and CF are measures of the peaks in the spectrum and would be expected to increase with the seeding of the defect. From Figure 46a it can be seen that the K value for the defect free test shows very little variation with temperature. However, the K value when the seeded defect is present shows a clear ascending trend, especially above an oil temperature of 36^{o}C. This was attributed to the increase of oil temperatures giving a decrease in the oil viscosity led to the decrease in the oil film thickness in contact area of the gear mesh.

Similar trends are observed with the CF, see Figure 46b. At lower oil temperatures CF and K values are not significantly different but above 36^{o}C the CF shows a clear indication of the presence of a defect.

It was concluded that both Kurtosis and Crest Factor provided an upward trend with oil temperature reflecting the presence of a fault and thinning of the oil film under a fixed load and speed conditions.

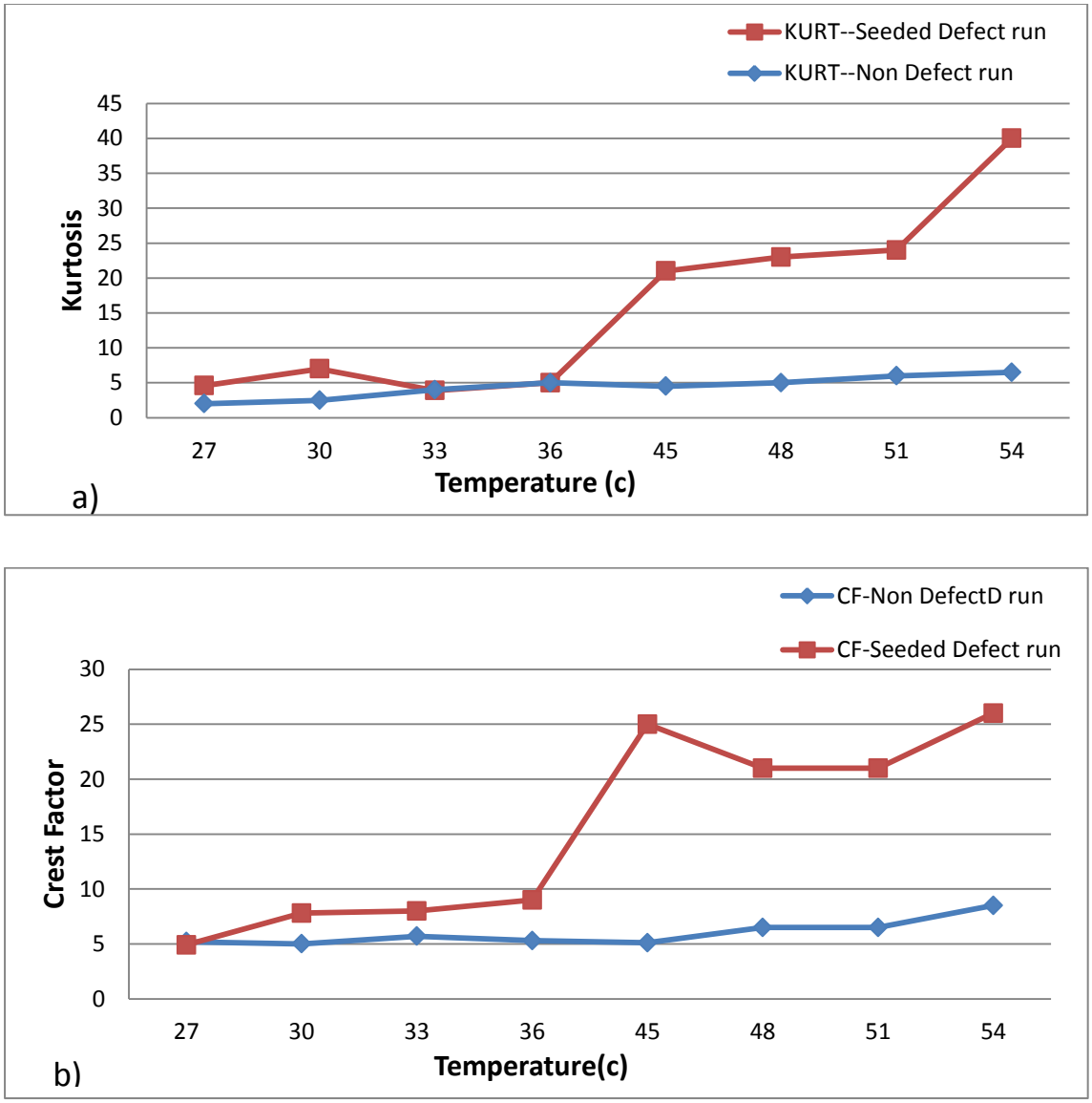

Figure 45: Statistical parameters of the AE first channel signals, a) kurtosis and b) Crest Factor.

It can be concluded from the results presented here that for constant speed and load, increasing oil temperature in the gear system or introducing a tooth fault had negligible effect on vibration r.m.s as measured at both the bearing pedestal and gearbox case.

The AE measurements made by the sensor on the gearbox casing also showed no significant change with seeded defect or change in oil temperature. This was attributed to high attenuation of AE signal before reached the sensor.

However, for the sensor on the gear, increasing oil temperature with the seeded fault had a considerable effect on Kurtosis and Crest Factor. Above 36^{o}C both these statistical measures gave a strong and positive indication of the presence of a defect.

6.2 Influence of Lubrication Film Conditions on AE

6.2.1 Test Instrumentation and Procedure

The AE sensor was placed near to the tooth root of the pinion gear as shown in Figure 47.

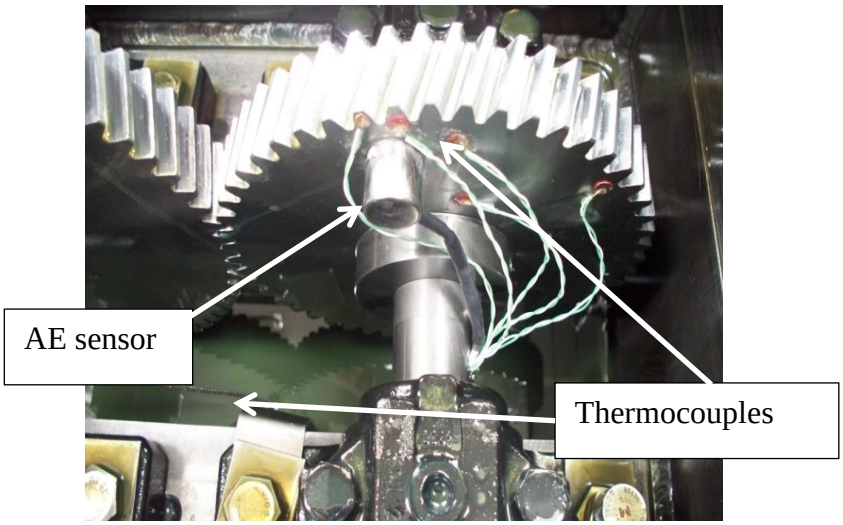

Figure 46: Locations of the AE sensor and thermocouples

This test involved observing AE generation levels under elastichydrodynamic (EHL) and hydrodynamic (HL) conditions.

Prior to the start of this test the gearbox was run for a period of 4 hours at 370 Nm load and a speed of 690 rpm until the temperature reached thermal balance, in this test was

about 43°C (-/+ 1°C). The liquid nitrogen was sprayed onto the rotating wheel gear through angled pipe so that no nitrogen directly impinged on the meshing area. While the nitrogen liquid was being sprayed on to the wheel, the temperature and AE r.m.s was measured in real-time, and AE waveforms were captured at different instances during the test. The flow of liquid nitrogen was halted when the temperature of the metal of the gear reached 0°C. After the supply of nitrogen was stopped the gearbox was allowed to continue operating hence the temperature of the lubricant increased gradually to about the same level as before the liquid nitrogen was introduced.

The AE r.m.s was measured and recorded in real time with a constant time of 100 ms and at a sampling rate of 10 Hz. AE waveforms were recorded every 30s at a sampling rate of 5 MHz. The AE waveforms captured represented approximately one revolution.

The oil viscosity at the measured pinion temperature was calculated using MacCoull's equations (Alexander, 1992). The film thickness was calculated from the measured gear temperature, and specific film thickness (λ) for gear metal was obtained by dividing oil film thickness by composite surface roughness ($\sigma_{r.m.s}$),(Dowson, 1977; Dowson, 1995). It was assumed the surface roughness remained constant ($\sigma_{r.m.s} = 2.5\ \mu m$) throughout the experiment.

6.2.2 Observations of AE Under Lubricated Conditions

Figure 48 shows a typical plot of temperature, specific film thickness and AE r.m.s as a function of time. It can be seen that at the start of the test (after the gear had run for about 4 hours and the operating temperature was stable the AE r.m.s level was constant for approximately 500s at about 0.155 Volts, see region A in Figure 48. The corresponding calculated specific film thickness remained below 1 during this period, corresponding to an EHL regime (Dowson and Ehret, 1999; Hamzah et al., 2008).

The instant the cooling nitrogen gas was applied (500 seconds into the test) there was a decrease in gear metal temperature and a rapid fall in AE r.m.s . However, this rapid fall was pre-empted by an initial rise in AE between 500 to 650 seconds, see Figure 48, which was attributed to the influence of the cooling on the microstructure of the gear metal. The drop in AE levels from 650s was a direct result of the increasing viscosity and film thickness of the oil film at the mesh. The AE r.m.s reached its minimum,

approximately 0.12 Volts when specific film thickness was at its maximum, λ= 9.9. The nitrogen supply was stopped when the gear temperature reached 0˚C. The gearbox continued operating and as such the temperature of lubricant and metal gradually returned to their initial levels, with a corresponding increase in AE levels as the specific film thickness decreased with an increase in temperature, see region C in Figure 48.

Samples of the AE raw waveforms captured at different times during the test are shown in Figure 49. For normal operating conditions (before cooling) the AE waveform showed transient bursts superimposed on a continuous waveform. The rate of generation of the transient bursts corresponded to the gear mesh frequency, see waveform A in Figure 49. Over the time period associated with region B the AE waveform amplitude decreased as specific film thickness increased and the AE bursts were less visible. Waveform C was captured at the minimum temperature region, region C in Figure 49, where specific film thickness was a maximum. At this point the captured waveform showed the lowest amplitude of the AE waveform. It was also noted that the transient bursts were hardly distinguishable from the continuous emissions from background noises such as oil film friction between mating surfaces and supporting bearings in the gearbox.

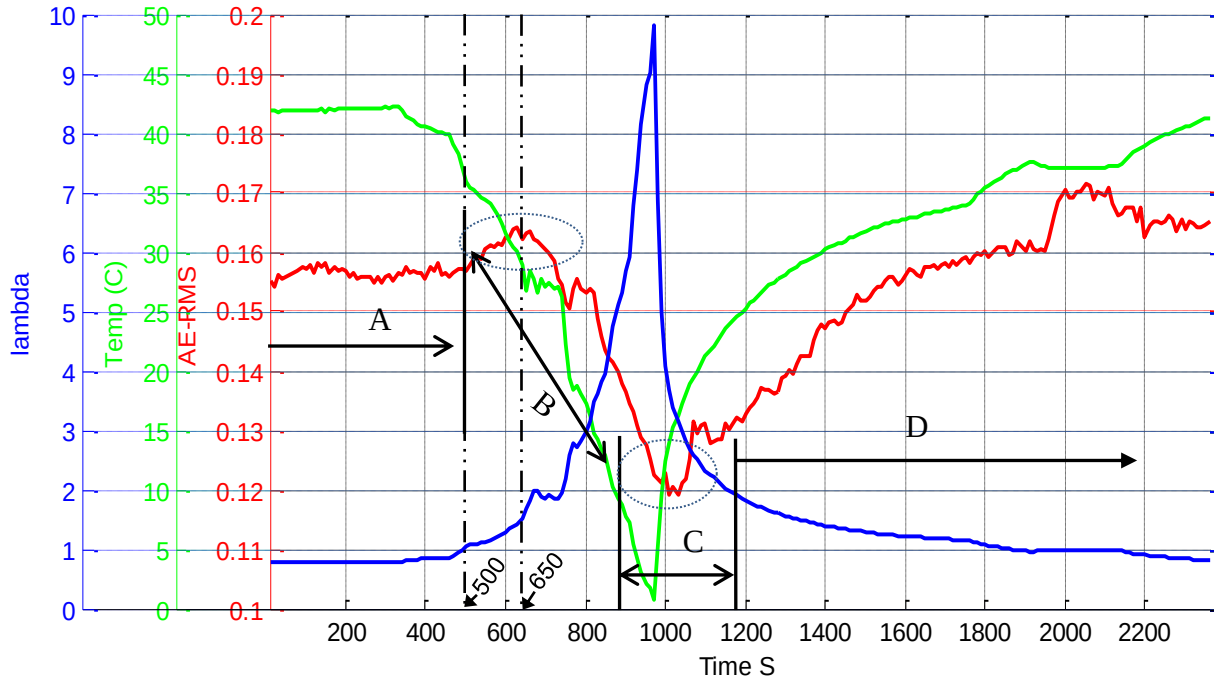

Figure 47: Gear temperature, specific film thickness and AE r.m.s with lubrication regime (system started dry, then oil was added and then system cooled).

The reduction in AE amplitude was attributed to there being no asperity contact at the gear mesh due to increased oil film thickness, similar to what occurs under the hydrodynamic lubrication (HL) regime. At this point the predicted λ value was 9.5, which is considered to be in the HL regime. (Boness et al., 1990; Hamzah et al., 2008) have concluded that asperity contact was non-existent under the hydrodynamic lubrication regime. However, even under HL conditions it is known that shearing of the oil film can generate AE. (Mirhadizadeh and Mba, 2009) have confirmed that in a properly maintained HL regime a principal source of AE is the friction in the shearing of the lubricant. After cooling, the system was allowed to return to its original operating conditions and the levels of AE increased as the lubrication regime moved from HL to EHL.

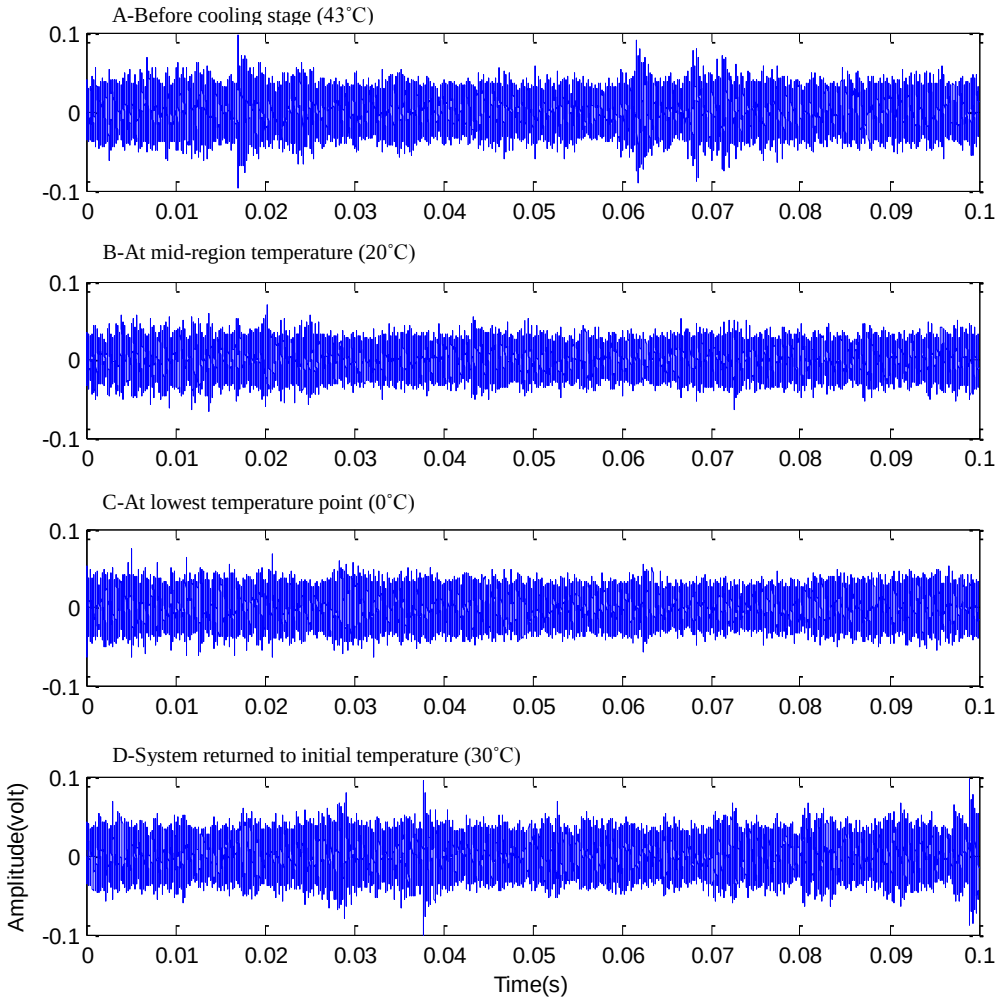

Figure 48: Influence of gear temperature and specific film thickness on AE waveforms (the waveforms corresponded the regions in Figure 48)

As the temperature of the gears increased and the specific film thickness reduced and the transient AE bursts were again observed in the waveform, see waveform D in Figure 49. This confi r.m.s that the lubrication regime had moved from HL back to EHL.

In conclusion: the results showed the AE levels could be used to identify the lubrication film regimes. A reduction in specific film thickness resulted in an increase in AE r.m.s levels and increasing the specific film thickness significantly reduced AE r.m.s levels. The results confirm the potential of AE technology to predict and quantify lubrication film regime under different operating conditions of helical gears.

6.3 Diagnosis During Dry and Lubricated Contact

6.3.1 Test Instrumentation and Procedure

This test used the same test-rig setup (Figure s 28 and 29) but the procedure for this test involved extracting lubricating oil from the gearbox. To achieve fully dry running conditions the gear teeth surface and gearbox housing were thoroughly cleaned with acetone. The test began by running the gears dry for a period of three minutes after which oil was slowly injected so that the boundary (BL), elastohydrodynamic (EHL) and hydrodynamic (HL) regimes could be established in succession. The oil was injected through a funnel which was positioned directly above the wheel gear but not at the position at gear mesh. After the oil returned to its normal level the same procedure was used in previous test.

The AE r.m.s and AE waveforms at the pinion were measured and recorded at the measured pinion temperature in the same way as in the tests described above. Also as above, the oil viscosity at the measured pinion temperature was calculated using MacCoull's equations.

6.3.2 Observations of AE Under Dry and Lubricated Conditions

Figure 50 shows AE r.m.s , specific film thickness and temperature as a function of time as the gears go through unlubricated to HL regimes. The rapid rise in the r.m.s value of the AE signal approximately 1.8 Volts during the initial stage of testing, was due to meshing of the unlubricated gears, see region A in Figure 50. Normally under this condition metal to metal contact dominates. The plot A in Figure 52 shows the AE waveform for dry conditions, it can be clearly observed that the high levels of AE were modulated by the gear mesh frequency. In unlubricated conditions the load is carried by tooth surface asperities which increase friction, energy loss and leads to excessive vibration and destruction of gear teeth (Tan and Mba, 2005a). The gears were run dry for 180s before the addition of a lubricant.

Oil was continuously added to the rotating gear wheel gear at rate of 10 ml/sec via a slot in the top gearbox cover. Once the oil touched the wheel teeth and entered the contact

area the AE r.m.s decreased rapidly reaching about 0.16 Volts, see region B in Figure s 50 and 51. This drop in AE r.m.s was a good indication that the addition of the oil had created a sufficient oil film to reduce asperity contact.

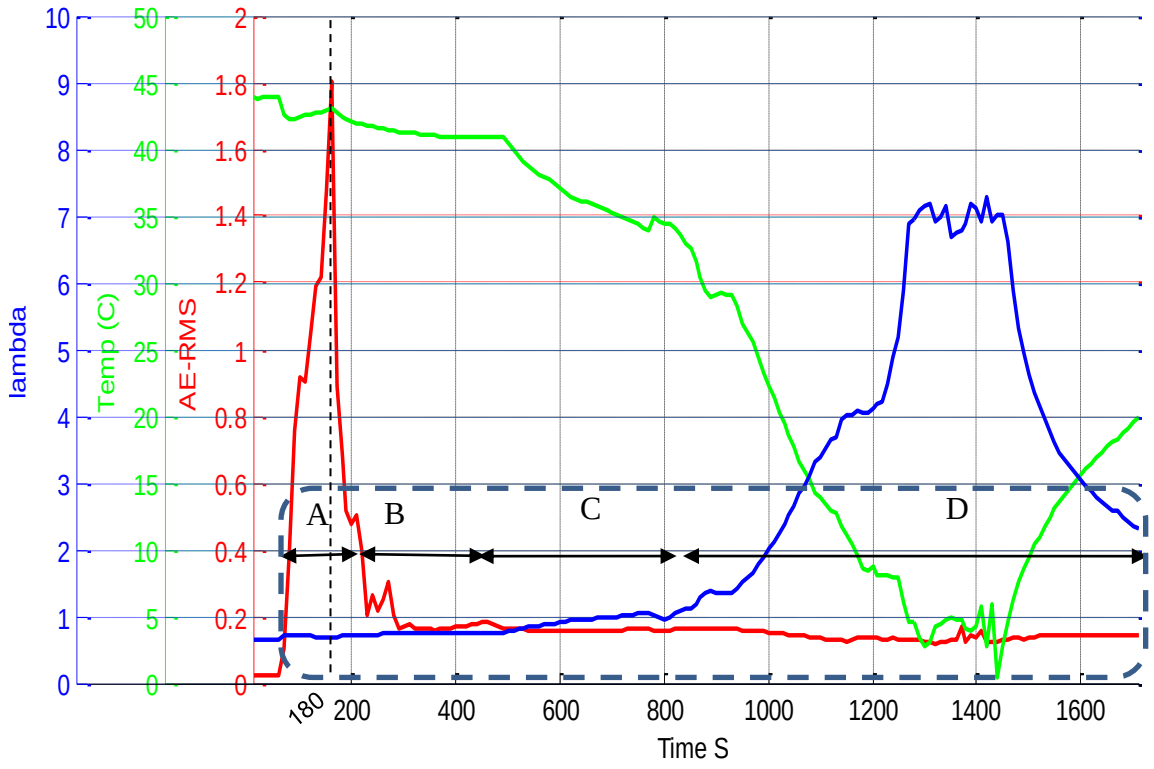

Figure 49: Influence of gear temperature and specific film thickness on AE r.m.s (system started dry, then oil was added and then system cooled).

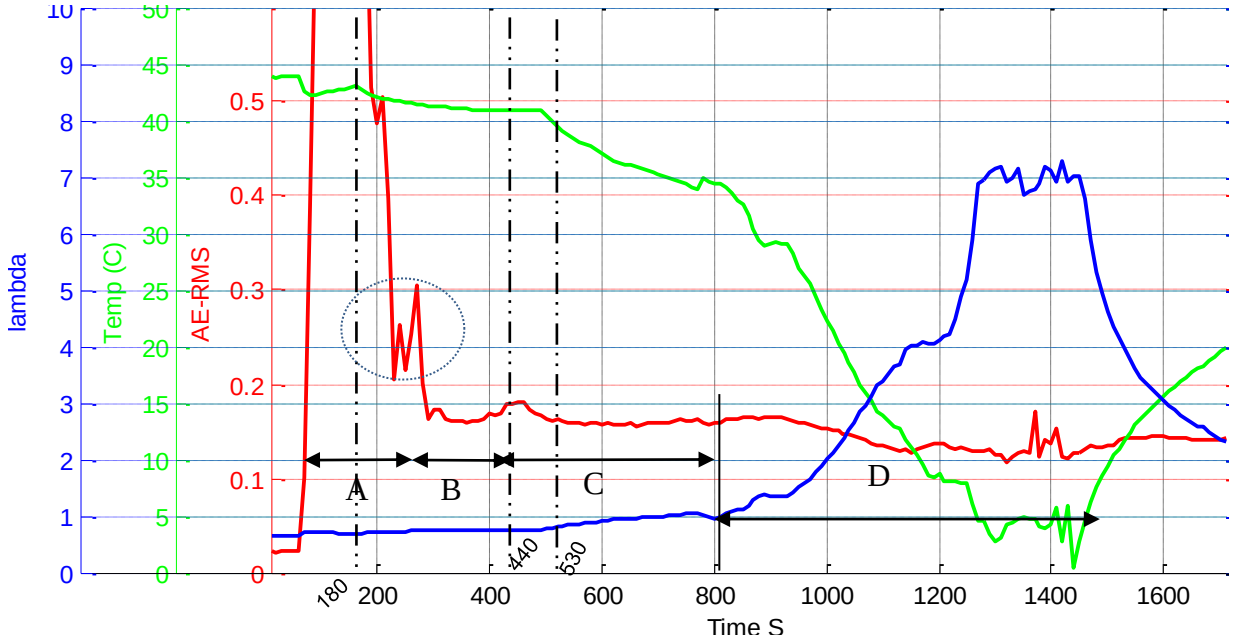

Figure 50: Gear temperature, specific film thickness and AE r.m.s as Figure 50 but enlarged

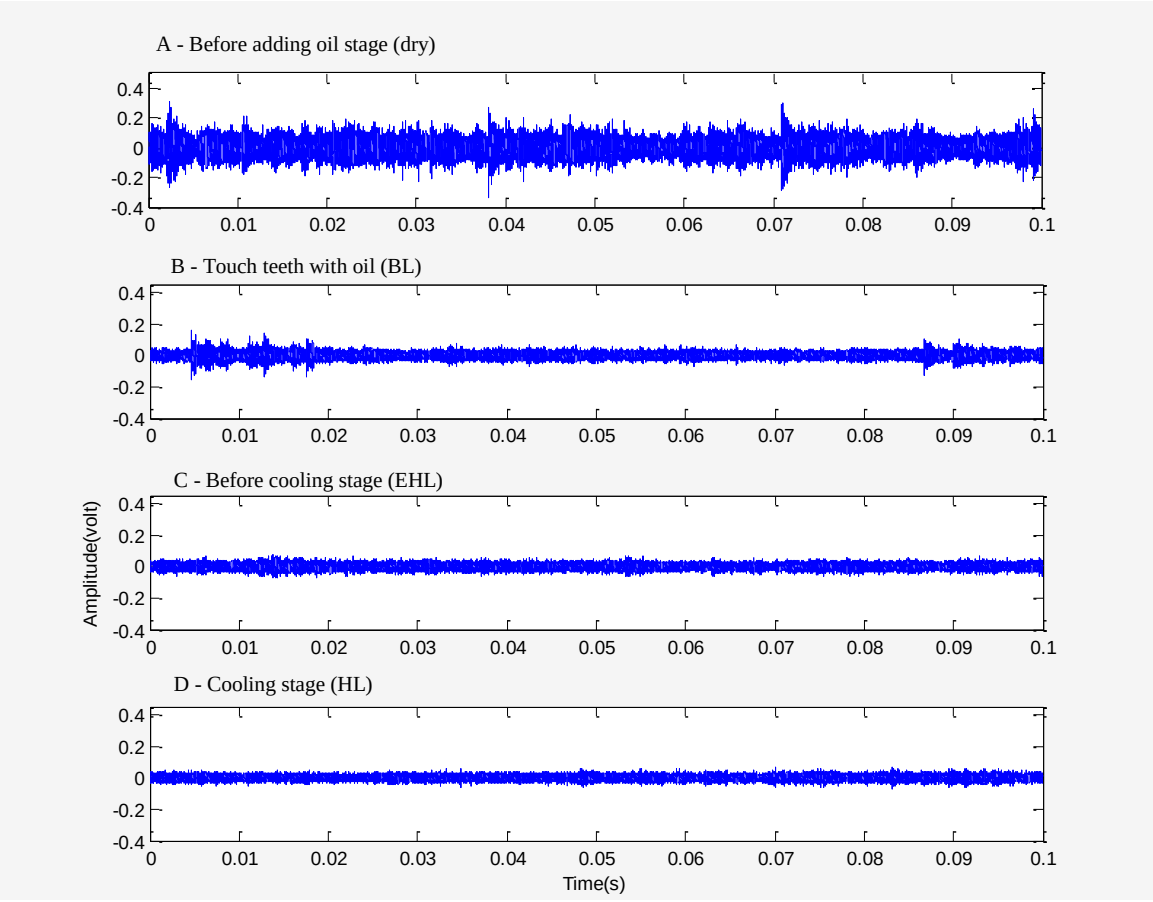

Figure 51: Influence of gear temperature and specific film thickness on AE waveforms (the waveforms correspond to the regions in Figure 50)

Region B of Figure s 50 and 51 represents the time frame from the instant oil was added to the gearbox to the point where the oil levels had reached a height such that the gear wheel teeth was in continuous contact with the oil in the sump. Within region B, during the initial stages fluctuating levels in AE r.m.s were noted. The calculated λ value was less than 1, suggesting a boundary lubrication regime. In addition, observations of the waveform characteristics associated with this region, see waveform B in Figure 52, showed transient AE bursts at the start of the signal but continuous type characteristics towards the end of the signal. Given that large transient bursts are directly associated with asperity contact at the mesh, this observed characteristic would suggest a contact region of varying levels of asperity contact during the shaft revolution, indicative of a boundary type regime.

Region C in Figure s 50 and 51 is associated with the period when the gears continuously dipped into the oil, i.e, there was now a sufficient lubrication supply. The AE r.m.s level in this region was 0.158 Volts and specific film thickness exceeded unity, $\lambda \geq 1$, so region C in Figure 51 is where the elastohydrodynamic regime became dominant.

The same procedure was followed as for the previous test and very similar results were observed; a decrease in AE r.m.s as specific film thickness increased, and vice-versa. These results indicate that AE technology can detect and distinguish the difference in oil film thickness and thereby the lubrication regimes (e.g. EHL or HL).

In conclusion the results of this study indicate that the direct contact between the helical gear teeth in dry conditions was a significant source of AE energy, confirming that asperity contact is an essential source of AE signals. The results also showed that level of the AE signal could be used to identify the lubrication film regime. A reduction in specific film thickness resulted in an increase in AE r.m.s level and increasing the specific film thickness significantly reduced AE r.m.s level. The results indicate the potential of AE technology to predict and quantify lubrication film regime under different operating conditions for helical gears.

6.4 Applicability of AE in Monitoring Defects During Dry and Lubricated Contact

6.4.1 Test Instrumentation and Procedure

The test setup was similar to that of the previous tests, i.e. the same back to back gearbox shown in Figure s 28 and 29.The teeth were damaged naturally by running the gears for a prolonged period. Eventually, spalls, 2 mm diameter and 2 mm in depth, were noted on six teeth, see circulated at teeth in Figure 53.

This test explores the influence of oil film thickness on the generation of AE from a defective helical gear. The test programme undertaken measured the AE energy generated during the mesh of a defective helical gear whilst simultaneously varying the thickness of the lubricating oil. The latter was accomplished by spraying the liquid nitrogen onto the test gear whilst it was in operation. This reduced the temperature of the metal of the gear which also reduced the lubricant temperature, thus increasing the lubricant viscosity and specific film thickness. The arrangement allowed the in-situ variation of the film thickness in a controlled manner.

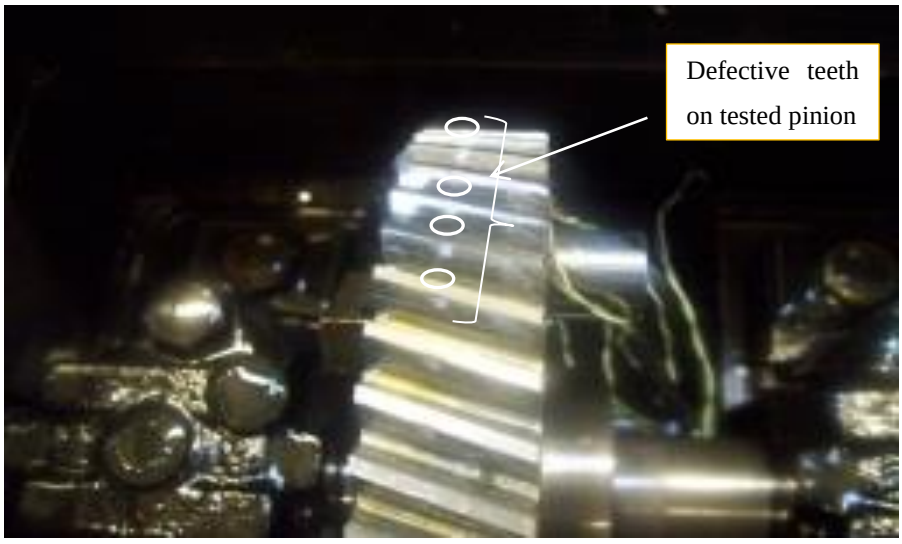

Figure 52: Defective Teeth – spalls of 2 mm diameter and 2 mm depth

To chieve fully dry running conditions the oil present in the gearbox was removed and then the gear teeth surfaces and gearbox housing were thoroughly cleaned with acetone, this was the same procedure as previously.

Again the AE r.m.s , AE waveforms were measured and recorded and the oil viscosity estimated at the measured pinion temperature, using the same approach as adopted in the previous tests.

6.4.2 Observation of The Signals in Time and Frequency Domains

Figure 54 presents the r.m.s value of the AE signal obtained with dry, EHL and HL lubrication regimes; regions 'A', 'B' and 'C' respectively. As explained previously under dry conditions the gear load is carried by tooth surface asperities. The gears were run dry for 200s before lubricating oil was added, see region 'A' in Figure 54. Figure 55 shows samples of AE raw waveforms captured at intervals during the test. Waveform 'A' in Figure 55 was associated with dry region, 'A' in Figure 54, and so on. Under dry running conditions it can be seen that there were transient bursts in the AE signal which were superimposed onto a continuous type emission. These were attributed to asperity contacts of the defective gears (dashed circle in waveform 'A')

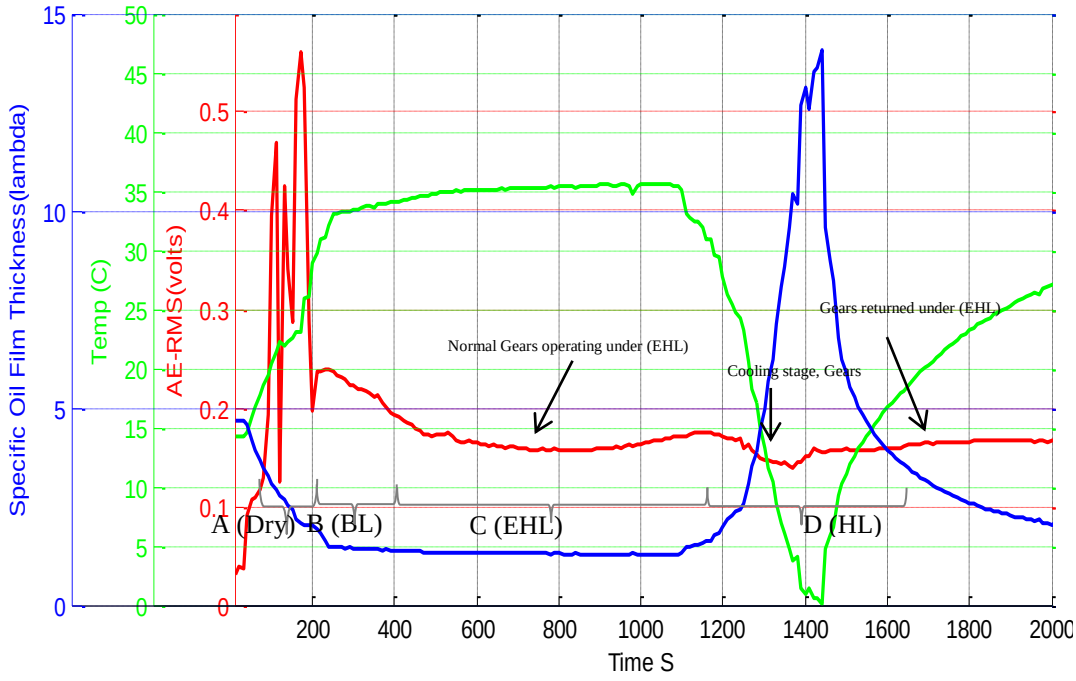

Figure 53: Influence of gear temperature and specific film thickness on AE r.m.s

Region ‘B’ of Figure 54 is associated with the period when the gears continuously dip into the oil (the gearbox operates under normal conditions). The AE r.m.s level had an average value of 0.17 Volts, and specific film thickness was greater than unity, $\lambda \geq 1$. Region ‘B’ in Figure 54 is indicative of a regime where EHL dominates. Waveform B in Figure 55 shows transient AE bursts which are noticeably smaller than those noted under dry conditions (region A). This significant reduction was predictable and attributed to the presence of an oil film in the meshing area, causing partial separation between corresponding asperities of defects (dashed circle in waveform B) on gear teeth in the contact area. Thus in the EHL regime the generation of AE amplitude is relatively lower than under dry conditions.

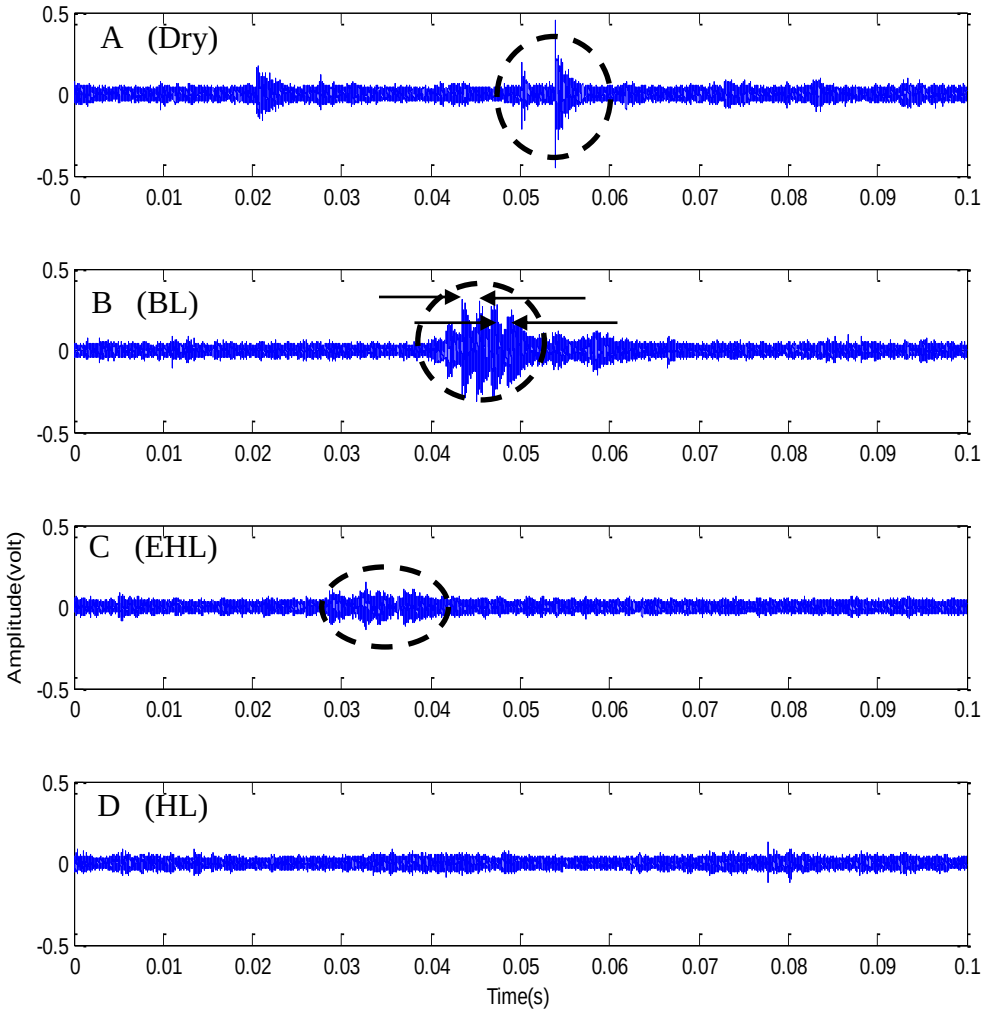

Figure 54: AE waveforms associated with regions ‘A’, ‘B’, ‘C’ in Figure 54

With the introduction of nitrogen into the operation at 1100 seconds there was a sharp decrease in gear metal temperature and a rapid fall in AE r.m.s . The drop in AE level was a direct result of increasing viscosity and oil film thickness at the meshing area. The AE r.m.s reached its minimum, approximately 0.13 Volts when the specific film thickness was at its maximum, $\lambda = 14$.

Waveform C in Figure 55 was captured in the minimum temperature region, where specific film thickness was a maximum and corresponding by the AE waveform showed the lowest amplitude. It was noted that transient bursts were hardly distinguishable from the continuous emissions. This confirmed that increasing oil film thickness decreased the AE generated from the defective gears. The increased film thickness under this region prevented the asperities in the defective region from meeting with the mating gear. This explains the lack of a transient AE burst associated with the defect in the captured waveform, see Figure 55.

The nitrogen supply was stopped when the gear temperature reached 0˚C, at about 1420 s, see region C in Figure 54. The gearbox continued operating and the temperatures of lubricant and metal gradually returned to their initial values, with a corresponding increase in AE levels as the specific film thickness decreased with increase in temperature. The AE signals associated with the presence of surface defects on the pinion tooth face showed no change in frequency content.

Statistical parameters obtained from the AE raw wavefo r.m.s ; Kurtosis (KURT) and crest factor (CF) were used to compare the effect of film thickness in measuring the presence of a defect, see Figure 55. These parameters were chosen on the basis that they are commonly used for condition monitoring of gears, and were used above, see Figure 56 because they were used above which demonstrated that both Kurtosis and Crest Factor could be used to detect the the presence of a fault, depending on oil temperature.

It can be seen that the highest levels of Kurtosis and Crest Factor were noted under dry conditions. The Kurtosis value rapidly decreased as the oil regime proceeded from dry to EHL. A similar reduction was noted for the CF. Further increases in film thickness resulted in further reductions of Kurtosis and CF values. These results were noted for all

experiments and reaffirm the finding that the level of film thickness greatly influences the generation of AE associated with defective gears.

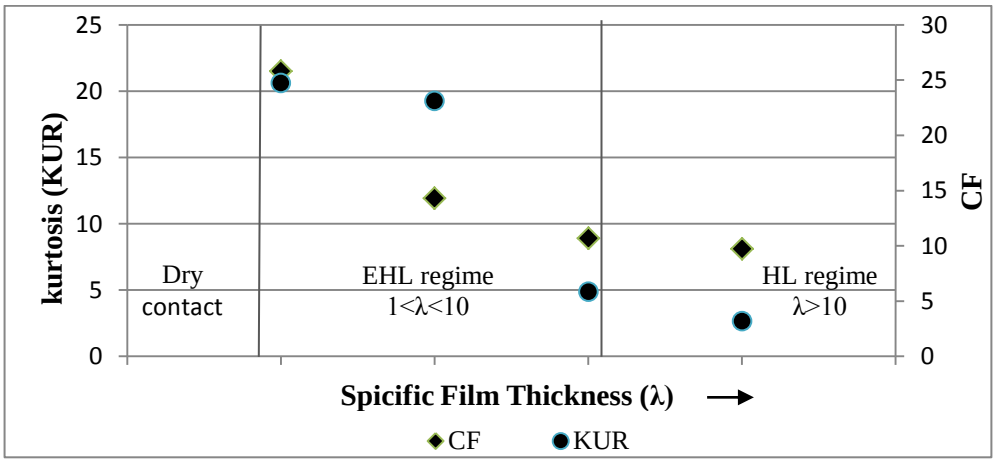

Figure 55: Statistical parameters associated with AE waveform for different lubrication regimes.

6.5 Spectral Kurtosis of AE Signal from Defective and Non-Defective Gear

The meshing of helical gears is progressive due to the gradual increase and decrease in contact length over a particular tooth face. Background noise masks the signal of interest and the Kurtosis obtained is low. When there is strong background noise the Spectral Kurtosis (SK) has been used instead of the global Kurtosis. The SK is a technique that calculates the Kurtosis locally in different frequency bands. SK has been used to identify a filter to select the part of the signal that is most impulsive, considerably reducing the background noise and improving the diagnostic capability and it is suggested that its application is appropriate here (Antoni, 2006; Sawahli and Randall, 2004).

Figure s 52 and 55 show peaks contained within the wavefo r.m.s , but the peaks are different in size and the time intervals between the peaks vary due to the helical gear's contact mechanism. In Figure 55 the interval exactly reflects passage of the wheel over the cracked pinion teeth. The existence of peaks showed that the signal contained a number of impulses, which should be detected using spectral kurtosis.

The use of SK would effectively de-noise the AE signals for both defect free and defective gear tests. The process involved calculating the Kurtogram for each signal for which the bandwidth and center frequency are required for the design of a band-pass filter. The determination of the SK was based on the algorithm developed by (Antoni and Randall, 2006; Antoni, 2007).

A Kurtogram of signals from defect free and defective gear tests are presented in Figure s 57and 58 respectively for each of the four lubrication regimes (dry, BL, EHL and HL). The center frequency (Fc) , bandwidth and max kurtosis were presented in Table 7.

Region (A)

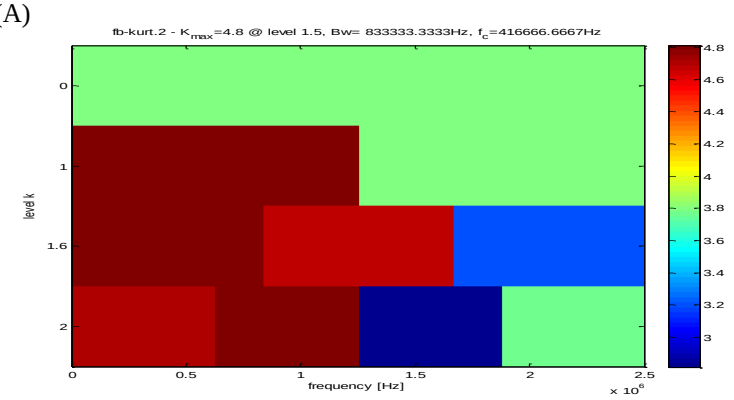

Region (B)

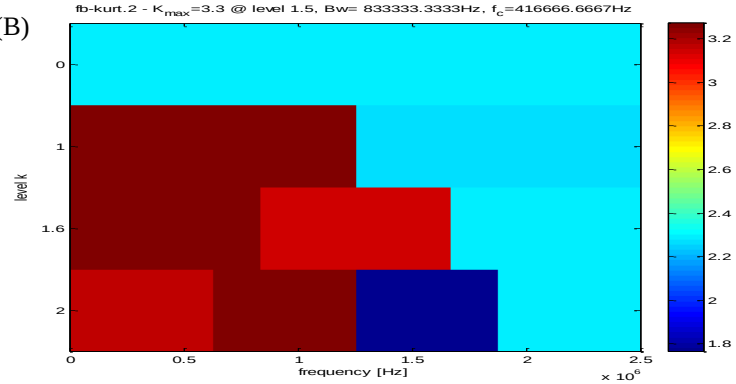

Region (C)

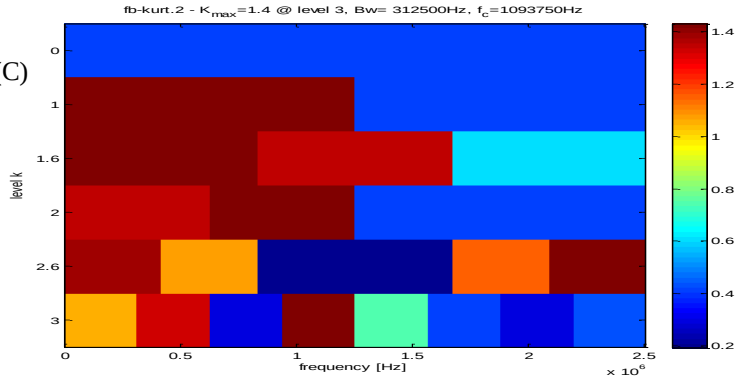

Region (D)

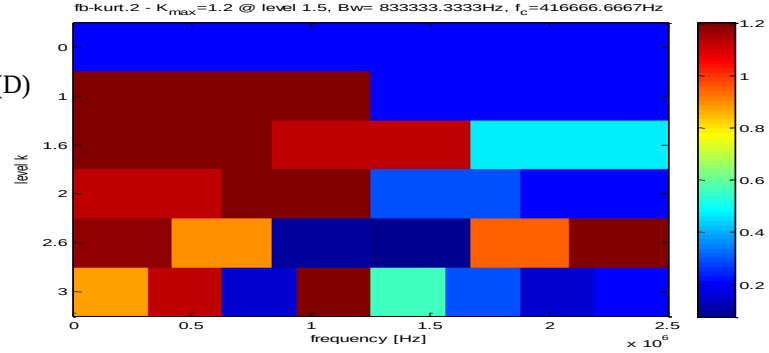

Figure 56: Kurtogram for defect free test; waveforms 'A' to 'D' correspond to regions 'A' to 'D' in Figure 50

Region (A)

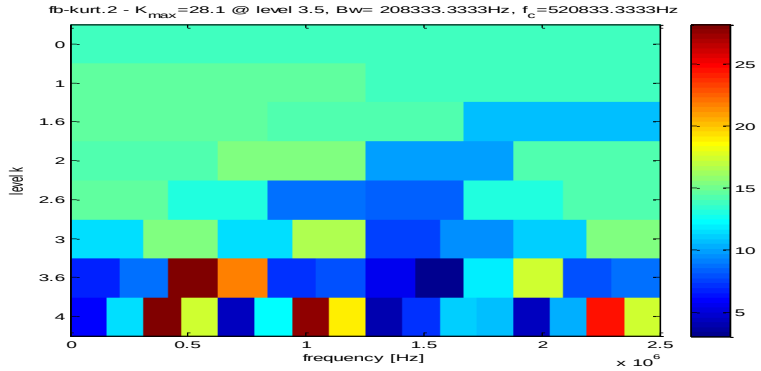

Region (B)

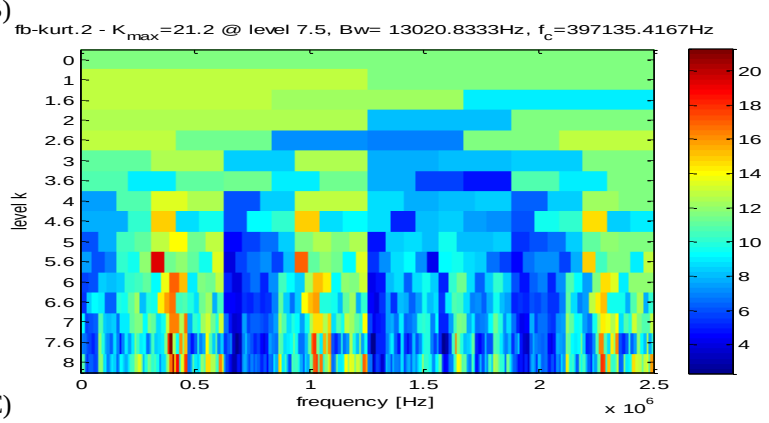

Region (C)

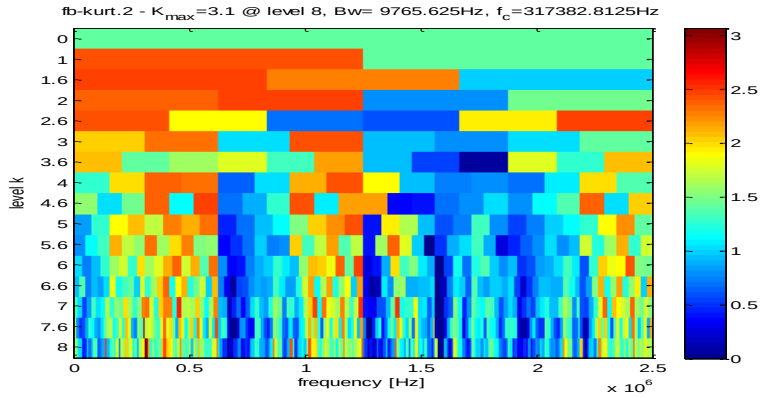

Region (D)

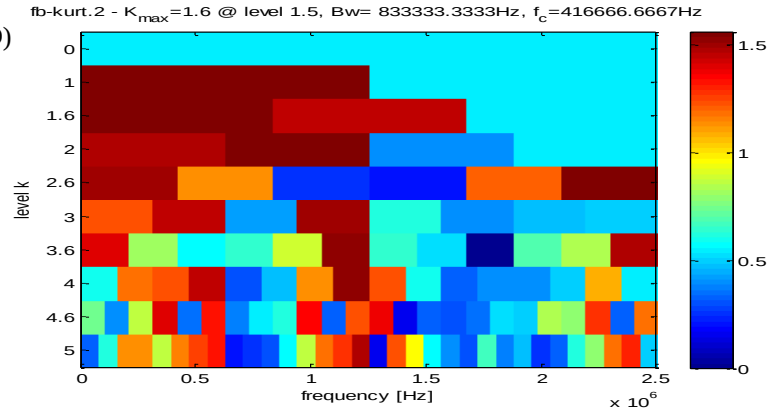

Figure 57: Kurtogram for defective gear test; waveforms 'A' to 'D' correspond to regions 'A' to 'D' in Figure 54

Table 7: Estimated optimum frequencies and bandwidths from Kurtogram

	Defect free gear test			Defective gear test			
Lubrication Regime	**Fc (MHz)**	**BW (KHz)**	**Kurt max**	**Fc (MHz)**	**BW (KHz)**	**Kurt max**	**Increase %**
Dry	0.4	833	4.8	0.5	208	28	500
BL	0.4	833	3.3	0.4	13	21	484
EHL	1	312	1.4	0.3	10	3.1	150
HL	0.4	833	1.2	0.4	833	1.6	25

The data presented in Table 7 shows two distinct and definite trends for the maximum value of the SK for a bandwidth of between 0 and 1 MHz for both the defect free test and defective gear test.

It can be seen that the SK values obtained from the defective gear tests are much higher than the corresponding values for the defect free gear tests; about 500% for dry running and decreased to about 25% for HL lubrication.

It is also clear that the data shows a decreasing value of SK with improved lubrication; dry through BL and EHL to the HL regime.

The original signals were band-pass filtered at the determined centre frequencies and the resulting time waveforms are presented in Figure s 59 for the defect free tests and Figure 60 for the defective gear test. From these Figure s it is obvious that filtered signals offered a higher level of signal to noise ratio showing the ability of SK based filtering for de-noising. Now, sharp peaks are clearly visible on all signals. They can be seen even on the signal obtained for the full film or HL regime, but with very low amplitude.

Region (A)
Dry regime

Original signals

Filtered signals

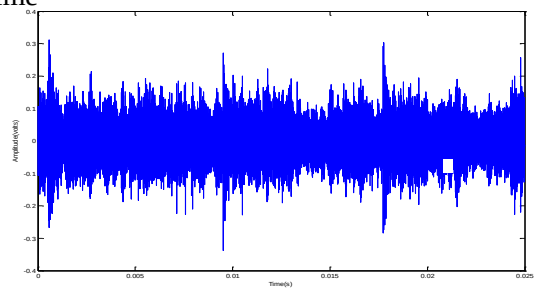

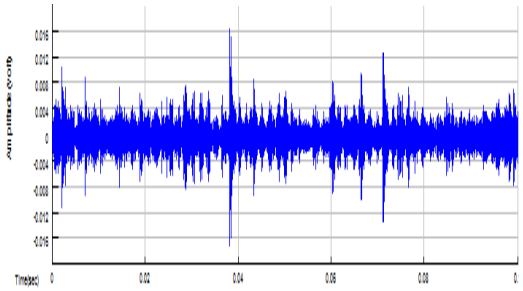

Region (B)
BL regime

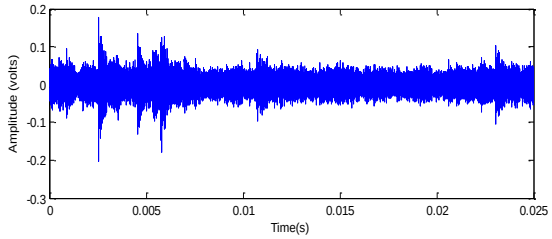

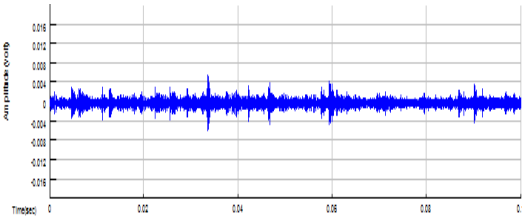

Region (C)
EHL regime

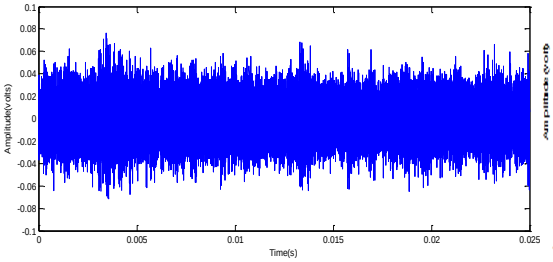

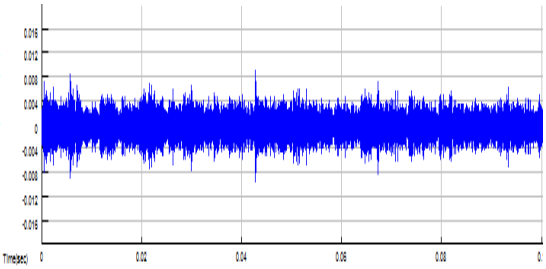

Region (D)
BL regime

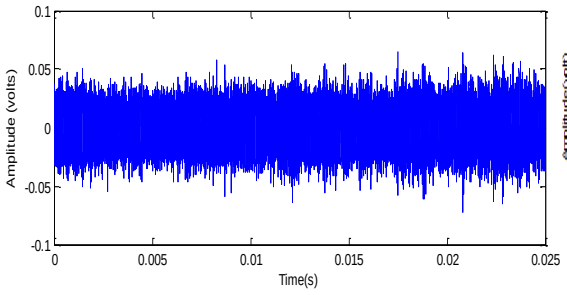

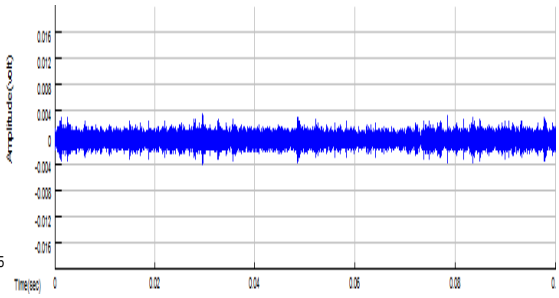

Figure 58: AE waveforms associated with filtered signals (defect free test)

Region (A)
Dry regime

Original signals

Filtered signals

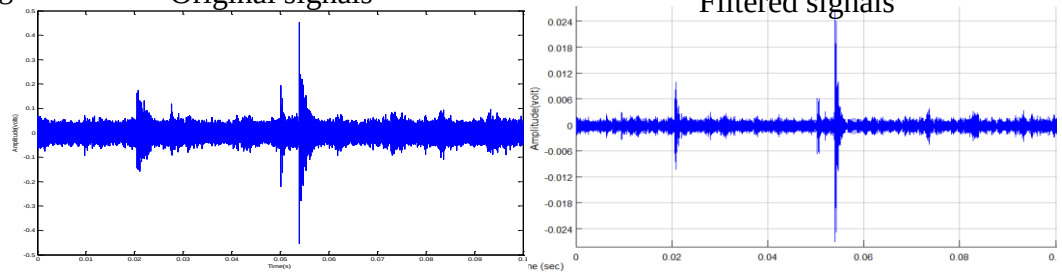

Region (B)
BL regime

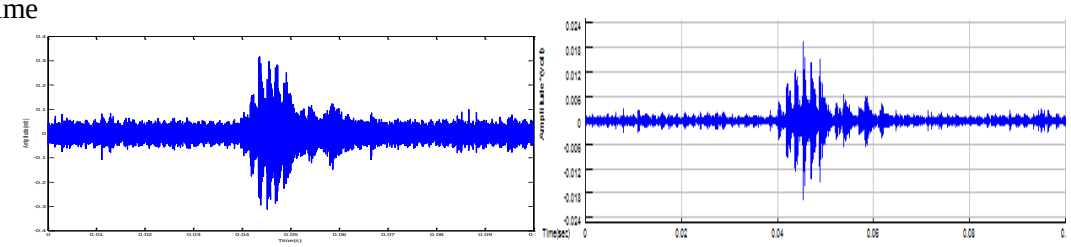

Region (C)
EHL regime

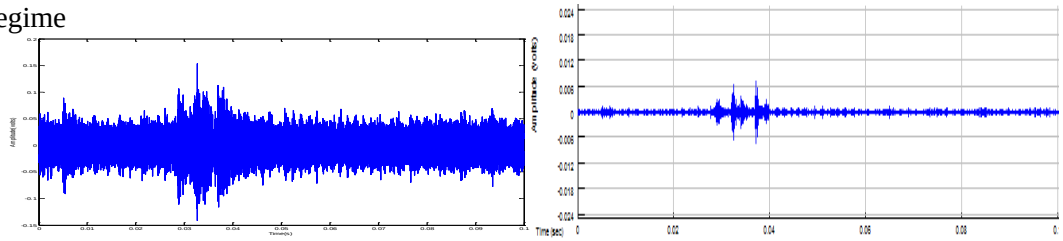

Region (D)
BL regime

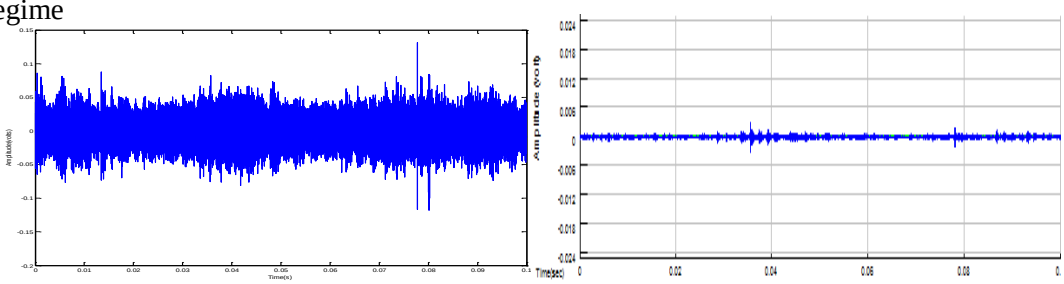

Figure 59: AE waveforms associated with filtered signals (test with defective gear)

Kurtosis (KURT) and Crest Factor (CF) are traditional methods to measure the smoothness of a signal and any increase in the spikiness of the signal profile will result in an increase in K and CF values. Both K and CF are used to detect the onset of machine failure, and have also been effective in monitoring the development of cracks and spall (Naid et al., 2009) (Tandon and Choudhury, 1999; Vecer et al., 2005). Here the relative abilities of K and CF to detect a gear fault have been compared before and after filtering.

The K values of the AE signals for the four lubrication regimes with no seeded fault (shown as regions A to D in Figure 51) prior to, and after, filtering are presented in Figure 61. It can be seen that the K value for the AE signal measured for the dry regime increased from 4.8 to 13 on filtering, and the increase for full film lubrication was 1 to 1.6. In every case the filtered K value was at least three times that obtained for the unfiltered signal, as can be seen from Figure 60, the presence of spikes was much more evident with the filtered wavefo r.m.s .

There was also an increase in the CF value on filtering the AE signal. This was not as dramatic as for the K values but still significant. In each lubrication regime the CF after filtering was at least 10% greater than for the unfiltered signal.

As expected the values of both K and CF decreased as the lubrication improved, and this is explained as due to the effect of the lubricating regime on the spikiness of the AE signal.

Figure 62 shows the K and CF values for AE signals from the defective gear test. For the dry regime the increase in CF levels rose from about 12.5 to about 14 on filtering and for full lubrication doubled from 8 to 16 on filtering the raw signal. However, K levels rose from 28 to 200 for the dry regime and levels rose from 1 to 2 at HL regime.

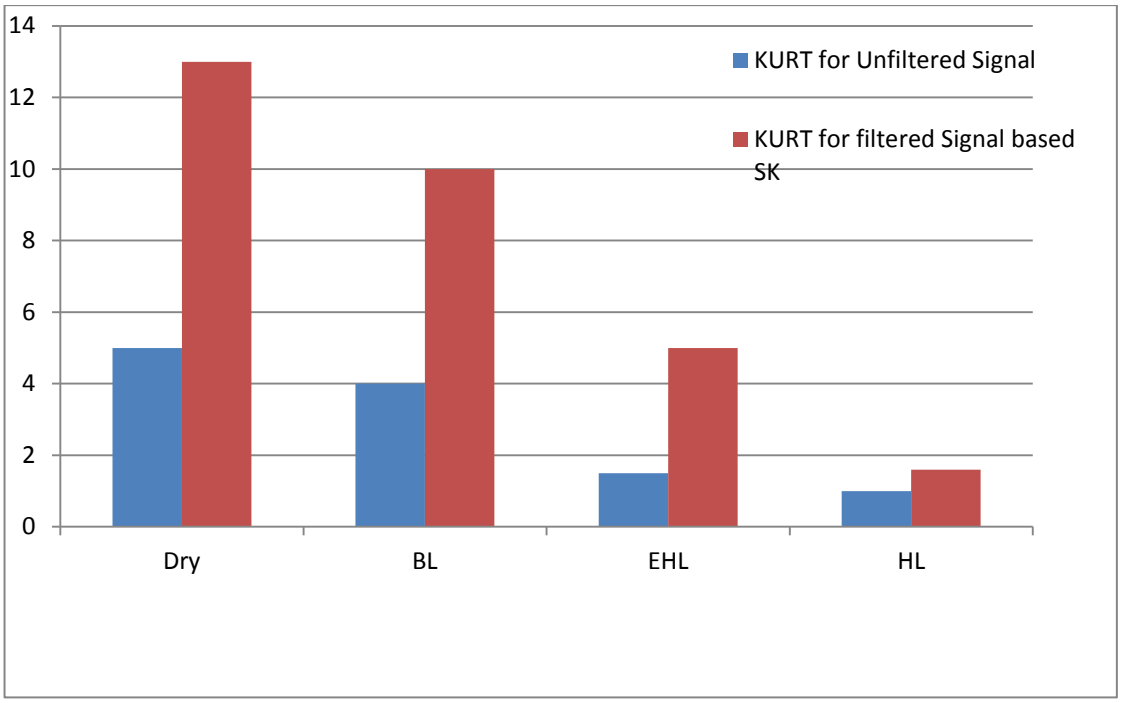

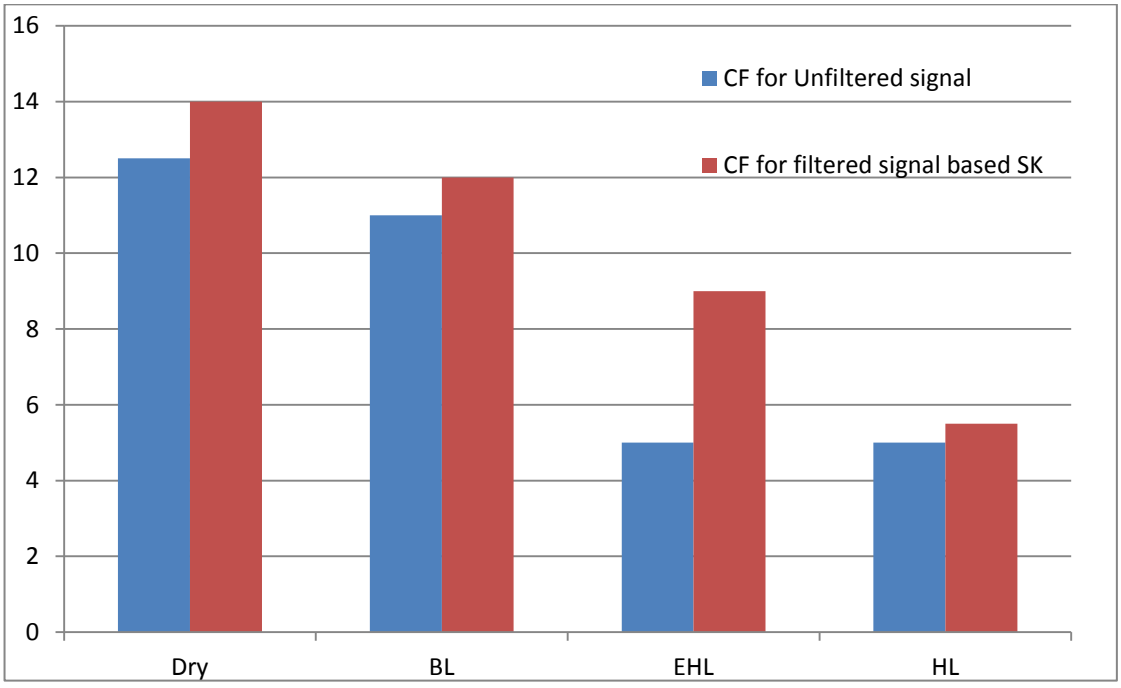

Figure 60: Effect of band pass filtering of raw AE signal on KURT and CF (Defect free gear test)

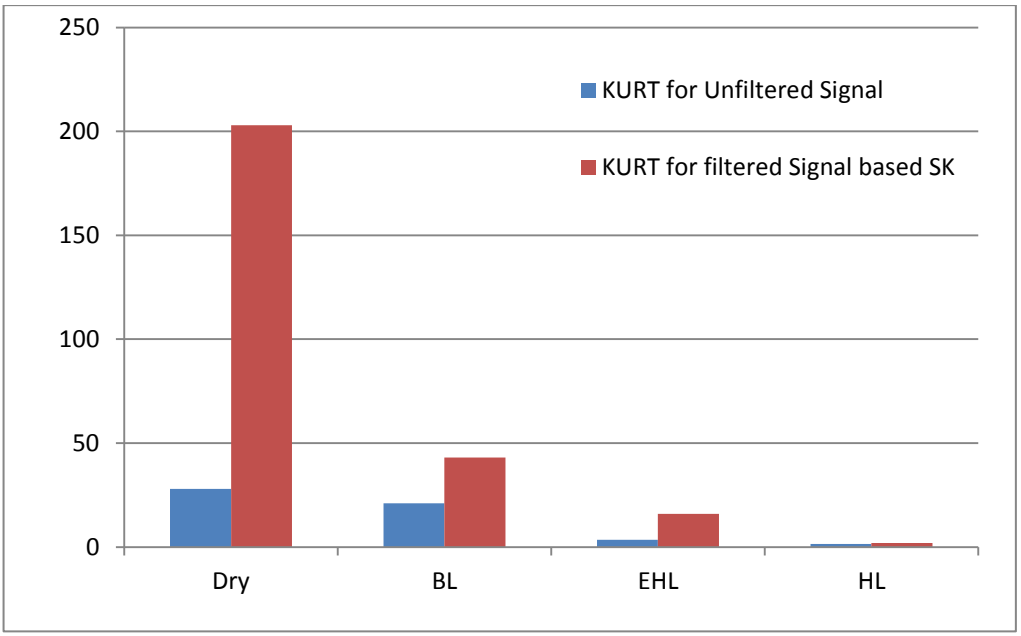

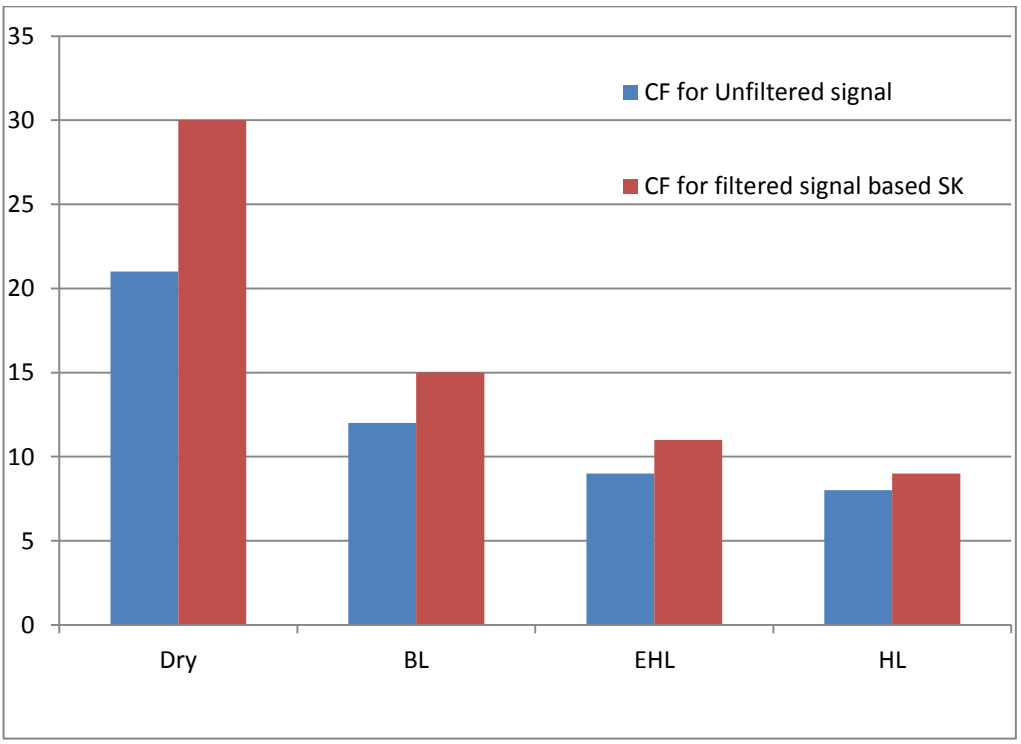

Figure 61: Effect of band pass filtering of raw AE signal on KURT and CF (defective gear test)

6.6 Correlation of AE r.m.s With Specific Film Thickness (λ)

Results showed the relationship between AE r.m.s and the calculated specific film thickness (λ) for both defect free and seeded defect tests. The test gears experienced three lubrication regimes from dry lubrication regime with λ =0 through BL, EHL and HL regimes. It was noted that the highest levels of AE r.m.s were in dry region, about 0.5 volts in the non-defective tests and 1 volt with seeded defects. There was a decrease in AE levels with the addition of lubricating oil; from direct (dry) contact to the BL region where the teeth were still in partial direct contact with λ about unity. It was clearly observed that the AE r.m.s levels were higher (0.20 volts) when the seeded defects were present than for the defect free test (0.16 volts).

The AE r.m.s levels decreased with increased thickness of lubricant film. It is believed that AE sources in this region come from either asperity contact and/or the elastic deformation of the teeth at contact. Again was clear that AE r.m.s levels obtained for seeded defects were higher. If asperity contact is the main contributor to AE activity, then when the specific film thickness increased to a value of λ = 9 when asperity contact would be expected to disappeared, there should be no further reduction in AE levels with increased lubrication.

6.7 General Observations

Significant events noticed and observed during the tests which will be important when analysing the AE signal in later sections are:

- At the point where liquid nitrogen was initially introduced onto the wheel (t =500 seconds), see Figure 48, there was a slight increase in AE activity which increased significantly when the temperature of the gear fell to below 35^{o}C. See regions 'A' and 'B' in Figure 48, and in particular the trace included within the dotted circle. This peak in AE r.m.s level lasted from about 500 to 650 seconds and occurred even though there was a continuous increase in specific film thickness (λ) during this time. This was attributed to the micro-structural change in the gear material as the temperature of the gear was reduced rapidly. This micro-structural change contributed to the generation of AE activity and thus increased the AE r.m.s level. After this micro-structural change was stabilised, the continuous increase in specific film thickness (λ) reduced the AE r.m.s level.

  During the actual tests, the effect of these macro- and micro-structural changes in gear metal due to the rapid change in temperature (from approximately 50ºC+/- to 0ºC) in a very short period of time (typically less than 10 minutes) caused extraneous AE activities. These extraneous AE activities contributed to the higher AE r.m.s . Also it was observed that the AE r.m.s started to decrease rapidly when temperature reached about 15°C.

- During the experiment, the oil mist generated as a result of churning of the oil formed a "frozen mist" as the oil temperature approached 0°C. This frozen oil mist was thrown into the gear mesh by the rotating wheel resulting in the generation of AE activity. This sudden increase in activity is shown in Figure 48 in the dotted circle in region 'C'. It was not possible to control the entry of the frozen mist into the gear mesh.
- The region between A and B (dotted circle) shown in Figure 51 also a sudden increase in AE r.m.s level as drops of oil were first dripped onto the gear wheel (at about 240s). It is suggested that adding oil in this manner and quantity results in oil drag and oil friction. This effect lasted for about 60s.

Chapter 7

Conclusions and Future Work

7 Conclusions and Future Work

7.1 Conclusions

An AE sensor was used to monitoring oil film thickness at contact area between the gear teeth in real-time for vary oil temperature conditions. At constant speed and load the operating temperature plays a role in surface fatigue and micropitting. As the temperature at the contact area increases, the oil viscosity is reduced and film thickness decreases. Thus a lubricant with too low an initial viscosity will become too thin and not provide adequate protection as the gear temperature increases leading to an increased rate of micropitting and surface fatigue.

A thorough analysis of oil film regime detection in helical gears has been presented. This analysis included a review of online condition monitoring methodologies for gears. In this research programme tests have been conducted, on a back-to-back gearbox, investigating the effects of changes in lubrication and gear temperatures at constant load and speed.

This research has investigated the application of acoustic emission to the identification of oil film regime in helical gear and used advanced signal processing techniques to analyse the AE signals, and several conclusions have been drawn based on the results and observations.

Firstly, mechanisms and factors that influence the generation of AE activities during helical gear mesh have been identified. The project has compared AE and vibration signals from the gears for condition monitoring and diagnosis of defect free and seeded surface defect on the gears in the presence of temperature variations. The AE signal showed better sensitivity for early diagnosis of the seeded damage compared to vibration. The AE signal showed a high sensitivity to identifying the presence of gear surface faults and was capable of detecting incipient damage in helical gears, far better than the vibration signals. Because pitch point contact for helical gear mesh is progressive pure rolling activities occur during meshing, resulting in the series of transient bursts that are so closely spaced as to form high amplitude continuous types of wavefo r.m.s .

Results presented here (Section 1.1) show that for constant speed and load, increasing the oil temperature in the gear system or introducing a tooth fault had negligible effect on vibration r.m.s as measured at both the bearing pedestal and gearbox case. The AE measurements for the sensor placed on the gearbox casing also showed no significant change with change in oil temperature or seeded defect. However, for the AE sensor on the gear the presence of the seeded fault had considerable effect on Kurtosis and Crest Factor of the AE signal when the temperature of the lubricating oil reached 36^{o}C.

The influence of calculated lubrication specific film thickness (λ) on AE generation was experimentally investigated and reported (Section 6.2). The change in specific film thickness, as calculated from the gear metal temperature, suggests that λ has a substantial effect on AE generation. The results obtained show an inverse relationship between specific film thickness λ and AE r.m.s level, strengthening the view that asperity contact is the main source of AE during helical gear meshing. The results confirm the potential of AE technology to predict and quantify lubrication film regime and suggests that the AE signal can be used for assessing the level of asperity contact under a variety of temperatures in real time operation. Because the level of asperity contact is influenced by the lubricant film thickness and surface roughness, AE technique can be a useful tool in detecting lubricating film breakdown and/or degradation of contact surfaces.

The investigation showed that in dry conditions (Section 6.3) a significant source of AE energy was direct contact between the helical gear teeth and the level of the AE signal demonstrated that this was a method that would readily detect dry gear running, further confirming that asperity contact is an important source of the AE signals. If accurately monitored the detection AE offers of running dry would, in practice, severely reduce the occurrence of gearbox destruction.

The rapid decline in the AE levels, resulting from introducing even a small amount of lubricating oil directly onto the gear provides evidence of the potential of AE technology to predict the transition from dry regime to the boundary regime BL. Its high sensitivity can provide an early warning of instability and it does not require measurements to be taken over a prolonged period to establish that gear distortions are occurring. In addition, it can provide a real-time indication of oil regime-dependent stability. Acoustic emission

technology has the potential to provide an effective lubrication regime monitoring system. The AE signal was lowest at the highest values of the specific film thickness and this is evidence to transition from the EHL to the HL regime. The results also showed that under lubricating conditions that completely separate the gear surface asperities, the generation of AE due to the presence of a defect may not be detectable over typical background noise.

Diagnosis of detective gear during dry and lubricated contact, which naturally degraded, has been investigated (Section 6.4) and the results provided the ability to identify gear defects under different lubricating regimes has been explored. It has been demonstrated that under lubricating conditions that completely separate the gear surface asperities, the generation of AE due to the presence of a defect may not be detectable over typical background noise level.

Spectral Kurtosis and Kurtograms were investigated as analysis tools for the AE signal for monitoring non-defective and naturally defective gears (Section 6.5). It was shown that the application these techniques was effective in de-noising the AE signals. The Kurtogram identified a frequency band in which the measure of the spikiness of the signal profile was greatest. Of the statistical parameters considered, variation of kurtosis values for the filtered raw AE data provides basis for a better understanding for lubricant film deterioration and fault progression.

7.2 Future Work

This research has made a contribution to knowledge; it has demonstrated that AE is a powerful diagnostic tool for identifying gear lubrication film regime and for early diagnosis of gear faults. This research has also opened new doors for the exploration of using AE signal analysis that could form the foundation for a significant advance in the application of AE for the prediction of the remaining life time of gears. The author hopes that the work presented in this thesis will stir the thoughts and generate new ideas in readers that will contribute to the advancement of gear engineering and the technologies used for detecting and diagnosing oil film thickness in geared transmission systems.

The findings of this research are encouraging and promising for the development of AE technology as preventative maintenance approach for early fault detection and prevention in all types of gearboxes. However further research is needed in critical areas. Recommendations for future work include:

- The signal from the gearbox casing typically experiences a high level of attenuation and it is expected, lower a SNR, making defect identification more challenging. In the future work the sensors on the casing might be mounted using such techniques as waveguides, and more advanced time/frequency analysis methods.

- Investigate the combined influence of wear, lubrication and contact mechanics on AE generation in helical gears. This could be realised by undertaking tests on specially designed machines such as a wear or tribology machine.

- Finding new technique for controlling and measuring the temperature inside the gear mesh would be very beneficial in obtaining a close approximation for the specific film thickness (λ) during gear operations. The use of liquid nitrogen during the tests was problematic particularly because of the formation of thick very low temperature lubricant mists at entered the gear mesh and generated unwanted AE signals. Varying the specific film thickness (λ) using other techniques would overcome this problem.

- Further work is needed to investigate the wear development of helical gears and correlate specific oil film thickness λ, asperity contact and wear rate.

hapter 8

References

8 References

Alexander, D. (1992), "The viscosity of lubricants", Lubrication, vol. 78, no. 3, pp. 1-16.

AlKazzaz, S., Ahmed, S. and Singh, G. (2003), " Experimental investigations on induction machine condition monitoring and fault diagnosis using digital signal processing techniques", Electric Power Systems Research, vol. 65, pp. 197-221.

Antoni, J. (2004), "The Spectral Kurtosis of non-stationary signals some properties and applications ", Proc Eurasip, , pp. 1167-1170.

Antoni, J. (2006), "The spectral kurtosis: A useful tool for characterising non-stationary signals", Mechanical Systems and Signal Processing, vol. 20, pp. 282-307.

Antoni, J. (2007), "Fast computation of the kurtogram for the detection of transient faults", Mechanical Systems and Signal Processing, vol. 21, pp. 108-124.

Antoni, J. and Randall, R. B. (2006), " The spectral kurtosis: Application to the vibratory surveillance and diagnostics of rotating machines", Mechanical Systems and Signal Processing, vol. 20, pp. 308-331.

Ashley, M. (2008), Mixing Lubricants: A Recipe For Trouble, machinerylubrication, U.S.

ASM. (ed.) (1992), Friction, Lubrication and Wear Technology, ASM International; 10th edition.

B. O. H, L. (2011), null, Aircraft Accident Report No: 2/2011, AAIB Bulletin, UK.

Balderston, H. L. (1969), "The detection of incipient failure in bearings", materials rvaluation, vol. 27, no. 6, pp. 121-128.

Bankim and Bernard, J. H. (1882), Frictional Heating Due to Asperity Interaction of Elastohydrodynamic Line-Contact Surfaces (unpublished Technical Paper), NASA.

Beattie, A. and Rumsey, M. (1999), "Non-Destructive Evaluation of Wind Turbine Blades Using an Infrared Camera", ASME Wind Energy Symposium,18th, Aerospace Sciences Meeting and Exhibit, 37th, Vol. 18th, Reno, Nevada.

Becker, W. T. and Shipley, R. J. (eds.) (2002), Failure Analysis and Prevention (ASM HandbookVolume 11), 10th ed, ASM, US.

Benabdallah, H. and Aguilar, D. (2008), "Acoustic emission and its relationship with friction and wear for sliding contact", Tribology Transactions, vol. 51, no. 6, pp. 738-747.

Benbouzid, M. E. H. (2000), "A review of induction motors signature analysis as a medium for faults detection", IEEE Transactions on Industrial Electronics, vol. 47, no. 5, pp. 984-993.

Board, D. B. (1975), "Incipient failure detection in high speed machinery", Vol. 10th Symposium, 23-25 April, San Antonio, .

Boczar, T. and Lorenc, M. (2004), "Determining the Repeatability of Acoustic Emission Generated by the Hsu-Nielsen Calibrating Source", Molecular and Quantum Acoustics, vol. 25, no. ., pp. 177-191.

Boness, R. and McBride, S. (1991), "Adhesive and abrasive wear studies using acoustic emission techniques", Wear, vol. 149, no. 1, pp. 41-53.

Boness, R., McBride, S. and Sobczyk, M. (1990), "Wear studies using acoustic emission techniques", Tribology International, vol. 23, no. 5, pp. 291-295.

Boyer, E. B. (1975), Failure Analysis and Prevention , Metal Handbook ed, Ohia, American Society for Metals., U.

Brüel and Kjaer. (1981), "(1981) Technical Review", vol. ISSN:0007- 2621, no. 2, pp. 38-40.

BS EN (2009), BS EN 1330-9:2009 Non-destructive testing— Terminology, , BS, UK.

BS EN 13477-1:2001. (2001), Non-destructive testing - Acoustic emission - Equipment characterization, Part 1, BS, UK.

Cairns, M. (1991), The Condition Monitoring of a Spur gearbox Using Noise and Vibration Measurements and Correlation (unpublished MSc thesis), Cranfield University, UK.

Capgo Pty Ltd. (2009), Fatigue Detection by Acoustic Emissions, Capgo Pty Ltd, available at: http://www.capgo.com/Resources/ConditionMonitoring/Acoustic.html (accessed 12/2012).

Choy, F. K. S., Huang, J. J. and Zakrajsek, R. F. (1994), Vibration signature analysis of a faulted gear transmission system, 106623. AIAA-94-2937, University of Akron, University of Akron.

ClickGreen, s. (2012), Offshore wind will play a vital role in the UK's future energy mix, report confi r.m.s , , ClickGreen, UK.

Copper, P. (1983), "Wear debris monitoring of rolling bearings", British Journal of NDT, vol. 25, no. 2, pp. 75-83.

Czichos, H. (1977), "Influence of asperity contact conditions on the failure of sliding elastohydrodynamic contacts", Wear, vol. 41, no. 1, pp. 1-14.

Da Silva, A. (1997), "Rotating machinery monitoring and diagnosis using short-time Fourier transform and wavelet techniques", Knoxville, T. (ed.), in: Proc. Int. Conf. Maintenance and Reliability, Vol. 1, pp. 14.01–14.15.

de Kraker, A. and Stakenborg, M. J. L. (1986), "Cepstrum analysis as a useful supplement to spectrum analysis for gear-box monitoring ", stress analysis: proceedings of the 8th international conference, Amsterdam, Netherlands, , May 12-16, Amsterdam, Netherlands, pp. 181-190.

Dempsey, P., Lewicki, D. and Decker, H. (2004), Investigation of Gear and Bearing Fatigue Damage Using Debris Particle Distributions.

, 2004-212883, NASA/TM.

Dowson, D. (1977), Elasto-hydrodynamic lubrication, 2nd ed, Pergamon, Oxford.

Dowson, D. (1995), "Elastohydrodynamic and micro-elastohydrodynamic lubrication", Wear, vol. 190, no. 2, pp. 125-138.

Dowson, D. and Ehret, P. (1999), "Past, present and future studies in elastohydrodynamics", Proceedings of the Institution of Mechanical Engineers, Part J: Journal of Engineering Tribology, vol. 213, no. 5, pp. 317-333.

Drago, T. (ed.) (1988.), Fundamentals of gear design, Butterworths ed, Boston, London.

Drouillard, T. F. (ed.) (1988), Introduction to acoustic emission, Material Evaluation ed, 46, 174-179.

Dwyer Joyce, R. S. (1995), Tribological Design Data, , Institution of Mechanical Engineers 1995, UK.

Dwyer, R. (1983), " Detection of non-Gaussian signals by frequency domain Kurtosis estimation", Acoustics, Speech, and Signal Processing, IEEE International Conference on ICASSP, Vol. 8, pp. 607-610.

Dwyer-Joyce, R. S. (ed.) (1995), Lubrication, 1st ed, Tribological Design Data Part 2.

E. Richard Booser, P. D. (1983), CRC HANDBOOK of LUBRICATION (Theory and Practice of Tribology)Volume IITheory & Design

, Volume II ed, Library of Congress, US.

Ebersbach, S., Peng, Z. and Kessissoglou, N. J. (2006), "The investigation of the condition and faults of a spur gearbox using vibration and wear debris analysis techniques", Wear, vol. 260, no. 1–2, pp. 16-24.

Eftekharnejad, B. and Mba, D. (2008), "Acoustic emission signals associated with damaged helical gears", Insight: Non-Destructive Testing and Condition Monitoring, vol. 50, no. 8, pp. 450-453.

Eftekharnejad, B. and Mba, D. (2009), "Seeded fault detection on helical gears with acoustic emission", Applied Acoustics, vol. 70, no. 4, pp. 547-555.

Envirocoustics S. A. (2007), Acoustic Emission Theory, Envirocoustics S. A.Publications, available at: http://www.envirocoustics.gr/acoustic_emission_theory_eng.htm (accessed 12/2012).

Eric Y, K., Andy, C. T., Bo-Suk, Y. and Vladis, K. (2007), "Experimental Study on Condition Monitoring of Low Speed Bearings : Time Domain Analysis", Fifth Australasian Congress on Applied Mechanics (ACAM 2007), Vol. 5th Australasian Congress on Applied Mechanics, 10–12 December, Brisbane, Australia, ACAM, .

Evans, J. S. and Hunt, T. M. (eds.) (2008), Machine & systems condition monitoring series– The oil analysis handbook, Firset ed, Coxmoor Publishing Company, Oxford, UK.

Faulstich, S. (2008), Windenergie Report Deutschland 2008, , Institut für Solare Energieversorgungstechnik (Hrsg.), Kassel.

Fernandes, P. and McDuling, C. (1997), "Surface contact fatigue failures in gears", Engineering Failure Analysis, vol. 4, no. 2, pp. 99-107.

Forrester, D. (1996), Advanced vibration analysis techniques for fault detection and diagnostic in geared transmission systems (PhD thesis), Swinburne University of Technology, Melbourne.

GABERSON, H. (2002), "The Use of Wavelets for Analyzing Transient Machinery Vibration", S.V.Sound and Vibration, vol. 36, pp. 12-17.

Gitin M, M. (ed.) (1994), Handbook of Gear Design, Second Edition ed, Tata McGraw-Hill,, ©1989, New Delhi, India ; Montréal.

Guangteng, G., Cann, P. M., Olver, A. V. and Spikes, H. A. (2000), "An experimental study of film thickness between rough surfaces in EHD contacts", Tribology International, vol. 33, no. 3–4, pp. 183-189.

Halme, J. and Andersson, P. (2010), "Rolling contact fatigue and wear fundamentals for rolling bearing diagnostics – state of the art", Proceedings of the Institution of Mechanical Engineers, Part J: Journal of Engineering Tribology, vol. 224, pp. 4.

Ham, C. W., Crank, E. J. and Rogers, W. L. (eds.) (1958), Mechanics of Machinery, McGraw-Hill.

Hamrock J, B., Steven, R. S. and Jacobson, B. O. (eds.) (2004), Fundamentals of Fluid Film Lubrication, Second ed, McGraw-Hill.

Hamzah, R. I., Al-Balushi, K. R. and Mba, D. (2008), "Observations of acoustic emission under conditions of varying specific film thickness for meshing spur and helical gears", Journal of tribology, vol. 130, no. 2.

Hamzah, R. I. and Mba, D. (2007), "Acoustic emission and specific film thickness for operating spur gears", Journal of tribology, vol. 129, no. 4, pp. 860-867.

Hamzah, R. I. and Mba, D. (2009), "The influence of operating condition on acoustic emission (AE) generation during meshing of helical and spur gear", Tribology International, vol. 42, no. 1, pp. 3-14.

Handbook of metric gears (ed.) Handbook of metric gears - Product guide and technical data: Catalog Q 410, .

Hasan, (2006), Gearbox Health Monitoring and Fault Detection Using Vibration Analysis (PhD thesis), Dokuz Eylül University, Dokuz Eylül.

Henning, D. (1988), "Josef Kaiser: His achievement in acoustic emission research

", Material Evaluation, vol. 46, no. 2, pp. 193-195.

Höhn, B. and Michaelis, K. (2004), "Influence of oil temperature on gear failures", Tribology International, vol. 37, no. 2, pp. 103-109.

Holroyd, T. (2000), Acoustic Emission & Ultrasonic, 1st ed, Coxmoor Publishing Company's. Oxford, UK.

Holroyd, T. and Randall, N. (1993), "Use of acoustic emission for machine condition monitoring", British journal of non-destructive testing, vol. 35, no. 2, pp. 75-78.

J, Y. and Quin˜o´nez, P. D. (2004), "Gear surface temperature monitoring", vol. IMechE Vol. 219 Part J: J. Engineering Tribology, pp. 99-105.

Jardine, A. K., Lin, D. and Banjevic, D. (2005), A review on machinery diagnostics and prognostics implementing condition-based maintenance, Technical report, CBM Lab, Department ofMechanical and Industrial Engineering, University of Toronto.

Jardine, A. K. S., Lin, D. and Banjevic, D. (2006), "A review on machinery diagnostics and prognostics implementing condition-based maintenance", Mechanical Systems and Signal Processing, vol. 20, no. 7, pp. 1483-1510.

Jiaa, C. L. and Dornfeld, D. A. (1990), "Experimental studies of sliding friction and wear via acoustic emission signal analysis", Wear, vol. 139, no. 2, pp. 403-424.

Jie, Z. and Drinkwater, B. W. (2006), "Acoustic measurement of lubricant-film thickness distribution in ball bearings", J. Acoust. Soc. Am., vol. 119, no. 2, pp. 863-871.

Johnson, M. L. (2012), Lubrication Technology , available at: http://www.sumitomodrive.com (accessed 06/05).

Joseph, R. D. (ed.) (2005), Gear materials, properties, and manufacture, Second Edition ed, ASM International, 2005.

Kaiser, J. (1950), A study of acoustic phenomena in tensile tests, Dr.-Ing. Dissertation, TechnicalUniversity of, Munich.

Kar, C. and Mohanty, A. R. (2006), "Multistage gearbox condition monitoring using motor current signature analysis and Kolmogorov–Smirnov test", Journal of Sound and Vibration, vol. 290, no. 1–2, pp. 337-368.

Keith, M. R. (2002), An introduction to predictive maintenance , Second ed, Elsevier Science, U.S.

Krantz, K. and Kahraman, A. (2004), "An Experimental Investigation of the Influence of Lubricant Viscosity and Additives on Gear Wear", Tribology Trans, vol. 47, pp. 138-148.

Kutz, M. (ed.) (2006), Mechanical engineers' handbook, 3rd ed, Wiley, Hoboken, N.J.

Le Sueur, H. E., (1978), Airworthiness of Hlicopters, 82(814), Aeronaut J, 82(814).

Lebold, M., McClintic, K. and Campbell, R. (2000), Review of vibration analysis methods for gearbox diagnostics and prognostics, 634, ed. pp. 623, Proceedings of the 54th Meeting of the Society for Machinery Failure Prevention Technology, Virginia Beach.

Lingard, S. and Ng, K. K. (1989), "An investigation of acoustic emission in sliding friction and wear of metals", Wear, vol. 130, no. 2, pp. 367-379.

Liu, H., Lin, J. and Liangsheng, Q. (1997), "FFT Spectral Entropy and its application in fault diagnosis", China Mech. Eng., vol. 4, no. E6.10, pp. 157-159.

Loutas, T. H. and Kalaitzoglou, J. (2007), "T.H. On the application of non-destructive testing techniques on rotating machinery", 4th International Conference on NDT, 11-14october, Chiania, Crete-Greece, NDT, .

Lucente, M. (2008), Condition monitoring system in wind turbine gearbox (MSc thesis), KTH, Stockholm, Sweden.

Luke, D., (2012), Changing a Gear: Gearbox Lubrication and Its Impact on Wind Turbine Lifespan, Wind Technology, Distributed with Renewable Energy World Magazine, UK.

Macconochie, I. O. and Newman, W. H. (1961), "The effect of lubricant viscosity on the lubrication of gear teeth", Wear, vol. 4, no. Issue 1, pp. 10-21.

Manufacturing Association American Gear (ed.) (1989), Geometry Factors for Determining the Pitting Resistance and BendingStrength of Spur, Helical, and Herringbone Gear Teeth, 1st ed, Manufacturing Association American Gear, US.

Martin, K. F. (1978), "A Review of friction prediction in gear teeth", Wear, vol. 49, pp. 201-238.

Mathew, J. (1989), Monitoring the vibration of rotating machine elements , 1, An overview. The Bulletin of the Center of Machine Condition Monitoring, Monash University.

Matthew G, B., Dr Rhys, P. and Dr Karen M, H. (2004), Detection of fatigue crack growth in aircraft landing gear, DGZfP-Proceedings BB 90, CD Lecture 27 EWGAE.

Mba, D. (2003), "Acoustic Emissions and Monitoring Bearing Health", STLE Tribol. Trans., vol. 46, no. 3, pp. 447-451.

Mba, D. and Rao, R. B. (2006), "Development of acoustic emission technology for condition monitoring and diagnosis of rotating machines; bearings, pumps, gearboxes, engines and rotating structures", Shock and Vibration Digest, vol. 38, no. 1, pp. 3-16.

McFadden, P. D. (1986), "DETECTING FATIGUE CRACKS IN GEARS BY AMPLITUDE AND PHASE DEMODULATION OF THE MESHING VIBRATION", Journal of Vibration, Acoustics, Stress, and Reliability in Design, vol. 108, no. 2, pp. 165-170.

McNiff, B. P. (1991), Variations in gear fatigue life for different wind turbine braking strategies, SERI/TP-257-3984; CONF-9009107--7, DOE; USDOE, Washington, DC (USA), United States.

Mechefske, C., G, S. and J, S. (2002), "Using Acoustic Emission to Monitor Sliding Wear", INSIGHT - The Journal of the British Society of Non-Destructive Testing, vol. 44, no. 8, pp. 490-497.

Miller, R. and McIntire, P. (eds.) (1987a), Acoustic emission testing. Nondestructive

, Second ed, Nondestructive testing handbook, American Society for Nondestructive Testing.

Miller, R. K. and McIntire, P. (eds.) (1987b), Nondestructive testing handbook, volume 5: Acoustic emission testing, 2nd ed, ASNT.

Mirhadizadeh, S. A. and Mba, D. (2009), "Observations of acoustic emission in a hydrodynamic bearing", Journal of quality in maintenance engineering, vol. 15, no. 2, pp. 193-201.

Muller, J. and Errichello, R. L. (2001), How to analyze gear failures, January, Geartech.

Naid, A., Gu, F., Shao, Y. and Ball, A. (2009), "Bispectrum analysis of motor current signals for fault diagnosis of reciprocating compressors", Key Engineering Materials, vol. 413 - 414, pp. 505-511.

NDT, E. R. C. (2013), Introduction to Acoustic Emission Testing, available at: http://www.ndted.org/EducationResources/CommunityCollege/Other%20Methods/AE/AE_Intro.htm (accessed 03/03).

Neale, M. J. (ed.) (1995), Tribology, 2nd ed, Butterworth-Heinemann, Oxford, UK.

Olver, A. V. (2002), "Gear lubrication - A review Part J. Journal of Engineering Tribology", vol. 216, pp. 255-267.

Paula. J, D. (2001), Gear Damage Detection Using Oil Debris Analysis, NASA / TM--2001-210936, NASA, Manchester, United Kingdom, September 4--6, 2001.

Pekka, V. (2006), Oil analysis in machine diagnostics, ISBN 951-42-8076-8, Acta Universitatis Ouluensis A, University of Oulu.

Peng, Z., Kessissoglou, N. J. and and Cox, M. (2005), "A Study of the Effect of Contaminant Particles in Lubricants using Wear Debris and Vibration Condition Monitoring Techniques", Wear, vol. 258, no. 11-12, pp. 1651-1662.

Peter Lynwander (1983), Gear Drive Systems: Design and Application, Volume 20 of Dekker Mechanical Engineering Series ed, Marcel Dekker.

Physical Acoustic Co. (2007), PCI-2 BASED AE SYSTEM USER's MANUAL, .

Pirro, D. M. and Wessol, A. A. (eds.) (2001), Lubrication Fundamentals, Second Edition: Revised and Expanded, Second Edition ed, CRC Press.

Reimche, W. and Südmersen, U. (2003), "Basics of Vibration Monitoring for Fault Detection and Process Control, vol. 6, pp. 2-6. Rio de Janeiro, Brazil (2003).", Vol. 6, Rio de Janeiro, Brazil, pp. 2-6.

Ribrant, J. and Bertling, L. (2007), "Survey of failures in wind power systems with focus on Swedish wind power plants during 1997-2005", Power Engineering Society General Meeting, 2007. IEEE, Vol. 22, 24-28 June 2007, Tampa, FL, pp. 1 - 8.

Robinson, J. C. (2001), " Detection and Severity Assessment of Faults in Gearboxes from Stress Wave Capture and Analysis", Society for Machinery Failure Prevention Technology (MFPT) 2001 Annual Conference, 2001.

Roylance, B. J. and Hunt, T. M. (eds.) (1999), Machine & condition monitoring series – Wear debris analysis, 1st ed ed, Coxmoor Publishing Company, Oxford, UK.

Ruqiang, Y. (2007), Base Wavelet Selection Criteria for Non-stationary Vibration Analysis in Bearing Health Diagnosis (PhD thesis), University of Massachusetts, Online PhD Thesis.

Samuel, P. D. and Pines, D. J. (2005), "A review of vibration-based techniques for helicopter transmission diagnostics", Sound and Vibration, vol. 282, pp. 475-508.

Sarychev, G. A. and Shchavelin, V. M. (1991), " Acoustic emission method for research and control of friction pairs", Tribology International, vol. 24, no. 1, pp. 11.

Sawahli, N. and Randall, R. (2004), "The application of spectral kurtosis to bearing diagnostics", Proc Acoustics (ed.), in: null, Noveember 2004, Australia, pp. 393.

Serrato, R., Maru, M. M. and Padovese, L. R. (2007), "Effect of lubricant viscosity grade on mechanical vibration of roller bearings", Tribology International, vol. 40, no. 8, pp. 1270-1275.

Shigley, J. E., Mischke, C. R. and Brown, T. H. (eds.) (2004), Standard handbook of machine design electronic resource, 3rd ed ed, McGraw-Hill, New York.

Shiroishi, J., Li, Y., Liang, S., Kurfess, T. and Danyluk, S. (1997), "BEARING CONDITION DIAGNOSTICS VIA VIBRATION AND ACOUSTIC EMISSION MEASUREMENTS", Mechanical Systems and Signal Processing, vol. 11, no. 5, pp. 693-705.

Smith, J. D. (1993), "A new diagnostic technique for asperity contact", Tribology International, vol. 26, no. 1, pp. 25-27.

Spinato, F., Tavner, P. J., van Bussel, G. J. W. and Koutoulakos, E., (2009), "Reliability of wind turbine subassemblies", vol. 3, no. 4, pp. 1-15.

Stokes, A. (ed.) (1992), Manual Gearbox Design, Butterworth-Heinemann Ltd.

Stribeck, R. (1902), " Die Wesentlichen Eigenschaften der Gieit- und Rollenlager--the key qualities of sliding and roller bearings. Zeitschrift des Vereines Seutscher Ingenieure", vol. 46, no. 38, pp. 1342-1348.

Tan, C. K. (2005), An Investigation on the Diagnostic and Prognostic Capabilities of Acoustic Emission on Spur Gearbox (PhD thesis), Cranfield University, UK.

Tan, C. K. and Mba, D. (2005), " Limitation of Acoustic Emission for Identifying Seeded Defects in Gearboxes", Nondestructive Evaluation, vol. 24, no. 1, pp. 11-28.

Tan, C. K., Irving, P. and Mba, D. (2007), "A comparative experimental study on the diagnostic and prognostic capabilities of acoustics emission, vibration and spectrometric oil analysis for spur gears", Mechanical systems and signal processing, vol. 21, no. 1, pp. 208-233.

Tan, C. K. and Mba, D. (2005a), "Experimentally established correlation between acoustic emission activity, load, speed, and asperity contact of spur gears under partial elastohydrodynamic lubrication", Proceedings of the Institution of Mechanical Engineers, Part J: Journal of Engineering Tribology, vol. 219, no. 6, pp. 401-409.

Tan, C. K. and Mba, D. (2005b), "Identification of the acoustic emission source during a comparative study on diagnosis of a spur gearbox", Tribology International, vol. 38, no. 5, pp. 469-480.

Tandon, N. and Choudhury, A. (1999), "A Review of Vibration and Acoustic Measurement Methods for the Detection of Damages in Rolling Element Bearings", vol. Tribology International, 32(8), no. 1999, pp. 469–480.

Tekeo, Y. and Takashi, F. (1982), "A new acoustic emission source locating system for the study of rolling contact fatigue", Wear, vol. 81, pp. 183-186.

Toutountzakis, T. and Mba, D. (2003), "Observations of acoustic emission activity during gear defect diagnosis", NDT & E International, vol. 36, no. 7, pp. 471-477.

Toutountzakis, T., Tan, C. K. and Mba, D. (2005), "Application of acoustic emission to seeded gear fault detection", NDT & E International, vol. 38, no. 1, pp. 27-36.

Townsend, D. P. and Akin, L. S. (1981), "Analytical and Experimental Spur Gear Tooth Temperature as Affected by Operating Variables", J. Mech. Des., vol. vol. 103, no. no. I, Jan., pp. 219-229.

Townsend, D. P. and Shimski, J. (1994), Evaluation of the EHL film thickness and extreme pressure additives on gear surface fatigue life, N ARL-TR-477. Perth, ASA Technical Report, Australia.

Tse, P., Yang, W. and Tam, H. (2004), "Machine fault diagnosis through an effective exact wavelet analysis", Journal of Sound and Vibration, vol. 4, no. 277, pp. 1005-1024.

Vahaviolos, S. J. (ed.) (1999), Acoustic Emission standards and technology update, stp1353 ed, ASTM.

Various, A. (2008), Operations Report 2007, OWEZ_R_000_20081023, Noordzee Wind, Noordzee Wind.

Vayionas, P. (1991), Design and Build of a Gearbox Test Rig for Condition Monitoring Through Vibration Analysis (unpublished MSc thesis), Cranfield University, Cranfield.

Vecer, P., Kreidl, M. and Smid, R. (2005), Condition Indicators for Gearbox Condition Monitoring Systems

, 45 (6), Acta, Polytechnica.

Vincent, O. (2007), Condition Monitoring of Gear Failure with Acoustic Emission (MSc thesis), Department of Mechanical Engineering Blekinge Institute of Technology Karlskrona, Sweden.

Walton, D. and Goodwin, A. J., (1998), "The wear of unlubricated metallic spur gears", Wear, vol. 222, pp. 103-113.

William, A. G. (ed.) (1992), Materials for Tribology, Elsevier Materials for Tribology ed, .

Wiśniewski, M. R. and Janczak, K. J. (1981), "Temperatures of meshing gears under conditions of elastohydrodynamic lubrication", Wear, vol. 67, no. 1, pp. 25-30.

Yesilyurt, I. (1997), Gear Fault Detection and Severity Assessment Using Vibration Analysis (Ph.D. thesis), Manchester, The University of Manchester.

Yesilyurt, I., Gu, F. and Ball, A. D. (2003), "Gear tooth stiffness reduction measurement using modal analysis and its use in wear fault severity assessment of spur gears", NDT & E International, vol. 36, no. 5, pp. 357-372.

9 Appendixes

APPENDIX A

Helical Gear geometry

Gear Specifications	
Normal module mn is mn = m cos ψ	
From geometry we have normal pitch as pn = p cos ψ	.
The pitch diameter (d) of the helical gear is: d = Z m = Z mn / cos ψ	
The axial pitch (pa) is: pa = p / tan ψ	
For axial overlap of adjacent teeth, b ≥ pa	
Normal module mn is pn = p cos ψ	
mn is used for hob selection. mn = m cos ψ	
The pitch diameter (d) of the helical gear is: d = Z m = Z mn / cos ψ	
The relation between normal and transverse pressure angles is tan Øn = tan Ø .cos ψ	
Basic Gear Formulas	
Pitch diameter (d)	d = zmn / cos β
Base diameter (db)	db = d cos αt
Root diameter (df)	df = da – 2h
Tip diameter (da)	da = d + 2ha
Addendum (ha)	ha = mn(1+xn)
Dedendum (hf)	-
Whole depth (h)	h = 2.25mn
Radial pressure angle (αt)	αt = tan-1(tan αn / cos β)
Tooth Thickness (t)	t = πmn / 2
mn = Normal module	
z = No of teeth	
α = Pressure angle	
αn = Normal pressure angle	
β = Helix angle	
xn = Normal coefficient of profile shift	
ψt = transverse pressure angle	
σo = base helix angle	
Gears Dimensions:	
da = tip diameter, pinion	da = 166.65 mm

do = base diameter, pinion	do = 150.06 mm
d = pitch diameter, pinion	d = 160.65 mm
Da = tip diameter, wheel	Da = 226.50 mm
Do = base diameter, wheel	Do = 205.97 mm
D = pitch diameter, wheel	D = 220.50 mm
f = gear face width	f = 25 mm
C = center distance	c = 190.58 mm
C = center distance	t = 51 teeth
σo = base helix angle	σo = 17.75o
mn = Normal module	mn = 3

Line of Contact Calculation for Helical Gear Equations from Merritt		
Nomenclatures		
pn = normal pitch	pn = π mn	
pa = axial pitch	pa = pn / sin β	
pot = transverse base pitch	pot = π do / t (3)	
ψt = transverse pressure angle	cos ψt = (do + Do)/ 2C (4)	
lp = length of path addendum contact, pinion	lp = lp = ½ √(da^2-do^2) – ½ d sin ψt	
lw = length of path addendum contact, wheel	lw = ½ √(Da^2-Do^2) – ½ D sin ψt	
Qctp = transverse contact ratio, pinion	Qctp = lp/pot (7)	
Qctw = transverse contact ratio, wheel	Qctw = lw/pot (8)	
Qct = transverse contact ratio	Qct = Qctp + Qctw (9)	
Qcn = Normal contact ratio	Qcn = Qct sec2 σo (10)	
Qca = axial contact ratio	Qca = f / pa (11)	
lcmin = minimum length of line of contact		
lc = maximum length of line of contact		

Since Qca lies between 2-Qct and 1, single line contact occurs over the axial length pa(2-Qct) and double line contact for the rest [109] given that the minimum length of line of contact, lcmin = pa (2Qca + Qct – 2) sec σo = **41.2965524** mm

The calculation of the maximum length of line of contact during helical gear mesh is given by, lc = lcmin Qct / (Qca + Qct -1) = **46.70** mm

Appendix B

Equivalent load per unit length at gear face width calculated from the torque laod

Torque [Nm]	Load [kN/m]
60.00	13.18
120.00	26.36
180.00	39.53
250.00	54.91
370.00	81.27

Line of contact calculation- continued	
π =	3.14
mn=	3.00
β=	17.75
sinβ=	0.30
Pn= πmn	9.43
Pa=pn/sinβ	30.93
do=	150.06
d=	160.65
da=	166.65
Do=	205.97
D=	220.50
Da=	226.50
σ=	17.75
sec σ=	1.05
sec² σ=	1.10
c=	190.58
f=	25.00
t=	51.00
Pot=πdo/t	9.25
cosψ=(do+Do)/2C	0.93
ψ=	20.93
sinψ=	0.36
lp=0.5*(da^2-do^2)^0.5-(.5*d*sinψ)	7.57
lw=0.5*(Da^2-Do^2)^0.5-(.5*D*sinψ)	7.75
Qctp=lp/Pot	0.82
Qctw=lw/Pot	0.84
Qct=Qctp+Qctw	1.66
Qcn=Qct sec² σ	1.82
Qca=f/Pa	0.81
2-Qct=	0.34
F=Total load applied on the tooth/teeth in *N*	
T= Torque applied on the wheel shaft in Nm	60.00
di,d2=Diameter of wheel and pinion in m	0.11

W= load per uint length in N/m	
F=d1/T*(N)*	544.22
w=F/*lc* *(Nlm)*	13.18
lcmin=pa(2Qca+Qct-2)sec σ *(mm)*	lc=lcmin Qct/(Qca+Qct-1) *(mm)*
41.2965524	46.70

Appendix C

Lubrication Specifications

Mobilgear 600 Series	629	636
cSt @ 40º C	150	680
cSt @ 100º C	15.8	39.2
Viscosity Index, ASTM D 2270	98	90
Pour Point, ºC, ASTM D 97	-27	-9
Flash Point, ºC, ASTM D 92	245	285
Density @15.6º C, ASTM D 4052, kg/l	0.89	0.91
Timken OK Load, ASTM D 2782, lb	65	65
4-Ball EP test, ASTM D 2783:		
Weld Load, kg	250	250
Load Wear Index, kgf	48	48
FZG Scuffing, DIN 51534, A/8.3/90, Fail Stage	12+	12+
Rust protection, ASTM D 665, Sea Water	Pass	Pass
Copper Strip Corrosion, ASTM D 130, 3 hrs @ 100º C	1B	1B
Demulsibility, ASTM D 1401, @ 54º C Time to 3ml emulsion, minutes @ 82º C	30	30

Appendix D

Thermocouples specifications

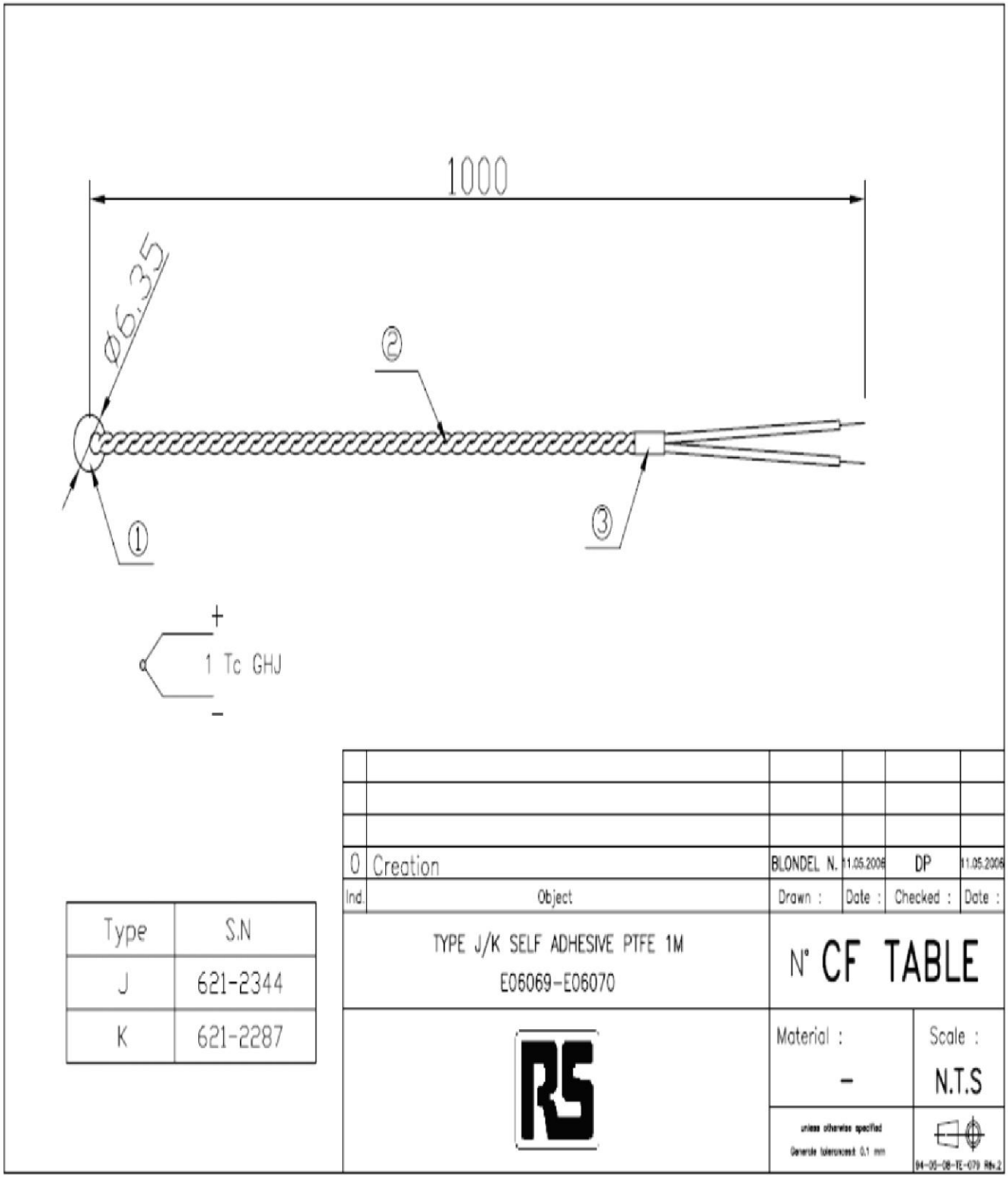

Appendix E

PM Series
Description
Suitable for a wide variety of industrial applications, the PM series is designed to transmit power and data signals at high speeds. Compatible with thermocouple and strain gauge instrumentation, the PM series is

designed to maintain reliable performance under adverse operating conditions. Continuous silver connections ensure minimal thermal error. Quick and easy to install and available with 8, 12 and 24 circuits.

Features

• Suitable for a wide variety of industrial applications
• Transmits power and data signals at high speeds
• Compatible with thermocouple and strain gauge instrumentation
• Reliable performance under adverse operating conditions
• Continuous silver connections ensure minimal thermal error
• Quick and easy to install
• Available with 8, 12 and 24 circuits

Benefits

• High rotational speed
Low torque required to drive this unit

High Speed Slip Ring Capsules

PM Series Specifications	
Terminals	Silver
Mounting	Flange mounted 4 holes ø5,1 mm equi-spaced on a 73,0 mm P.C.D.
Cooling Air Pressure	1.4kg / cm2
Brush Lifting Air Pressure	4.2 kg / cm2
Maximum Voltage	50 volts
Temperature Range	-20ºC to +90ºC
Maximum Current	2.5 amps

**Please note that the operational life of the unit is dependent upon rotational speed, environment and temperature.*

Note: Operation at maximum rotational speed requires cooling air to be supplied through the inlet and outlet ports provided.

Series	Part Number	Number of Ways	Length Diameter	Weight gm	Starting Torque g-cm	Maximum Speed RPM
PM-08	80038-950	8	132 mm	1000	290	12,000
PM-12	80039-950	12	147 mm	1140	406	12,000
PM-24	80027-950	24	216 mm	1820	812	12,000

PM Series Dimensions

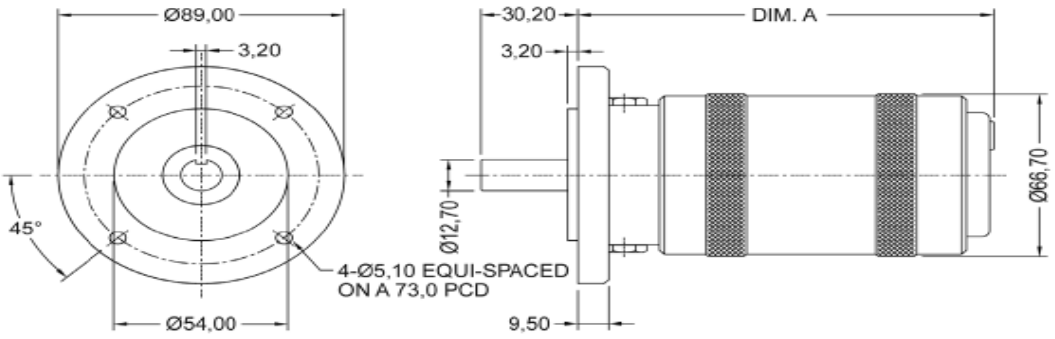

Dimensions in millimeters